A STUDY OF TIME DELAYS ON A SINGLE CYLINDER AND A CYLINDER IN AN ARRAY OSCILLATING IN UNIFORM FLOW

By

JIAQI CAI

Master of Science

Tianjin University

Tianjin, China

1986

Submitted to the Faculty of the
Graduate College of the
Oklahoma State University
in partial fulfillment of
the requirements for
the Degree of
DOCTOR OF PHILOSOPHY
July, 1995

A STUDY OF TIME DELAYS ON A SINGLE CYLINDER AND A CYLINDER IN AN ARRAY OSCILLATING IN UNIFORM FLOW

Thesis Approved:

Thesis Adviser

Dean of the Graduate College

ACKNOWLEDGMENTS

I would like to express my sincere appreciation to my major adviser, Dr. Peter M. Moretti for his intelligent supervision, constructive guidance, support and inspiration. My thanks also go to the other members of my committee: Dr. Kenneth Bell, Dr. Frank W Chambers, Dr. Richard L Lowery-- for guidance and suggestions in the completion of this research.

To some of my friends who provided suggestions, assistance and friendship for this study, my hearty thanks: Dr. Mingchun Dong, Dr. Ye Tian, Dr. G. X. Chen, Mr. Lapmou Tam, Mr. Tzerkun Lin, Mr. Wenchieh Tang, and everyone at the MAE machine workshop.

My wife, Yijing Zhang, must be thanked for her consideration, enthusiasm, encouragement, understanding and substantial help throughout this whole process.

I would like to say a very special thank-you to my parents and my grandmother who have taught me more than I usually care to admit. Certainly, none of this would have been possible without them. And I also thank my brother Jiazhen and my sisters Jiaqing and Jiaxin for their encouragement.

And if I left anyone out- I am sorry, but you know my intentions are always good even if my memory is not.

Finally, I would like to thank the School of Mechanical and Aerospace Engineering for the financial support during these four and half years of study.

TABLE OF CONTENTS

LIST OF TABLES

LIST OF FIGURES

NOMENCLATURE

A	Oscillation amplitude
$\overline{A}$	Non-dimensional oscillation amplitude
c	Speed of sound
c_f	Skin friction factor
c_{fs}	Steady component of skin friction factor
c_{fu}	Oscillating component of skin friction factor
C_D	Drag Coefficient
c_p	Pressure coefficient
c_{po}	Variation range of pressure
D	Cylinder diameter
f	Oscillation frequency
F	Strength of the convection
g	Gravity acceleration
H	Shape factor
l	Length of the fluid stream
m	Mass
K	Stability constant
P	Pressure
R	Cylinder radius
Re	Reynolds number
$S(\lambda)$	Shear correlation
t	Time

$\bar{t}$	Non-dimensional time
T	Pitch in a cylinder array
$\frac{1}{D}$	Pitch to diameter ratio
U	Flow velocity
$\bar{U}$	Non-dimensional flow velocity
U_{cr}	Critical flow velocity
U_{∞}	Free stream velocity
x	X-coordinate
$\bar{x}$	$\frac{x}{R}$
$\bar{x}_s$	Separation point
y	Y-coordinate
$\bar{y}$	$\frac{y}{R}$
z	Elevation
α	Phase angle
β	Transverse velocity component
δ	Logarithmic decrement of mechanical damping
δ_1	Displacement thickness
δ_2	Momentum thickness
Δt	Time step
$\Delta\bar{t}$	Non-dimensional time step
Δx	Grid size
$\Delta\bar{x}$	Non-dimensional grid size
ε	Non-dimensional oscillation velocity
$\phi(x,y,t)$	Potential function
λ	Boundary parameter

μ	Dynamic viscosity
ν	Kinematics viscosity
ρ	Density of fluids
τ	Time Delay
τ_o	Shear stress
ω	Oscillation circular oscillation frequency
$\overline{\omega}$	Non-dimensional circular oscillation frequency

CHAPTER I

PROBLEM STATEMENT

1.1 Background

Cylinder arrays subjected to cross-flow are commonly found in heat exchangers, steam generators, and condensers in the power-generation, chemical, and petrochemical industries. Since the 1970's, with increasing flow velocities and larger units used in order to enhance heat transfer and reduce cost, many notorious failures have occurred in the power generating and chemical industries, leading to extensive damage and to costly and time-consuming repairs (Paidoussis 1979, 1981).

During the last 20 years, extensive research has been carried out to identify the excitation mechanisms responsible for the vibrations and to provide guidelines for the safe design of new equipment. Reviews of the state-of-the-art in these excitation phenomena have been compiled by Blevins (1990), Chen (1984, 1991), Moretti (1986, 1993), Paidoussis (1987) and Weaver et al. (1987).

The mechanisms involved in the cross-flow-induced vibration of cylinder arrays may be broadly classified as turbulent buffeting, vortex shedding (with or without acoustic resonance), and fluid-elastic instability. These are all identified as possible sources of vibrations, depending on the design and operating condition of the heat exchanger. Fluid-elastic instability or whirling is generally recognized as the flow-induced vibration mechanism most commonly causing failure in industrial heat-exchanger cylinder arrays, so it is by far the most important mechanism. Hence the prediction of the critical flow velocity of fluid-elastic instability is very important.

Since the early 1970's, a number of studies have been conducted on fluid-elastic instability both of a practical and a theoretical nature (Chen et al., 1987; Paidoussis, 1987; Weaver et al., 1987). Chen (1978,1981) proposed a semi-empirical model in which displacement, velocity, and acceleration dependent fluid force coefficients would be used in a linearized equation of motion in order to predict the fluid-elastic instability of a cylinder array. Tanaka and Takahara (1980) were able to experimentally determine these unsteady force coefficients for water flow through a square array as well as the motion of the cylinder in question and its nearest four neighboring cylinders. Chen then used these force coefficients to complete his unsteady model, extending the predicted stability model to air flow; good agreement with experimental results was found. The major shortcoming associated with Chen's semi-empirical model is that all of the relevant fluid force coefficients have to be measured for every array configuration over the entire range of reduced flow velocity, which is very tedious and time consuming. To avoid this extensive experimental work, several different simple fluid-elastic instability models based on time delay have been developed to predict the critical velocity for an arbitrary geometry (Marn and Catton, 1992; Price and Paidoussis, 1992; Yetisir and Weaver, 1992). The time delay here means the delay between the cylinder motion and the associated flow perturbation; the major advantages of this kind of model are that no measured fluid force coefficients are required and that it considers the effects of cylinder array configuration and the pitch-to-diameter ratio directly. While each of the models is successful in reproducing some features of experimental results and field experience, each of them uses a different value of time delay between the cylinder displacement and the velocity close to the cylinder. The solutions are very sensitive to variations in the value of time delay used (Lever and Weaver 1982). Since there is no theoretical or experimental study on the time delay, it is generally obtained from semi-empirical equations. Each researcher's equation has a form which results from his postulation of the fundamental time delay phenomenon, and at least one coefficient which is arbitrarily adjusted to obtain the desired overall result when the

time-delay is entered into a particular stability model. The time delay values obtained vary widely; for example, for a rotated-triangle (30 degree) array with pitch-to-diameter ratio of 1.5, the Yetisir & Weaver model (1992) yields a time delay about three times larger than that of Price et al.(1992). The reason for this dramatic difference is that the fluid dynamics producing the time delay is not well understood, and therefore time delay is introduced artificially into the model.

1.2 Weaver's Time Delay Model

Weaver's time delay model is based on the following assumptions: (a). The channel flow is incompressible and inviscid; (b). A quasi-steady Bernoulli equation can be used; (c). The time delay results from the fluid inertia in the approaching flow channel in a cylinder array.

Conceptual problems with Weaver's model are three-fold: Firstly, assumptions (a) and (c) contradict each other, since low-Mach-number irrotational flows follow the governing equation:

$$\rho\frac{D\vec{V}}{Dt} = \rho\vec{g} - \nabla\vec{p}$$

which does not give rise to time delays. Secondly, in assumption (b) the quasi-steady Bernoulli equation:

$$\frac{p}{\rho} + \frac{1}{2}V^2 + gz = \text{const}$$

is not adequate for vibrational studies, as the unsteady terms are not negligible. Thirdly, Weaver's model does not account for the unsteady wake effects, which are considered to play a very important role in time delay and are essential to the excitation mechanism.

1.3 The Current Time Delay Model and Main Results

To answer the first objection, our approach is to look for the time delays which can explain self-sustaining oscillations in the viscous part of the flow, with the governing equation:

$$\rho \frac{D\vec{V}}{Dt} = -\vec{\nabla} p + \mu \nabla^2 \vec{V}$$

which, in the vicinity of the cylinder, reduces to the unsteady boundary layer equation:

$$\frac{\partial (U\delta_1)}{\partial t} + \frac{\partial (U^2 \delta_2)}{\partial x} + U\delta_1 \frac{\partial U}{\partial x} = \frac{\tau_0}{\rho}$$

To answer the second and third objections in section 1.2, we look for the action of the time delay on the fluid forces not through the Bernoulli equation applied to the main channel, but through the aerodynamic lift due to the shifts in boundary layer separation. From the viewpoint of fluid dynamics, when the flow is across the cylinder, there is a thin boundary layer near the cylinder which will be separated at a certain location on the cylinder (flow separation), with the separated flow forming unsteady wakes downstream. When the cylinder is oscillated in the flow, the oscillation will cause a change in the boundary layer near the cylinder, which will affect the separation point and the wake flow. Therefore oscillation changes the separated flow, but the response of separated flow to oscillation is not immediate. As a result of the time delay there is a phase lag between the oscillation and the separated flow due to the delayed response of the boundary layer to the changed flow conditions. As flow separation is influenced by boundary layer development, and the time delay is attributed to the boundary layer development, it is possible to predict the time delay by solving the unsteady boundary layer equation.

In this study, an attempt is made to understand the physical mechanism of time delay and develop a theoretical model for time delay based on fundamental fluid dynamics theory. Then experimental measurements are made to verify the theoretical results. Our research attempts to improve the physical description of time delay and give a physical insight into the fluid mechanics. This report describes the theory and the solution procedure, and presents the theoretical results. Finally, the experimental results are presented and compared to the theoretical results. The existence of time delay is found by

solving the unsteady boundary-layer momentum-integral equation numerically. Time delay for a single cylinder with transverse or streamwise oscillation was investigated. Based on the studies for a single cylinder, the time delay for a cylinder array has been investigated and reported. The results show that the oscillation frequency and oscillation amplitude do not affect the time delay very significantly for either a single cylinder or a cylinder array, so that it can be concluded that the velocity perturbation does not affect time delay either. For a single cylinder the time delay does depend on the measurement location with respect to the oscillating cylinder. In the region of $0.09 \leq \bar{x} \leq 1.06$, the time delay increases near linearly with the x-coordinate; in the region of $1.06 < \bar{x} \leq 1.80$ the rate of change increases with the time delay increasing exponentially. For a single cylinder, comparing the time delay for transverse and streamwise oscillation, it was found that the behavior of the time delay for a streamwise oscillation was similar to that for the transverse oscillation, but a time delay with transverse oscillation was larger than that for the streamwise oscillation. It also shows that the fluctuation of momentum thickness changes with the location; the fluctuation decays from $\bar{x} = 0.09$ to $\bar{x} = 1.26$, but it increases when $\bar{x} > 1.26$, which is different from the assumption used in Yetisir & Weaver's model (1992).

For a cylinder array, the results show that Reynolds number and oscillation frequency do not affect the outer layer velocity distribution very significantly; but the pitch-to-diameter ratio T/D influences the outer layer velocity very significantly; with the increase of the T/D ratio, the velocity decreases, which is the same as that expected. The results show that with the increase in oscillation amplitude the velocity increases at certain time.

Regarding the time delay of a cylinder array, it was found that the time delay changes with the location; in the region near the stagnation point there is a jump in the time constant, after $\bar{x} \geq 0.18$ the time delay increases with the location linearly; but the effect of oscillation frequency and amplitude on time delay is very small. The pitch-to-

diameter ratio greatly influences the time delay such that with the increase of pitch-to-diameter ratio, the time delay increases compared to a single cylinder. The time delay, for a cylinder in an array in the region from the point near stagnation point to $\bar{x} = 1.44$, is larger than that for a single cylinder, but after this region the time delay for a single cylinder is larger than that of a cylinder array; in other words, the increased ratio of time delay for a single cylinder is greater than that of a cylinder array. Finally, a comparison with Weaver's model has been made. As the current time delay model and Weaver's model have different mechanisms of time delay, it is impossible to compare these two models directly. However it is found that the predictions of these two models are all independent of Reynolds number.

From the experimental results, the following conclusions can be drawn: the time delay is caused by the development of the boundary layer, which is in good agreement with what we expected and demonstrated numerically; before the separation point, it was found from the measurements that the flow perturbation and cylinder oscillation correlate closely, without time delay or phase lag; near the separation point (about 85 degrees), time delay is detected between cylinder oscillation and flow perturbation; after the separation point, time delay still exists, but the value of time delay is different from moment to moment and from location to location, so that the time delay in the wake cannot be described in a simple way; if the hot film moves with the cylinder but outside the boundary layer, there is no time delay found between the cylinder oscillation and the mean flow, small high-order perturbation was observed overlaid on the fundamental fluctuation in our experiments.

CHAPTER II

LITERATURE SURVEY

The extensive studies of flow-induced vibration can be dated back to the early 1970's. Since then considerable research has been conducted on fluid-elastic instability both of a experimental and a theoretical nature (Chen et al., 1987; Paidoussis, 1987; Weaver et al., 1987). These studies include empirical stability criteria, mathematical models, and scaled-models or full-scale evaluation tests. The results have improved understanding of the instability mechanism and provided guidelines for practical design. However, there are still some rather serious deficiencies both in understanding the mechanism of fluid-elastic instability in cylinder arrays and in the prediction of instability. This will be detailed in a later section.

2.1 Experimental Studies

Because of the complexity of the flow field in a cylinder row or array, it is very difficult to predict critical velocity theoretically under different conditions. Researchers in various countries have conducted many experimental studies with regard to fluid-elastic instability, which can be grouped in several areas as follows:

2.1.1 Stability constants

Much of the pioneering work on fluid-elastic instability of cylinders in cross flow was done by Connors (1970). Connors developed a semi-empirical model, based on the motion of cylinders which he had observed commonly in a single cylinder row. After Connors presented his famous expression for the prediction of fluid-elastic instability critical velocity,

$$\frac{U_{cr}}{fD} = K\left[\frac{m\delta}{\rho D^2}\right]^{0.5}$$

extensive experimental and analytical studies were motivated by the need to develop design guidelines. Experimental data was collected to obtain suitable values of K, applicable to cylinder arrays of different geometry, in different fluids, etc. (Chen, 1984; Connors, 1978; Grover and Weaver, 1978; Pettigrew et al., 1978; Soper, 1980; Weaver, 1987; Zdravkovich and Norman, 1978). Details may be found in the review of Prettigrew and Taylor (1992). It was found that K=*9.9*, obtained by Connors, is not conservative for all cylinder arrangements. Soper (1980) suggested K_{min}=*2.0* for rotated (parallel) triangular arrays; Connors (1978), from experiment on square-geometry arrays, proposed $K = 0.37 + 1.76\frac{T}{D}$ for $1.41 < \frac{T}{D} < 2.12$*1*, where $\frac{T}{D}$ is pitch to diameter ratio of the cylinder array, leading to K_{min}=2.9. However, it was the value of K_{min}=*3.0* proposed by Prettigrew et al. (1992) that obtained the most widespread acceptance in practical industrial design.

2.1.2 Effect of different system parameters

There are many parameters that affect the critical flow velocity: for instance, upstream turbulence will affect critical velocity. Southworth and Zdravokovich's experiment (1975) in a wind tunnel shows that turbulence causes the beginning of fluid elastic instability to shift to a higher flow velocity. But Chen's experiment (1981) in a water tunnel found turbulence could stabilize or destabilize the tube array depending on the characteristics of the turbulence.

Having different individual 'vacuum' natural frequencies for each cylinder in an array is called detuning. In general, the detuning of a cylinder array increases the critical velocity (Chen and Jendrzejczyk, 1981).

Pitch-to-diameter ratio T/D has a significant effect on fluid-elastic instability for some cylinder arrays. Soper (1983) noticed that the factor K increases with T/D for triangles and rotated square arrays, but the effect of T/D is very small for normal square and rotated triangle cylinder arrays.

2.1.3 Measurement of flow field

It should be stated that understanding the flow field around cylinder arrays subjected to cross-flow is important in order to understand the fluid dynamics between the cylinder array and the flow, and to identify and quantify the important system parameters. Unfortunately, our physical understanding of the flow field in cylinder arrays is rather poor due to the complex flow patterns in interstitial and downstream flow. Heinecke and Mohr (1982) measured the steady and unsteady flow forces acting on a cylinder and the response of the cylinder to these forces. Their measurements show that four kinds of exciting mechanisms exist, which are vortices, buffeting, galloping and fluid-elastic instability. Chen and Jendrzejczyk (1987) measured the fluid forces acting on a square in-line array of cylinders subject to turbulent flow with a pitch-to-diameter ratios of 1.33 and 2.0 respectively, and the critical velocity measured is in good agreement with that calculated with the unsteady force coefficients. Oengoeren and Ziada (1992) measured the unsteady fluid forces acting on a square cylinder array with a pitch ratio of 1.95 in air cross flow; they investigated the effects of Reynolds number and the row depth on fluctuating forces. From their measurements the fluctuating lift and drag coefficients were obtained. Their results agree well with those measured by Chen and Jendrzejczzyk (1987).

Many researchers have studied vortex shedding from an oscillating circular cylinder. They found that when a cylinder is vibrating in a cross flow, vortex shedding can be dramatically altered. The flow generated by vortex shedding around a forced oscillating cylinder is very different from that for a fixed one. It is found that the vortex shedding frequency is captured by the oscillating frequency over a range of reduced

velocities, that is, the well-known 'lock-in' phenomenon (Bearman, 1984; Bishop and Hassan, 1964; Cheng and Moretti, 1991, 1992; Griffin and Hall, 1991; Stasby, 1976). An oscillating cylinder will also change the fluctuating drag coefficient C_D; Tanida et al. (1973) reported an increase in C_D for an oscillating cylinder. Bublitz (1972) measured the unsteady pressure on an oscillating circular cylinder in transverse flow; his results show that the mean values of pressure coefficient C_p are different from those for the rest of the cylinders. Comparing with the case of the cylinder at rest, it is found that the separation point is shifted forward in the case of oscillation.

The pressure distribution around a cylinder in an array is very complex, and only limited data is available, although this data is important in understanding the flow field as well as in obtaining the necessary force coefficients for response calculations. Zdravkovich and Namork (1980) measured the fluctuating time-averaged pressure distribution around a cylinder located in different rows of a triangle array with a transverse pitch ratio of 1.375, longitudinal 1.875, for *Re=110,000* in a wind tunnel. They found the pressure distribution in the first two cylinder rows was very different from that in the rest of the array, indicating a different structure of the flow at different positions in the array. Zdravkovich and Stonebanks (1990) investigated the flow field behind a single row and two rows of cylinders, their experiment showed non-uniform flow across the row even though the approaching flow was uniform and the cylinders were uniformly spaced; their experiment identified the regions of greatest non-uniformity behind a single and two rows of cylinders. They found the flow was meta-stable and could switch intermittently. This phenomenon is supported by the extensive flow visualization experiments carried out by Moretti and Cheng (1988, 1989) for different configurations of cylinder array. Zdravkovich (1991) found the meta-stable interstitial flow could be stabilized by placing guide vanes behind a single row of tubes, and once the interstitial flow is stabilized, it becomes uniform as well. Recently, Ljungkrona and Bengt (1992) did an experimental

investigation of mean and r.m.s. pressures on cylinder surfaces for two in-line square cylinder arrays with pitch-to-diameter ratios of 1.26 and 1.75, respectively. They found a non-symmetric distribution for both mean-pressure coefficient and r.m.s. pressure coefficient in the tighter array, but symmetric results for the 1.75 ratio.

Studies of the interstitial, downstream flow and local dynamic pressure distribution are required for us to understand the mechanism of fluid-elastic instability, to give some new insights into the physics of the flow field, and vibration mechanism, and thereby to predict the critical velocity of fluid-elastic instability. This will lay a foundation for predicting fluid-elastic instability theoretically.

2.2 Theoretical Studies

It is impossible at present to determine the critical velocity for all different cylinder arrays under different flow conditions, so a systematic theoretical method must be developed to predict the fluid-elastic instability. Roberts (1966) first studied the dynamic instability of a cylinder row in cross flow. He discovered that flow-direction motion of alternate cylinders could cause changes in wake-pairing downstream of the row. He postulated that the switch of jet-like flow between adjacent cylinders is significantly affected by the motion of the cylinders: thus, when one cylinder moves, the wakes behind and the pressure distributions around the moving cylinder and neighboring cylinders are modified, in synchronism with the cylinder motion. For purely streamwise motions, it was found that in the course of a cycle of oscillations, energy may be extracted from the flow, thus leading to an amplified oscillation. However, in closely packed arrays, streamwise motion may not be the first instability observed.

After Roberts, other researchers developed theoretical models to predict the onset of fluid-elastic instability of cylinder arrays in cross flow. These models can be classified by their underlying flow theory as follows:

2.2.1 Quasi-static semi-analytical models

Connors (1970), expanding on Roberts' work on a single row of cylinders, including motions in both streamwise and transverse directions, simplified the exciting forces by the assumption that, in most practical cases, the oscillating frequency is too high to permit jet switching to actually take place. He systematically displaced the three controlled cylinders according to relative motion which corresponded to his free-oscillation observations, and measured the force coefficients statically for various relative positions of the cylinders, thus establishing force-displacement relations empirically. The quasi-static assumption was made that the dynamic fluid forces at any instantaneous position of the cylinder (after subtracting jet-switching forces) are the same as the static fluid forces. Connors obtained the same simple expression as Roberts relating the critical flow velocity of fluid elastic instability U_{cr} in a cylinder array to the system parameters.

$$\frac{U_{cr}}{fD} = K\left[\frac{m\delta}{\rho D^2}\right]^{0.5}$$

where f is the frequency of oscillation; D is the cylinder diameter; m is the mass of the cylinder per unit length; δ is the logarithmic decrement of mechanical damping; and ρ is the fluid density. In Connors' study, K was found to be equal to 9.9 for a short tube row at 1.41 pitch-to-diameter ratio.

Blevins (1974) obtained similar results using stability criteria in a more general manner. He obtained additional values of K for non-uniform cylinder stiffness and damping. Up to that point it appears that Connors' semi-empirical equation can be extended to all types of arrays of cylinders; one only needs to know the appropriate value of K.

Connors-Blevins' expression derived from quasi-static theory is simple and very useful. However, with the accumulation of new experimental results, it was found that the

expression is not always applicable and there is some experimental data which cannot be explained by their expression. For instance, Weaver and Grover (1978) have found that the critical flow velocity varied as the damping parameter raised to power 0.21, rather than 0.5 as suggested by Connors' expression. Southworth and Zdravkovich (1975) have shown that even if all cylinders but one are held rigidly immobile, that one cylinder still becomes unstable, contrary to Connors' theory which requires a certain pattern of inter-cylinder displacements.

These are a few of the questions which have been raised concerning the universal validity of the Connors-Blevins theoretical model. As a result, fundamental work was reinitiated to find new theoretical models.

2.2.2 Unsteady semi-analytical models

One can speculate that vibration of the type which cannot be explained by the Connors-Blevins theoretical model is due to unsteady fluid-dynamic force components. To account for non-quasi-static forces, Chen (1978,1983) and Tanaka et al. (1980,1981, 1982) developed unsteady semi-analytical models. Chen formulated the system of cylinder-cylinder interactions and obtains expressions for coupled inertial, damping, and stiffness (displacement-dependent) terms. Tanaka et al. measured the unsteady forces on oscillating cylinders in an in-line square array, with the unsteady force coefficients obtained from their measurement, which have been used to generate stability curves which give good agreement with measured stability data for this in-line square array. An important fundamental contribution of this model lies in the identification of two distinct mechanisms which can individually cause flutter-type fluid-elastic instabilities.

Fluid-damping-controlled instability occurs for low values of $\frac{m\delta}{\rho D^2}$ typical of liquid flows. It is the dynamic instability caused by the fluid damping force: when the flow velocity exceeds a certain value, the modal damping becomes negative and the system

becomes unstable. The energy transferred from flow to cylinder is attributed to the cylinder velocity, so it may be called a 'velocity mechanism'.

For high values of $\frac{m\delta}{\rho D^2}$ typical of gas flows, however, the mechanism is dominated by the fluid-dynamic 'stiffness effect', i.e., a position-dependent mechanism, so that inter-cylinder positions are important. This mechanism requires motion of more than one cylinder. Generally, of course, both mechanisms are at work, but their relative importance is different for different $\frac{m\delta}{\rho D^2}$ values.

This model is one of the most successful models available to date, as it gives the most detailed insights into the instability mechanism (Chen and Jendrzejczyk, 1982). The success of this model depends on the accuracy of the unsteady force coefficients, which can only be obtained through tedious measurement at present, which is the major shortcoming of this model and limits its practical application Numerical techniques for motion-dependent fluid forces of cylinders are desired, which could be developed only after we have a good understanding of the physics of the flow field. Unfortunately, the studies on the physics of the flow field is very limited. Once these fluid force coefficients can be estimated numerically or theoretically, this model is very attractive and promising.

2.2.3 Analytical models

To avoid the difficulty of measuring or estimating the fluid force coefficients, several so-called analytical models are developed. Basically, there are two different analytical models so far. One was developed by Lever and Weaver (1982, 1986a, 1986b). This model is based on the experimental observation, both in air and water cross flows, that a single flexible cylinder among rigid ones does become unstable at essentially the same U_{cr} as in an all-flexible array (Blevins et al., 1981; Southworth et al., 1975; Weaver et al., 1978, 1981a). From the flow visualization studies of Weaver et al. (1985, 1987), it

was found that the mean area of a streamtube is constant over the streamtube length. Therefore, it was assumed that it is sufficient to analyze the motion of a single cylinder in the array, where the mean area of a streamtube remains constant. A model was then developed considering the motions of just one cylinder, surrounded by immobile neighbors. The forces leading to destabilization are considered to arise from flow redistribution in the 'channel' formed by the dividing streamlines of sub-channel flows, where the flow distribution is caused by cylinder motion, with an appropriate phase lag (time delay) due to fluid inertia; thus both velocity and displacement-dependent forces are part of the model. This model can predict the fluid-elastic instability threshold at lower values of the mass-damping parameter as the excitation mechanism is dominated by negative damping; but at higher values of the mass-damping parameter the coupling between cylinders is dominant, so a flexible array of cylinders should be considered to model fluid-elastic instability. Recently, Yetishir and Weaver (1992) modified the Lever and Weaver model by introducing a linear superposition to account for the effect of the motion of neighboring cylinders. So the theoretical model of Lever and Weaver can be extended to a flexible array of cylinders through modification.

Price and Paidoussis (1984, 1986a, 1986b, 1992) developed a so-called constrained-mode approach, based on quasi-steady theory, which deals with only a small kernel of cylinders properly to account for the coupling between cylinders instead of a full array of flexible cylinders to save computational effect. The approach assumes any two adjacent cylinders in an array have motions of equal magnitude and may be either in or out-of-phase with each other. To compute the fluid forces on the cylinder, they introduced two time delay terms, one of them to account for the time delay between individual cylinder motion and the fluid dynamic forces, another for the time delay between the motion of a cylinder and its effect being felt by adjacent cylinders. The model can predict the instability thresholds both for lower and higher values of the mass-damping parameters.

Rzentkowski and Lever (1992) modified the Lever and Weaver model to predict the non-linear fluid-elastic behavior of a cylinder array. They modified the model with a cylinder-amplitude dependent time delay, their modification improved the model's post-stable prediction, which further indicates the importance of time delay in the model. Marn and Cotton (1992) presented a new approach to the idea introduced by Lever and Weaver in the complex plane.

The advantage of this analytical model over the other models is its simplicity, as no empirical coefficients are required to describe the essential behavior of the system. The numerical solution of this model is in very good qualitatively with the experimental data, so it seems that the analytical model is on the right track, and the future is very promising. But the major problem regarding this model is how to estimate the very important parameter of time delay in this model. So far there is no systematic investigation to this parameter. Each researcher chooses his own time delay function based on his understanding of time delay.

2.3 The Gap in the Time Delay Studies

The crucial parameter in the analytical model is the time delay associated with the cylinder motion and flow perturbation. The model solutions are very sensitive to the variations of the time lag (Lever and Weaver, 1982). Unfortunately, so far there is no experimental investigation of the time delay available in the literature. Researchers have proposed different time delay functions based on speculative models.

Based on the experimental observation of a jet switch behind a row of cylinders, Roberts (1966) estimated the time delay between cylinder motion and fluid force to be $\tau = 10\frac{D}{U}$. Lever and Weaver (1982) proposed the estimation of time delay function based on a hydraulic analogy, the time lag is $\tau = \frac{l}{U}$, where l is the length of the fluid

stream under consideration and U is the steady gap flow velocity; following the work of Simpson and Flower (1977), Price et al. (1990) proposed the time lag to be $\tau = \mu \frac{D}{U}$, where μ is taken as being of order 1 in their model; D is the diameter of cylinder, U is reference gap flow velocity.

These time delay functions are very different for a same configuration of cylinder under same flow conditions. For example, considering a rotated triangle array with pitch to diameter ratio of 1.5, the l in Lever and Weaver model is about 4.3D; their time delay is about 3 times larger than that of the Price et al model, and the time delay from Roberts' expression is 9 times larger that of the Price et al model. The different time delay estimates will generate different fluid-elastic instability curves. The reason for this big difference for the same parameter is that the fluid dynamics producing such a time delay is not well understood, and artificial values are introduced into both models to make them fit known results. The solution to this problem may depend on the understanding of the physics of cylinder motion and the associated flow perturbation. To the best of our knowledge, there is no rigorous physical model for estimating the time delay.

In Weaver's time delay model, it is assumed that the channel flow is incompressible and inviscid so that a quasi-steady Bernoulli equation can be used and the time delay results from the fluid inertia in the approaching flow channel.

Conceptual problems with Weaver's model are three-fold: Firstly, the assumption of incompressible flow and the assumption of time delay, since for low-Mach-number irrotational flows the governing equation is Euler's equation, which does not give rise to time delays. Secondly, the quasi-steady Bernoulli equation is not adequate for vibrational studies, because the unsteady terms are not negligible. Thirdly, Weaver's model did not account for the unsteady wake effects, which are considered to play a very important role in time delay and are essential to the excitation mechanism.

With regard to the above conceptual problems of Weaver's time delay model, our approach is to look for the time delays which can explain self-sustaining oscillations in the viscous part of the flow with Navier-Stokes equations, which, in the vicinity of the cylinder, reduces to the unsteady boundary layer equation. Instead of using the quasi-steady Bernoulli equation to look for time delays, we look for the action of the time delay on the fluid through the aerodynamic lift due to the shifts in boundary layer separation. From the viewpoint of fluid dynamics, when the flow is across the cylinder, there is a thin boundary layer near the cylinder which will be separated at certain locations on the cylinder (flow separation). The separated flow forms unsteady wakes downstream. When the cylinder is oscillating in the flow, the oscillation will cause a change in the boundary layer near the cylinder, which will affect the separation point and the separated flow. Therefore oscillation changes the separated flow, but the response of separated flow to oscillation is not immediate, because of the time delay (phase lag) between the oscillation and separated flow (wake) due to the delayed response of the boundary layer to the changed flow conditions. As flow separation is caused by boundary layer development, time delay is contributed to the boundary layer development, it is possible to predict the time delay by solving the unsteady boundary layer development.

In this study, an attempt is made to understand the physical mechanism of time delay and develop a theoretical model for time delay based on fundamental fluid dynamics theory. Based on theoretical study, an experimental study has been done too. This study attempts to improve the physical description of time delay, to give physical insight into the fluid mechanics, and to develop a theoretical method to estimate the time delay.

CHAPTER III

APPROACH FOR A SINGLE CYLINDER

3.1 The Description of the Flow Field Around the Cylinder

The flow field around a cylinder in a cylinder array is very complex. It can be simplified by dividing it into two regions: the thin region near the cylinder surface (boundary layer), where viscosity effects are important; and the far region, where the flow is assumed to be inviscid. The pressure gradient is impressed upon the boundary layer from the far region. According to boundary layer theory, the pressure gradient in the y direction is negligible, so the pressure gradient will be the same for both boundary layer and outer layer at a certain x location. In the far region, potential flow theory is applied. Across the interface between the two regions, velocity (and therefore streamwise pressure gradient) are then matched, so that the two regions are related by the pressure gradient of the far region flow.

The analyses of the two regions are linked: the pressure field imposed by the far region flow controls the development of the boundary layer; for example, an adverse streamwise pressure gradient ultimately leads to flow separation. Conversely, the location of the separation point affects the far region flow and downstream flow.

3.2 The Description of Time Delay

As stated by Lever and Weaver (1986a) and Price and Paidoussis (1992), the effects of cylinder motion may not be felt instantaneously throughout the cylinder array; there is a delay between a flexible cylinder's motion and the resulting fluid disturbances, we call this delay a time delay.

In a cylinder array, when a cylinder is oscillating, the forces acting on the cylinder are unsteaddary layer will be unsteady too. Before the fluid-elastic instability occurs, the oscillation amplitude is very small compared to the cylinder's diameter D, with nondimensional cylinder oscillation velocity $\varepsilon = \overline{A}\,\overline{\omega} \leq 0.05$. It is possible to start the analysis with the solution for a cylinder at rest, impose an oscillatory perturbation, as long as the acoustic wave length of the perturbation is large compared to the diameter of the cylinder, that is, c/f >> D, where c is the speed of sound in the fluid; f is the oscillating frequency, and D is the diameter of cylinder. The analysis is identical for a cylinder oscillating in a mean flow.

When a cylinder is oscillating in the flow, the consequent changes in the free stream velocity will cause the movement of the upstream stagnation point. If the flow velocity is everywhere low compared to the speed of sound in the fluid, the changes of the pressure field can be assumed to be instantaneous; but the boundary layer on the cylinder will take time to respond

The separation point of a boundary layer in the steady flow occurs where the product of the boundary layer thickness and the (adverse) pressure gradient is equal to some value that depends on Reynolds number, surface roughness and the free stream turbulence et al. Although the pressure gradient will respond to the oscillation immediately, the boundary thickness will take time to grow. If the cylinder is moving downward, then the boundary layer on the cylinder surface will thicken quickly and the separation point will move to upstream; on the other hand, if the cylinder is moving upward, the boundary thickness on the cylinder surface will decrease, causing the separation point to move downstream. After a certain time Δt the boundary layer thickness will develop completely, with the separation point returning to its equilibrium position as shown in Figure 1. The behavior on the other side of the cylinder is opposite. In the words, the boundary layer profile at the stagnation point and separation point is always out of phase or time delay at any instant of time. The movements of the separation

point will affect pressure fluctuation and lift and drag force fluctuation, therefore time delay will also affect the fluid forces on the cylinder. Time delay causes the fluid elastic instability to happen, and if the cylinder is rigid (no oscillation) there will be no time delay, which explains why the fluid elastic instability will not occur if all the cylinders are rigid in the cylinder array.

3.3 The Range of Interested Non-dimensional Circular Frequency

It is well known that the vortex shedding from a cylinder occurs when

$$\frac{fD}{U_\infty} = 0.2$$

Fluid elastic instability usually happens (Prettigrew et al., 1991) when

$$4 < \frac{U_\infty}{fD} < 100$$

Defining the non-dimensional circular frequency

$$\overline{\omega} = \omega \frac{R}{U_\infty} = 2\pi f \frac{R}{U_\infty} = \pi \frac{fD}{U_\infty}$$

where R is the radius of the cylinder.

For vortex shedding

$$\overline{\omega} = 0.2\pi$$

and for fluid elastic instability

$$0.01\pi < \overline{\omega} < 0.25\pi$$

As the time delay is most important for fluid elastic instability, here we will concentrate our study on the non-dimensional circular frequency range

$$0.01\pi < \overline{\omega} < 0.40\pi$$

3.4 The Mathematical Model of Time Delay

Considering the flow over a curved body shape as shown in Fig. 2, where the boundary layer thickness is small compared to the wall radius of curvature, so the

equations for a Cartesian system are also valid for general curved-wall flows. The x coordinate can be taken in the direction of the cylinder surface, the y coordinate can be measured at right angles to it. Thus the coordinate consists of curves which are parallel to the surface of the cylinder and of straight lines perpendicular to them, the corresponding velocity components are denoted by u and v, respectively.

As we are only interested in the global properties of the boundary layer, it is convenient to use an integral representation of the boundary layer. Here we use the momentum-integral boundary layer equation (Schlichting, 1979):

$$\frac{\partial(U\delta_1)}{\partial t}+\frac{\partial(U^2\delta_2)}{\partial x}+U\delta_1\frac{\partial U}{\partial x}=\frac{\tau_0}{\rho} \qquad (1)$$

Where U=U(x,t) is the flow velocity at the outer edge of the boundary layer;

$\delta_1=\int_0^\infty \frac{(U-u)}{U}dy$ is the displacement thickness of the boundary layer; u is the flow velocity in the boundary layer; $\delta_2=\int_0^\infty \frac{(U-u)u}{U^2}dy$ is the momentum thickness of the boundary layer; τ_0 is the shear stress on the cylinder surface, and ρ is the density of the fluid.

For generality, we define dimensionless variables as follows:

$$\overline{U}=\frac{U}{U_\infty}$$

$$\overline{u}=\frac{u}{U_\infty}$$

$$\overline{x}=\frac{x}{R}$$

$$\overline{y}=\frac{y\sqrt{\mathrm{Re}}}{R}$$

$$\bar{t} = t\frac{U_\infty}{R}$$

$$\bar{\omega} = \omega\frac{R}{U_\infty}$$

$$c_f = \frac{\tau_0\sqrt{\mathrm{Re}}}{\rho U_\infty^2}$$

Where R is the radius of the cylinder, Re is the radius Reynolds number $\mathrm{Re} = \frac{\mathrm{RU}_\infty\rho}{\mu}$ and c_f is the skin friction factor of the cylinder.

By the definition of displacement and momentum thickness, we can find the corresponding dimensionless thicknesses are as follows:

$$\bar{\delta}_1 = \frac{\sqrt{\mathrm{Re}}}{R}\delta_1$$

$$\bar{\delta}_2 = \frac{\sqrt{\mathrm{Re}}}{R}\delta_2$$

Substituting all the dimensionless variables into equation (1), we obtain the dimensionless form of the momentum integral equation:

$$\frac{\partial(\bar{U}\bar{\delta}_1)}{\partial\bar{t}} + \frac{\partial(\bar{U}^2\bar{\delta}_2)}{\partial\bar{x}} + \bar{U}\bar{\delta}_1\frac{\partial\bar{U}}{\partial\bar{x}} = c_f \qquad (2)$$

To simplify the above equation, it is convenient to link together $\bar{\delta}_1$ and $\bar{\delta}_2$ through a shape factor H,

$$H = \frac{\bar{\delta}_1}{\bar{\delta}_2} \qquad (3)$$

Substitution of H into equation (2) gives:

$$H(\overline{U}\frac{\partial\overline{\delta}_2}{\partial\overline{t}}+\overline{\delta}_2\frac{\partial\overline{U}}{\partial\overline{t}})+\overline{\delta}_2(H+2)\overline{U}\frac{\partial\overline{U}}{\partial\overline{x}}+\overline{U}^2\frac{\partial\overline{\delta}_2}{\partial\overline{x}}=c_f \qquad (4)$$

The equation (4), the governing equation of the boundary layer, is a time-dependent, non-linear partial differential equation, which can be solved only by either approximate methods or numerical methods. Here we will use a numerical method.

To attempt to solve equation (4) numerically, firstly, we should know H, $\overline{U}$ and c_f, which are very different for different geometric configurations, flow conditions and oscillation directions etc.. These parameters are different for a single cylinder with transverse oscillation or streamwise oscillation and they are also different for a single cylinder and a cylinder array. Next we are going to discuss how to determine these parameters for a single cylinder with transverse oscillation and a single cylinder with streamwise oscillation respectively.

3.5. The Determination of $\overline{U}$, H and c_f

3.5.1 Outer region velocity $\overline{U}(x,t)$

(i). Transverse oscillation of a single cylinder

Outside the boundary layer which is adjacent to a solid boundary, the fluid may be considered inviscid and the methods of potential flow are applicable. This assumption is valid not only for steady flow but also for unsteady flow as the flow outside the boundary layer can still be assumed inviscid for unsteady flow. In other words, when a cylinder is oscillating transversely in uniform flow, the flow field around the cylinder can still be divided into two regions: the thin region near the cylinder surface (boundary layer), where the viscosity effects are important, and the far region, where the flow is assumed to be inviscid. The pressure gradient is impressed upon the boundary layer from the far region. So in the far region the inviscid flow theory or potential flow theory can be applied.

In a two dimensional unsteady potential flow, the momentum equations are Euler equations as follows:

$$X-\frac{1}{\rho}\frac{\partial P}{\partial x}=u\frac{\partial u}{\partial x}+v\frac{\partial u}{\partial y}+\frac{\partial u}{\partial t} \tag{5a}$$

$$Y-\frac{1}{\rho}\frac{\partial P}{\partial y}=u\frac{\partial v}{\partial x}+v\frac{\partial v}{\partial y}+\frac{\partial v}{\partial t} \tag{5b}$$

The continuity equation is:

$$\frac{\partial \rho}{\partial t}+\frac{\partial(\rho u)}{\partial x}+\frac{\partial(\rho v)}{\partial y}=0 \tag{6}$$

If the flow is incompressible, then ρ is constant, and equation (6) reduces to the kinematic expression:

$$\frac{\partial u}{\partial x}+\frac{\partial v}{\partial y}=0 \tag{7}$$

When the flow is inviscid or potential, it is irrotational flow; mathematically, there exists a scalar function or potential function $\phi(x,y,t)$ which serves to describe completely a particular set of conditions in space and time. Although the potential is a scalar quantity, a vector function called its gradient can be derived from a potential function by partial differentiation. For a velocity potential, the positive gradient of the potential is called the velocity of flow:

$$u=\frac{\partial \phi(x,y,t)}{\partial x} \tag{8a}$$

$$v=\frac{\partial \phi(x,y,t)}{\partial y} \tag{8b}$$

If the fluid is assumed to be incompressible, then substitution of the velocity components from Eqs. (8) into the equation of continuity leads to what is known as the Laplace equation:

$$\frac{\partial^2 \phi}{\partial x^2}+\frac{\partial^2 \phi}{\partial y^2}=0 \tag{9a}$$

$$\nabla^2\phi = 0 \tag{9b}$$

Hence, its solution would be an expression for ϕ, the velocity potential, as a function of the coordinates and the time. With the known velocity potential satisfying the boundary conditions, the velocity field may be found from the derivatives of the velocity potential [Eqs. (8)]. The pressure distribution throughout the fluid may then be obtained from the appropriate form of Euler's equation, which will be discussed from next section in detail.

As the Laplace equation is linear, if ϕ_1 and ϕ_2 satisfy the Laplace equation, their sum will also be a solution as long as the boundary conditions after superposition are the same as the given boundary conditions.

For the unsteady flow, as the flow is incompressible the Laplace equation is still satisfied and the superposition method is still valid. The only difference is the boundary conditions are dependent on the time. If the velocity field is found, the pressure field could be obtained from an unsteady form of the Euler's equation.

From the above discussion, we can find the outer layer potential flow when a cylinder is oscillating in the transverse direction to the mean flow: If the coordinates are fixed on the cylinder, the outer layer potential flow will be the superposition of steady uniform flow U_∞ and unsteady flow $A\omega\cos\omega t$ which is caused by the perturbation velocity component.

For given coordinates, the flow velocity caused by U_∞ will be

$$U_1(x,t) = 2U_\infty \sin x \tag{10}$$

From the unsteady flow component $A\omega\cos\omega t$

$$U_2(x,t) = 2A\omega\cos\omega t \sin(x+\frac{\pi}{2}) \tag{11}$$

So the outer potential flow velocity is the sum of $U_1(x,t)$ and $U_2(x,t)$. That is,

$$U(x,t) = U_1(x,t) + U_2(x,t) \tag{12a}$$

$$U(x,t) = 2U_\infty \sin x + 2A\omega\cos\omega t\cos x \tag{12b}$$

$$\frac{U(x,t)}{U_\infty} = 2(\sin x + \frac{A\omega}{U_\infty}\cos\omega t \cos x) \qquad (12c)$$

Eq.(12) can be expressed in the following dimensionless form:

$$\bar{U}(\bar{x},\bar{t}) = 2(\sin\bar{x} + \varepsilon\cos\bar{\omega}\ \bar{t}\cos\bar{x}) \qquad (13a)$$

Where

$$\bar{A} = \frac{A}{R}$$

$$\bar{\omega} = \omega\frac{R}{U_\infty}$$

$$\varepsilon = \bar{A}\,\bar{\omega}$$

$$\bar{x} = \frac{x}{R}$$

$$\bar{U}(x,t) = \frac{U(x,t)}{U_\infty}$$

$$\bar{t} = t\frac{U_\infty}{R}$$

These parameters are non-dimensional amplitude, circular frequency, velocity perturbation, distance, outer layer velocity and time, respectively.

(ii). Streamwise oscillation of a single cylinder

For streamwise oscillation, similarly using the superposition method, the outer flow velocity for streamwise oscillation is:

$$\bar{U}(\bar{x},\bar{t}) = 2\sin\bar{x}(1+\varepsilon\cos\bar{\omega}\ \bar{t}) \qquad (13b)$$

3.5.2. Shape factor H

As we mentioned before, the shape factor is a function of x for the cylinder, which has different values for different locations in boundary layer (Thwaites, 1949): Following the work by Thwaites, to find H and steady flow skin-friction factor c_f at first we need to calculate λ for a specific $\bar{x}$, where λ is a parameter as follows:

$$\lambda = \bar{\delta}_2^2 \frac{d\bar{U}}{d\bar{x}} \tag{14}$$

$\bar{\delta}_2^2$ can be calculated by the following equation for given $\bar{x}$ as suggested by Thwaites:

$$\bar{\delta}_2^2 = \frac{0.45}{\bar{U}^6} \int_0^{\bar{x}} \bar{U}^5 d\bar{x} \tag{15}$$

where $\bar{U}$ is the outer layer flow velocity, which is equal to $\bar{U} = 2\sin(\bar{x})$

so

$$\bar{\delta}_2^2 = \frac{0.45}{2\sin(\bar{x})^6} * \left(\frac{8}{15} - \cos(\bar{x}) + \frac{2}{3}\cos^3(\bar{x}) - 0.2\cos^5(\bar{x})\right) \tag{16}$$

For specific $\bar{x}$, $\bar{\delta}_2^2|_{\bar{x}} = \frac{0.45}{\bar{U}^6|_{\bar{x}}} \int_0^{\bar{x}} \bar{U}^5 d\bar{x}'$, then $\lambda|_{\bar{x}} = \bar{\delta}_2^2|_{\bar{x}} \left.\frac{d\bar{U}}{d\bar{x}}\right|_{\bar{x}}$

where

$$\left.\frac{d\bar{U}}{d\bar{x}}\right|_{\bar{x}} = 2\cos(\bar{x}) \tag{17}$$

But a singularity occurs at the stagnation point, where $\bar{x} = 0.0$. In order to get a finite value for $\bar{\delta}_2^2$, L'Hospital's rule has to be used:

$$\bar{\delta}_2^2|_{\bar{x}=0} = \frac{0.45 \frac{d}{d\bar{x}} \left(\int_0^{\bar{x}} \bar{U}^5 d\bar{x}' \right)}{\frac{d}{d\bar{x}} \left(\bar{U}^6 \right)}$$

$$\bar{\delta}_2^2|_{\bar{x}=0} = \frac{0.45}{6 \left.\frac{d\bar{U}}{d\bar{x}}\right|_{\bar{x}=0}} = 0.0375$$

so

$$\lambda|_{\bar{x}=0} = \bar{\delta}_2^2 \left.\frac{d\bar{U}}{d\bar{x}}\right|_{\bar{x}=0} = 0.0826 \tag{18}$$

Once the δ_2^2 and λ have been obtained from given outer layer velocity $\overline{U}(x)$, the other parameters H and c_f can be calculated through shear correlation $S(\lambda)=\frac{c_f\overline{\delta}_2}{\overline{U}}$ and shape factor $H(\lambda)=\frac{\overline{\delta}_1}{\overline{\delta}_2}$. Here, we use the following correlations (Fei, et al. 1989):

for $0 \le \lambda \le 0$.

$$H = 2.61 - 3.75\lambda + 5.24\lambda^2 \tag{19a}$$

$$S(\lambda) = 0.22 + 1.57\lambda - 1.82\lambda^2 \tag{19b}$$

$$\overline{c}_f = \frac{\overline{U}}{\overline{\delta}_2}(0.22 + 1.57\lambda - 1.82\lambda^2) \tag{19c}$$

for $-0.1 < \lambda < 0$

$$H = \frac{0.0731}{0.14 + \lambda} + 2.088 \tag{20a}$$

$$S(\lambda) = 0.22 + 1.402\lambda + \frac{0.018\lambda}{0.107 + \lambda} \tag{20b}$$

$$\overline{c}_f = \frac{\overline{U}}{\overline{\delta}_2}(0.22 + 1.402\lambda + \frac{0.018\lambda}{0.107 + \lambda}) \tag{20c}$$

It should be noticed that the H and $\overline{c}_f$ from Eqs. (19) and (20) are different for steady flow and unsteady flow, which depends on what velocity distribution is. From steady flow the H will be that of steady flow. Similarly, from unsteady flow the H will be that of unsteady flow.

3.5.3 The skin-friction factor c_f

(i) Transverse oscillation of a single cylinder

When a cylinder is oscillating transversely in the uniform flow, the skin-friction factor includes two parts: that is, the oscillating component c_{fu} and the steady component c_{fs};

$$c_f = c_{fs} + c_{fu} \tag{21}$$

According to Glauert (1956), the oscillating component of the skin-friction can be obtained as follows:

$$\frac{\tau}{\rho\beta^2} = (\frac{cv}{\beta^2})^{1/2}\{\chi'(0) - A\}e^{i\omega t} \tag{22}$$

where $c = 3.6\frac{U_\infty}{D}$, β is transverse velocity component, $\beta = A\omega$;

$$\chi'(0) - A = 0.4213\frac{i\omega}{c} + O(\frac{\omega^2}{c^2})$$

so

$$\frac{\tau}{\rho\beta^2} = (\frac{cv}{\beta^2})^{1/2} 0.4213\frac{i\omega}{c}e^{i\omega t} \tag{23}$$

To rearrange and simplify the above equation, we have:

$$\frac{\tau\sqrt{Re}}{\rho U_\infty^2} = 0.3140\frac{\omega^2 R^2}{U_\infty^2}\frac{A}{R}ie^{i\omega t} \tag{24}$$

In the dimensionless form, the Eq.(24) becomes:

$$c_{fu} = 0.3140\overline{A}\,\overline{\omega}^2 ie^{i\overline{\omega}\,\overline{t}} \tag{25}$$

As there is meaning only for the real part, the real part of c_{fu} is :

$$c_{fu} = -0.3140\overline{A}\,\overline{\omega}^2 \sin\overline{\omega}\,\overline{t} \tag{26}$$

Finally, the skin-friction factor c_f for a cylinder with transverse oscillation will be:

$$c_f = c_{fs} - 0.3140\overline{A}\,\overline{\omega}^2 \sin\overline{\omega}\,\overline{t} \tag{27}$$

Where: c_{fs} is the skin-friction factor for steady flow, which can be obtained from Eqs. (19) and (20).

(ii) Streamwise oscillation of a single cylinder

For streamwise oscillation, the skin friction factor c_f is different from that for transverse oscillation. Lighthill (1954) studied the unsteady incompressible boundary layer over a fixed cylinder of arbitrary cross-section when the free stream is fluctuating with small amplitude about a steady mean flow. For incompressible flow, this problem is mathematically the same as if the cylinder were oscillating with the same fluctuating velocity in a uniform flow. Therefore we can use the approximate skin friction factor c_f that he obtained.

for $\bar{\omega} < 10$, then $\tau = \tau_w + \varepsilon e^{i\omega t}(\frac{3}{2} + \frac{i}{2}\omega U \rho \delta_1)$

for $\bar{\omega} > 10$ $\tau = \tau_w + \varepsilon \mu U \left(\frac{\omega}{\nu}\right)^{1/2} e^{i(\omega t + \frac{\pi}{4})}$

where τ_w is the shear stress of steady boundary layer of the cylinder, L is the characteristic length, for cylinder L=2R.

In the dimensionless form, the above two equations are as follows:

$$c_f = c_{fs}(1 + \frac{3\varepsilon e^{i\bar{\omega}\bar{t}}}{2}) + \frac{\varepsilon}{2} e^{i\bar{\omega}\bar{t}} i\bar{\omega}\,\bar{U}(\bar{x}) H\bar{\delta}_2,$$

and

$c_f = c_{fs} + \varepsilon \bar{U}(\bar{x})\sqrt{\bar{\omega}} e^{i(\bar{\omega}\bar{t} + \frac{\pi}{4})}$ respectively.

There is meaning only to the real part, which is:

For $\bar{\omega} < 10$

$$c_f = c_{fs}(1 + \frac{3\varepsilon}{2}\cos\bar{\omega}\bar{t}) - \frac{\varepsilon}{2}\bar{\omega}\bar{U}(\bar{x}) H\bar{\delta}_2 \sin\bar{\omega}\bar{t} \qquad (28a)$$

For $\bar{\omega} > 10$

$$c_f = c_{fs} + \varepsilon \bar{U}(x)\sqrt{\bar{\omega}}\cos(\bar{\omega}\bar{t} + \frac{\pi}{4}) \qquad (28b)$$

Now we are able to estimate $\overline{U}(\overline{x},\overline{t}), H(\overline{x})$ and c_f. So we are able to solve equation (4) numerically to find the time delay of a single cylinder for both transverse and streamwise oscillations.

3.6 The Numerical Scheme to Solve Time Delay

To solve equation (4) a two dimensional finite difference scheme is used. Under the discretization, the point $(\overline{x},\overline{t})$ is represented by $(i\Delta\overline{x}, j\Delta\overline{t})$, where $\Delta\overline{x}$ is the grid size, and $\Delta\overline{t}$ is the time step.

Equation (4) was arranged as follows:

$$\frac{\partial\overline{\delta}_2}{\partial\overline{t}}+\frac{\overline{U}}{H}\frac{\partial\overline{\delta}_2}{\partial\overline{x}}=\frac{c_f}{H\overline{U}}-\frac{\overline{\delta}_2}{\overline{U}}\frac{\partial\overline{U}}{\partial\overline{t}}-\frac{\overline{\delta}_2(H+2)}{H}\frac{\partial\overline{U}}{\partial\overline{x}} \tag{29}$$

To discretize equation (29), the spatial derivative is represented by upwind finite difference:

$$\frac{\partial\overline{\delta}_2}{\partial\overline{x}}=\frac{\overline{\delta}_{2i}^{j}-\overline{\delta}_{2(i-1)}^{j}}{\Delta\overline{x}} \tag{30}$$

The temporal derivative is represented as follows:

$$\frac{\partial\overline{\delta}_2}{\partial\overline{t}}=\frac{\overline{\delta}_{2i}^{j+1}-\overline{\delta}_{2i}^{j}}{\Delta\overline{t}} \tag{31}$$

So the finite difference form of the equation (29) becomes:

$$\overline{\delta}_{2i}^{j+1}=\frac{\overline{U}\Delta\overline{t}}{H\Delta\overline{x}}\overline{\delta}_{2(i-1)}^{j}+\overline{\delta}_{2i}^{j}\left(1-\frac{\overline{U}\Delta\overline{t}}{H\Delta\overline{x}}-\frac{\Delta\overline{t}}{\overline{U}}\frac{\partial\overline{U}}{\partial\overline{t}}-\frac{(H+2)\Delta\overline{t}}{H}\frac{\partial\overline{U}}{\partial\overline{x}}\right)+\frac{c_f\Delta\overline{t}}{H\overline{U}} \tag{32}$$

where $\frac{\overline{U}\Delta\overline{t}}{H\Delta\overline{x}}$, $\frac{c_f\Delta\overline{t}}{H\overline{U}}$ and $-\frac{\overline{U}\Delta\overline{t}}{H\Delta\overline{x}}-\frac{\Delta\overline{t}}{\overline{U}}\frac{\partial\overline{U}}{\partial\overline{t}}-\frac{(H+2)\Delta\overline{t}}{H}\frac{\partial\overline{U}}{\partial\overline{x}}$ are evaluated at the node i and j time step.

To solve Eq. (32), the initial and boundary conditions must be assigned. The initial condition is: $\overline{\delta}_2$ is zero throughout the computational domain from $\overline{x}=0.0$ to $\overline{x}=1.8$ rad, that is, $\overline{\delta}_2(x,0)=0.0$.

From the results of boundary layer of steady flow (Schlichting, 1979), the first derivative of $\overline{\delta}_2$ with respect to $\overline{x}$ is zero, therefore the boundary condition is :

$$\left.\frac{\partial \overline{\delta}_2}{\partial \overline{x}}\right|_{\overline{x}=0.0} = 0.0 \tag{33}$$

that is

$$\frac{\overline{\delta}_{2i}^{j} - \overline{\delta}_{2(i-1)}^{j}}{\Delta \overline{x}} = 0.0 \tag{34}$$

hence $\overline{\delta}_{22}^{j} = \overline{\delta}_{21}^{j}$ for every time step. Once we have initial and boundary conditions, equation (4) can be solved numerically.

CHAPTER IV

APPROACH FOR A CYLINDER ARRAY

In the previous studies, based on our understanding of fundamental fluid mechanics, the theoretical model of time delay for a single cylinder with streamwise or transverse oscillation has been developed. The studies give physical insight into the time delay, which is the basis of attacking time delay in cylinder rows and cylinder arrays. The time delays for cylinder rows and cylinder arrays are most important as fluid-elastic instability usually happens in the cylinder array. It should be stated that the flow field around the cylinder array is much more complicated than that of a single cylinder. Our understanding of the flow field around cylinder arrays subjected to cross-flow is important in order to understand the fluid dynamics between the cylinder array and the flow, and to identify and quantify the important system parameters. Unfortunately, our physical understanding of the flow field in cylinder arrays is rather poor due to the complex flow pattern in interstitial and downstream flow, which causes difficulties in solving the time delays with respect to a cylinder array. Therefore several simplifying assumptions have been made about the flow field.

4.1 The Description of Fluid-elastic Instability in Cylinder Arrays

During the last 20 years, many papers have been published concerning the fluid-elastic instability in a cylinder array (Blevins, 1990; Chen, 1984, 1991; Moretti, 1986,1993; Paidousis, 1987 and Weaver et al., 1987). From these studies, some important features can be summarized as follows:

(1). The fluid-elastic instability is similar to flutter and is related to the dynamic response of the cylinder and fluid-structure interactions;

(2). There are two distinct mechanisms which can lead to fluid-elastic instability: (i) a negative fluid-damping mechanism which occurs at lower values of mass damping parameter ($\frac{m\delta}{\rho d^2}$), and which happens even if there is only one flexible supported cylinder in a cylinder array; (ii) a fluid-stiffness controlled type of mechanism resulting from the fluid coupling between the neighboring cylinders, which usually occurs at high values of the mass damping parameter ($\frac{m\delta}{\rho d^2} > 200$);

(3). The geometry of the cylinder array affects the stability boundary. (Soper, 1983);

(4). The viscosity of the fluid has little effect on the critical velocity of fluid-elastic instability, as verified by experimental results for different fluids or for the same fluid at different temperature.

4.2 Assumptions

As the flow pattern around the cylinder rows or cylinder arrays is much more complicated than that around a single cylinder, the determination of time delays is more difficult. To apply the developed theoretical model for a single cylinder to cylinder rows or cylinder arrays, some simple assumptions are introduced as follows:

(1). The boundary layer on the surface of the cylinder in the cylinder rows or cylinder arrays is laminar, so the correlations Eqs.(19) & (20) of shape factor H for a laminar boundary layer can still be applied.

(2). As the flow pattern in the cylinder rows or cylinder arrays is different from that of single cylinder, the skin-friction factor c_f will be different too, but as the boundary layer is still laminar, the correlation $S(\lambda) = \frac{c_f \overline{\delta}_2}{U}$ is still valid for the oscillation of the cylinder in the cylinder array. Once we know the outer layer velocity distribution, it is possible to calculate the skin-friction factor c_f from the above correlation.

(3). The fluid-elastic instability is assumed to occur only in the transverse direction, which has been assumed by many researchers. (Chen et al., 1984; Prettigrew and Taylor, 1991)

With the above assumptions, we still cannot determine the time delays for a cylinder in cylinder rows or cylinder arrays without knowing the outer layer velocity distribution around a cylinder, which will be addressed in detail below.

4.3 The Pressure Distribution Around a Cylinder in a Cylinder Array

Due to the complexity of the flow field in a cylinder array, and the difficulty of experimentation, there is no complete velocity measurement data or theoretical analysis concerning the cylinder in the cylinder array. But there are some papers investigating the pressure distribution on the surface of the single cylinder in a jet-like flow path surrounding by walls. (Okamoto, et al., 1975; Bearman et al., 1978; Muraoka et al., 1984). From the boundary layer theory, the pressure gradient in the y direction is nearly zero, or the transverse pressure gradient is negligible; that is, $\frac{\partial p}{\partial y} \approx 0,\ p = p(\bar{x})\ only.$ Since the pressure gradient will be the same for both the boundary layer and outer layer at the same location, it is possible to convert the experimental pressure distribution around a cylinder to the outer layer velocity distribution through the Navier Stokes equations.

(1). The pressure distribution on the surface of the single cylinder in a jet-like flow path

Okamoto et al. (1975) studied the pressure distribution on the surface of the single cylinder in a jet-like flow path surrounded by parallel walls. The measurement results obtained are shown in Figure 3, where $c_p(\bar{x})$ is the non-dimensional pressure distribution or pressure coefficient:

$$c_p(\bar{x}) = \frac{p(\bar{x}) - p_\infty}{1/2\rho U_\infty^2} \tag{35}$$

(2). The pressure distribution on the surface of a single cylinder in a cylinder array

From the studies of Nishikawa et al. (1977) and Kobayashi (1976), it was found that the pressure distribution in Figure 3 might be a typical pattern even in a cylinder array. So the non-dimensional pressure distribution $c_p(\bar{x})$ on the surface of a single cylinder in the cylinder array is assumed as shown in Figure 4, where $\bar{x}_s$ is the separation point; c_{po} is the variation range of the pressure; μ is the ratio of pressure decrease at separation point; $\bar{x}_p$ is the point where minimum pressure occurs.

According to Nakamura et al. (1992), the non-dimensional pressure can be expressed as in the following equation:

$$c_p(\bar{x}) = 1.0 - c_{po}\sin^2\left(\frac{\pi}{2\bar{x}_p}\bar{x}\right) \quad (0 \le \bar{x} \le \bar{x}_s) \tag{36a}$$

$$c_p(\bar{x}) = 1 - (1-\mu)c_{po} \qquad (\bar{x} > \bar{x}_s) \tag{36b}$$

where $\bar{x}_p = \dfrac{\pi \bar{x}_s}{2\sin^{-1}(\sqrt{1-\mu})}$, c_{po}, the variation range of the pressure, is a function of cylinder displacement y in the transverse direction and the pitch-to-diameter ratio $\dfrac{T}{D}$ in a cylinder array. Based on the measurement data, they recommended:

$$c_{po}(y,\frac{T}{D}) = 277.6(\frac{y+D}{T} - 0.25)^4 + 3.1 \tag{37}$$

where T is the pitch of a cylinder array.

Eq. (36) shows that the pressure distribution is also a function of the separation point $\bar{x}_s$. Although the separation point $\bar{x}_s$. is a function of the displacement of cylinder y, pitch-to-diameter ratio $\frac{T}{D}$ and oscillation velocity $\frac{\partial y}{\partial t}$, the separation point is not what we are most interested in, and the present study assumes that $\bar{x}_s$ is a constant to make the problem simple. From Hara's measurement data for a cylinder array (Hara, 1989), the steady separation point $\bar{x}_s$ is about 130^o away from stagnation point (2.27 rad) based on the average value of test data. As the present study is more interested in time delay instead of separation point, $\bar{x}_s$ may be fixed at 130^o (2.27 rad). From Tomonichi et al. (1992), the ratio of pressure decrease is $\mu = 0.1$. So $c_p(\bar{x},\bar{t})$ in the Eq. (36) can be decided completely as follows:

$$c_p(\bar{x}) = 1.0 - \left[277.6\left(\frac{y+D}{T} - 0.25 \right)^4 + 3.1 \right] \sin^2\left(\frac{\pi}{2\bar{x}_p} \bar{x} \right) \tag{38}$$

In our developed theoretical model of time delay for a single cylinder, we need to determine the outer layer flow velocity distribution $\bar{U}(\bar{x},\bar{t})$ of a cylinder array instead of $c_p(\bar{x},\bar{t})$, so it is necessary to convert $c_p(\bar{x},\bar{t})$ into $\bar{U}(\bar{x},\bar{t})$ by using the Navier-Stokes equations.

(3). The determination of $\bar{U}(\bar{x},\bar{t})$ from $c_p(\bar{x},\bar{t})$

For the non-inertial coordinates shown in Figure 1, as the boundary thickness is small compared to the diameter of cylinder D, in the region where is just outside the boundary layer, δ_1 can be considered as the streamline of outer-layer flow. As the

coordinate is along with the cylinder surface (streamline). In other words, $\frac{\partial^2 U}{\partial y^2}$ term is negligible. The one dimensional unsteady Navier Stokes equation can be applied in this streamline, that is:

$$\frac{\partial U}{\partial t} + U\frac{\partial U}{\partial x} = -\frac{1}{\rho}\frac{\partial p}{\partial x} + \nu\frac{\partial^2 U}{\partial x^2} \tag{39}$$

or $$\frac{\partial U}{\partial t} + U\frac{\partial U}{\partial x} - \nu\frac{\partial^2 U}{\partial x^2} = -\frac{1}{\rho}\frac{\partial p}{\partial x} \tag{40}$$

where ν is the kinematic viscosity and ρ is the density of the fluid. The non-dimensional parameters are defined as follows:

$$\bar{U} = \frac{U}{U_\infty}$$

$$\bar{t} = t\frac{U_\infty}{R} \tag{41}$$

$$\bar{x} = \frac{x}{R}$$

$$c_p = \frac{p - p_\infty}{1/2\rho U_\infty^2}$$

$$\mathrm{Re} = \frac{RU_\infty}{\nu}$$

Where c_p is the pressure coefficient, and Re is radius Reynolds number, then:

$$U = \bar{U}U_\infty$$

$$x = \bar{x}R$$

$$p = p_\infty + \frac{1}{2}\rho U_\infty^2 c_p \tag{42}$$

$$t = \bar{t}\frac{R}{U_\infty}$$

Substitution of Eqs. (42) into Eq. (40) yields the non-dimensional form of Navier-Stokes equation:

$$\frac{\partial \overline{U}}{\partial \overline{t}} + \overline{U}\frac{\partial \overline{U}}{\partial \overline{x}} - \frac{1}{\mathrm{Re}}\frac{\partial^2 \overline{U}}{\partial \overline{x}^2} = -\frac{1}{2}\frac{\partial c_p}{\partial \overline{x}} \tag{43}$$

where:

$$c_p(\overline{x}) = 1.0 - c_{po}\sin^2\left(\frac{\pi}{2\overline{x}_p}\overline{x}\right) \quad (0 \le \overline{x} \le \overline{x}_s)$$

$$\overline{x}_p = \frac{\pi \overline{x}_s}{2\sin^{-1}(\sqrt{1-\mu})}$$

$$c_{po} = c_{po}(y, \frac{T}{D}) = 277.6(\frac{y+D}{T} - 0.25)^4 + 3.$$

$$y = A\sin\omega t$$

Defining non-dimensional displacement and amplitude $\overline{y} = \frac{y}{R}$ and $\overline{A} = \frac{A}{R}$ respectively, the non-dimensional displacement is $\overline{y} = \overline{A}\sin\overline{\omega}\,\overline{t}$, and the variation range of the pressure c_{po} is:

$$c_{po} = 277.6\left[\frac{D}{T}\left(1+\frac{\overline{y}}{2}\right) - 0.25\right]^4 + 3. \tag{44}$$

So

$$c_p(\overline{x}) = 1.0 - \left\{277.6\left[\frac{D}{T}\left(1+\frac{\overline{y}}{2}\right) - 0.25\right]^4 + 3.1\right\}\sin^2\left(\frac{\pi}{2\overline{x}_p}\overline{x}\right) \tag{45}$$

For given μ=0.1 and $\overline{x}_s$,=2.27, the $\frac{\pi}{\overline{x}_p} = \frac{2\sin^{-1}(\sqrt{1-\mu})}{\overline{x}_s} = 1.10$, so

$$\frac{\partial c_p}{\partial \overline{x}} = -\frac{\pi}{2\overline{x}_p}c_{po}\sin\left(\frac{\pi}{\overline{x}_p}\overline{x}\right) = -0.55c_{po}\sin(1.10\overline{x}) \tag{46}$$

Combining Eqs. (44) and (46) gives:

$$\frac{\partial c_p}{\partial \bar{x}} = -\left\{152.68\left[\frac{D}{T}\left(1+\frac{\bar{y}}{2}\right)-0.25\right]^4 + 1.705\right\}\sin(1.10\bar{x}) \tag{47}$$

Let:

$$\frac{1}{2}\left\{152.68\left[\frac{D}{T}\left(1+\frac{\bar{y}}{2}\right)-0.25\right]^4 + 1.705\right\}\sin(1.10\bar{x}) = f(\bar{y},\frac{D}{T},\bar{x}) \tag{48}$$

hence:

$$-\frac{1}{2}\frac{\partial c_p}{\partial \bar{x}} = f(\bar{y},\frac{D}{T},\bar{x}) \tag{49}$$

The Eq. (43) becomes:

$$\frac{\partial \bar{U}}{\partial \bar{t}} + \bar{U}\frac{\partial \bar{U}}{\partial \bar{x}} - \frac{1}{\mathrm{Re}}\frac{\partial^2 \bar{U}}{\partial^2 \bar{x}} = f(\bar{y},\frac{D}{T},\bar{x}) \tag{50}$$

To solve Eq. (50), we are able to convert the pressure distribution of a cylinder array $c_p(\bar{x},\bar{t})$ into the velocity distribution $\bar{U}(\bar{x},\bar{t})$ of a cylinder array.

4.4 The Velocity Distribution of Outer-layer

(1). Initial and boundary conditions

To solve velocity distribution from equation (50), the initial and boundary conditions have to be decided first.

The initial condition for Equation (50) can be set to be the same as the potential flow around a single cylinder. That is,

$$\bar{U}(\bar{x},0) = 2\sin\bar{x} \tag{51}$$

Similar to single cylinder oscillation, the non-inertial transformation of the governing equations (50) to a reference frame that is fixed relative to the oscillating cylinder simplifies the specification of boundary conditions at the cylinder. When the cylinder is oscillating, the stagnation point varies with time. As it is assumed that the oscillation amplitude is very small compared to the cylinder diameter D, the variation of

stagnation point is very small; and the boundary layer develops from $\bar{x} = 0.0$, so a no slip boundary condition for outer layer velocity distribution at $\bar{x} = 0.0$ can be applied, that is:

$$\bar{U}(0,t) = 0.0 \tag{52}$$

If the right side boundary is chosen near the separation point, as the pressure gradient tends to be zero after separation as shown in Figure 4, the right boundary condition can be set to zero velocity gradient, that is,

$$\left.\frac{\partial \bar{U}}{\partial \bar{x}}\right|_{\bar{x}=\bar{x}_r} = 0.0 \tag{53}$$

(2). The solution technique and finite difference formulation

The governing equation for velocity distribution is:

$$\frac{\partial \bar{U}}{\partial \bar{t}} + \bar{U}\frac{\partial \bar{U}}{\partial \bar{x}} - \frac{1}{Re}\frac{\partial^2 \bar{U}}{\partial^2 \bar{x}} = f(\bar{y}, \frac{D}{T}, \bar{x}) \tag{50}$$

Eq. (50) contains a convection term, a diffusion term $\frac{1}{\mathrm{Re}}\frac{\partial^2 \bar{U}}{\partial^2 \bar{x}^2}$ and a source term $f(\frac{D}{T}, \bar{y}, t)$. The above equation is rearranged in the following general form:

$$\frac{\partial \bar{U}}{\partial \bar{t}} + \frac{\partial}{\partial \bar{x}}\left(\frac{1}{2}\overline{UU}\right) - \frac{\partial}{\partial \bar{x}}\left(\frac{1}{\mathrm{Re}}\frac{\partial \bar{U}}{\partial \bar{x}}\right) = f(\bar{y}, \frac{D}{T}, \bar{x}) \tag{54}$$

The typical grid point cluster for the one dimensional problem is shown below:

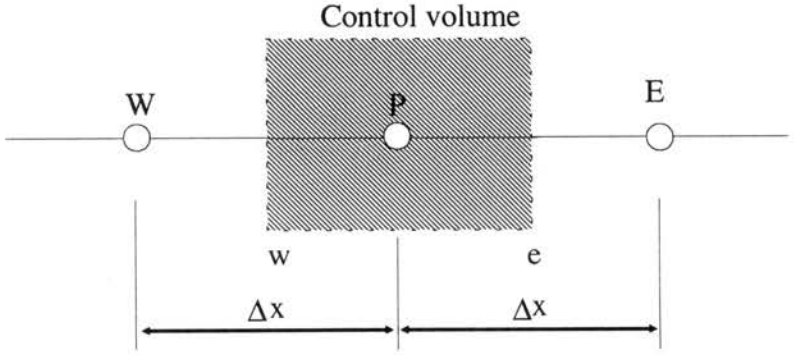

The finite difference equation can be obtained by integrating Eq. (50) over the

control volume and expressing the result in terms of neighboring point values. The value of the convection and diffusion terms is the surface integral of the convective and diffusive flux, resulting in:

$$\left[U_P^{j+1}-\overline{U}_P^j\right]\Delta\bar{x}+\Delta\bar{t}\left[\frac{1}{2}\overline{U}^j\overline{U}^j-\frac{1}{\mathrm{Re}}\frac{\partial U^j}{\partial\bar{x}}\right]_e-\Delta\bar{t}\left[\frac{1}{2}\overline{U}^j\overline{U}^j-\frac{1}{\mathrm{Re}}\frac{\partial U^j}{\partial\bar{x}}\right]_w=f\left(\frac{D}{T},\bar{y}_P,\bar{t}\right)\Delta\bar{t} \tag{55}$$

Where j refers to known values at time $\bar{t}$, while $j+1$ is the unknown values at time $\bar{t}+\Delta\bar{t}$. For the representation of the convective and diffusive terms over the control volume, a hybrid scheme is used (Patankar, 1980), which is the combination of the so-called central and upwind differences. The convection-diffusion discretization equation for the hybrid scheme is:

$$\Delta\bar{t}\left[\frac{1}{2}\overline{U}^j\overline{U}^j-\frac{1}{\mathrm{Re}}\frac{\partial U^j}{\partial\bar{x}}\right]_e-\Delta\bar{t}\left[\frac{1}{2}\overline{U}^j\overline{U}^j-\frac{1}{\mathrm{Re}}\frac{\partial U^j}{\partial\bar{x}}\right]_w=a_P\overline{U}_P^j-a_E\overline{U}_E^j-a_W\overline{U}_W^j \tag{56}$$

Where

$$\begin{aligned}
a_E&=\left[\left[-F_e,D_e-\frac{F_e}{2},0.0\right]\right]\\
a_W&=\left[\left[F_w,D_w+\frac{F_w}{2},0.0\right]\right]\\
a_P&=a_E+a_W+(F_e-F_w)
\end{aligned} \tag{57}$$

Here the symbol $\left[\left[-F_e,D_e-\frac{F_e}{2},0.0\right]\right]$ denotes the greatest of the three terms and is the same as $\left[\left[F_w,D_w+\frac{F_w}{2},0.0\right]\right]$. And $F_e=\left(\frac{1}{2}\overline{U}^j\right)_e$, $F_w=\left(\frac{1}{2}\overline{U}^j\right)_w$ indicate the strength of

the convection (or flow), $D = \dfrac{1}{\Delta\bar{x}\,\mathrm{Re}}$ is the diffusion conductance, which is a constant for uniform grid and constant Re.

Substitution of Eq. (54) into Eq.(53), the final one-dimensional discretization equation can now be written as:

$$\overline{U}_P^{j+1} = a_P' \overline{U}_P^j + a_E' \overline{U}_E^j + a_W' \overline{U}_W^j + S(P) \tag{58}$$

Where

$$a_E' = a_E \frac{\Delta\bar{t}}{\Delta\bar{x}} \tag{59a}$$

$$a_W' = a_W \frac{\Delta\bar{t}}{\Delta\bar{x}} \tag{59b}$$

$$a_P' = \left(1.0 - a_P \frac{\Delta\bar{t}}{\Delta\bar{x}}\right) \tag{59c}$$

$$S(P) = f\left(\frac{D}{T}, \bar{y}, \bar{t}\right) \tag{59d}$$

Thus Eq. (56) linking each $\overline{U}$ at a point P with its two neighboring point values, adding initial and boundary conditions, the velocity distribution can be determined for the whole computational domain.

4.5 The Shape Factor H(x,t) and Skin-friction Factor $c_f(x,t)$

In a cylinder array, as the outer layer velocity is different from that of single cylinder, it changes with locations and time, Eq. (15) becomes:

$$\bar{\delta}(x,t)_2^2 = \frac{0.45}{\left[\overline{U}(x,t)\right]^6} \int_0^{\bar{x}} \left[\overline{U}(x,t)\right]^5 d\bar{x} \tag{60}$$

Because we do not know the analytical formula of $\overline{U}(x,t)$, Eq.(60) should be evaluated by numerical integration; once we get $\bar{\delta}_2^2$, λ can be calculated by Eq.(14):

$$\lambda(x,t) = \bar{\delta}_2^2 \frac{d\bar{U}}{d\bar{x}} = \bar{\delta}_2^2 \frac{\bar{U}(i,t) - \bar{U}(i-1,t)}{\Delta x} \tag{61}$$

Finally, the shape factor H(x,t) and friction factor $c_f(x,t)$ can be obtained by Eqs.(19) and (20), that is:

For $0 \le \lambda \le 0$.

$$\begin{aligned} H(x,t) &= 2.61 - 3.75\lambda + 5.24\lambda^2 \\ S(\lambda) &= 0.22 + 1.57\lambda - 1.82\lambda^2 \\ c_f(x,t) &= \frac{\bar{U}(x,t)}{\bar{\delta}_2}(0.22 + 1.57\lambda - 1.82\lambda^2) \end{aligned} \tag{62}$$

For $-0.1 < \lambda < 0$

$$\begin{aligned} H(x,t) &= \frac{0.0731}{0.14 + \lambda} + 2.088 \\ S(\lambda) &= 0.22 + 1.402\lambda + \frac{0.018\lambda}{0.107 + \lambda} \\ c_f(x,t) &= \frac{\bar{U}(x,t)}{\bar{\delta}_2}(0.22 + 1.402\lambda + \frac{0.018\lambda}{0.107 + \lambda}) \end{aligned} \tag{63}$$

The above formulas of shape factor H and skin-friction factor c_f for a cylinder in the cylinder array are first introduced by us; and they might fill the gap where there are no formulas for these two factors in the unsteady flow of a cylinder array.

We now have got all the parameters and solution techniques that are needed for solving the time delays of a cylinder array. As the Eqs. (4) and (50) are coupled, they should be solved at the same time to get the time delay.

CHAPTER V

THEORETICAL RESULTS

5.1 The Results for a Single Cylinder with Transverse Oscillation

Using the developed theoretical model in chapters 3, the time delays of a single cylinder with transverse or streamwise oscillation are investigated. The computational domain is from $\bar{x} = 0.0$ to $\bar{x} = 1.8$, where $\bar{x} = 1.8$ is the approximated separation point that is used in developing the boundary layer equation; boundary layer equations are only valid for a thin layer which is not valid after separation occurs. The computational domain was then divided into grids of 100 intervals, so that the grid size is $\Delta\bar{x} = 0.018$. With coordinates defined as before, the velocity distribution just outside the boundary layer for transverse oscillation is: $\bar{U}(\bar{x},\bar{t}) = 2(\sin\bar{x} + \varepsilon\cos\bar{\omega}\ \bar{t}\cos\bar{x})$. The stagnation streamline is thus instantaneously directed towards $\bar{x} = \tan^{-1}(\varepsilon\cos\bar{\omega}\,\bar{t})$. As the momentum thickness is undetermined at the separation point , the first node is chosen away from but close to the stagnation point, which is $\bar{x}_0 = 0.09$ for transverse oscillation. After the numerical stability analysis the time step is chosen $\Delta\bar{t} = 0.01$ for a single cylinder but for a cylinder array $\Delta\bar{t} = 0.001$. It should be noted that the 'separation point' here is only a nominal term used to indicate the end of the computational domain.

5.1.1 The development of momentum thickness

Figure 5 shows the development of boundary layer momentum thickness with time at different locations between the stagnation and separation points, when the velocity perturbation is $\varepsilon = \bar{\omega}\bar{A} = 0.01$ and the oscillation frequency is $\bar{\omega} = 0.2\pi$. It can be found from this figure that the momentum thickness grows from zero to steady periodic, which

will take a certain time t to reach steady periodic, where t is called a time constant. And time constants are different for different locations as shown in Figure 5, which will be discussed in the next section.

5.1.2 The influence of oscillation frequency, amplitude and location on time delay

From Figure 5 we can find that the time constant increases with the increase in distance from the stagnation point. As the time constant changes for different locations, there are different time constants for different positions. As discussed in Chapter 3, the stagnation point will respond to the flow perturbation instantaneously, but the response at the other locations inside the boundary layer will take a certain time as the changes are communicated by the boundary layer development and there will be a time difference between the stagnation point and a specific location to reach steady periodic. We call this time difference a time delay. For instance, the time constants of locations $\bar{x} = 0.09$ and $\bar{x} = 1.80$ are 0.22 and 1.59 respectively as shown in the Figure 6. It should be noted that the curve of stagnation point has been shifted up in this figure so that it is easy to compare the time constant difference. So the time delay at the location $\bar{x} = 1.80$ with $\varepsilon = 0.01$ and $\bar{\omega} = 0.2\pi$ is $\tau = 1.37$ as shown in the Figure 6.

Figure 7(a-c) and Table 1 show the changes of the time constant, time delay and phase lag with the different locations and different oscillation frequencies with velocity perturbation $\varepsilon = 0.05$. From the Figure 7(a) and Table 1 it can be found that: The time constant changes with the locations. And it can also be found that the oscillation frequencies do not influence the time constant very much.

Figure 7(b) shows the time delay vs. locations at different frequencies. As Figure 7(b) is obtained by subtracting the time constant of $\bar{x} = 0.09$ from every point, this figure is similar to Figure 5(a). From this figure it is easy to see that time delays do increase

with the increase of locations, and the trend is the same as for the time constant. The oscillation frequencies do not affect the time delay.

The time delay can be also converted into the phase lag α, which is the product of time delay τ and the corresponding oscillation frequency $\overline{\omega}$. The phase lag results are shown in the Figure 5(c) and Table 1. It can be seen from the figure that phase lag increases with the increase of oscillation frequency

To investigate the effect of oscillation amplitude on the time constant, Figures 8(a-c) and Table 2 show the influences of oscillation amplitude at different locations with oscillation frequency $\omega = 0.20\pi$. From these figures it can be found that the oscillation amplitude does not affect the time delay. As the product of oscillation frequency and amplitude is the velocity perturbation, it can be concluded that the velocity perturbation does not affect time delay either.

5.2 The Comparison with Streamwise Oscillation

To compare the time delay of transverse oscillation with streamwise oscillation, the time constant, time delay and phase lag for streamwise oscillations are computed, the results are shown in Figure 9(a-c), Figure 10(a-c), Table 3 and Table 4. Figure 9(a-c) is for different oscillation frequencies; and Figure 10(a-c) is for different oscillation amplitudes. From these figures and tables, we can find that the behavior of time delay for streamwise oscillation is similar to that for transverse oscillation. From Figure 11, it is shown that the time constant of streamwise oscillation is smaller than that of transverse oscillation; and the variation of time constant for streamwise oscillation is less than that for transverse oscillation.

To investigate the effect of first node location on time constant, the locations of first node are changed from $\overline{x} = 0.018$ to $\overline{x} = 0.18$ with $\overline{\omega} = 0.20\pi$ and $\varepsilon = 0.01$. The results are shown in Table 5, it can be found from Table 5 that time constants change for the points near the first node with the variation of first node location; but variations of the location of first node do not affect the time constants in the locations away from the first node. So it is reasonable and valid to choose the first node at $\overline{x}_0 = 0.09$.

5.3 The Results of a Cylinder Array with Transverse Oscillation

5.3.1 Outer layer velocity distribution

Figure 12 shows the velocity distribution of a pitch-to-diameter ratio T/D=1.44 cylinder array at different times, where the oscillation frequency is $\overline{\omega} = 0.20\pi$, oscillation amplitude is $\overline{A} = 0.01$ and Reynolds number Re=2000, and the initial condition is set to $\overline{U}(x,0) = 2.0 \sin x$. This figure shows that the outer layer velocity grows with the increase of time until t=0.3. When time is greater than 0.3, the velocity does not change very much with the increase of time, which means that the velocity reaches periodic steady after time is greater than 0.3. Figure 13 shows the effect of Reynolds number on outer layer velocity distribution. From this figure it is easy to see that Reynolds number does not affect the velocity distribution very much.

To study the effect of pitch-to-diameter ratio T/D on outer velocity distribution, T/D is changed from 1.10 to 2.0, and the results are shown in Figure 14. From this figure we can find that the ratio of T/D influences the outer layer velocity very significantly. With the increase of T/D ratio, the velocity decreases, which is what we expect, because the gap between the cylinders is getting larger with the increase of pitch-to-diameter ratio.

Figure 15 shows the effect of oscillation frequency on outer layer velocity. In this figure the oscillation frequency is changed from $\omega = 0.01\pi$ to $\omega = 0.50\pi$ with fixed oscillation amplitude A=0.01, Reynolds number Re=2000.0 and pitch-to-diameter ratio 1.44 at time is equal to 2.0. From this figure we can find that the effect of oscillation frequency on outer layer velocity is negligible.

Figure 16 shows the effect of oscillation amplitude on outer layer velocity distribution with fixed oscillation frequency, Reynolds number and pitch-to-diameter ratio. This figure indicates that the outer layer velocity is getting larger with the increase of oscillation amplitude at certain time.

5.3.2 The time constant, time delay and phase lag for a cylinder array

Figure 17(a-c) and Table 6 show the effect of oscillation frequency on time constant, time delay and phase lag for different locations with fixed oscillation amplitude

$\overline{A} = 0.01$, Reynolds number Re=2000 and pitch-to-diameter ratio T/D=1.44. Figure 16(a) is the time constant vs. locations at different frequencies, from this figure we can find that the time constant changes with the locations.

Figure 18(a-c) and Table 7 show the effect of oscillation amplitude on time constant, time delay and phase lag. It can be found from this figure and table that the oscillation amplitude does not change the time delay very much, so the phase lag is independent of oscillation amplitude also.

Figure 19(a-c) and Table 8 show the effect of pitch-to-diameter ratio on time constant, time delay and phase lag with fixed oscillation frequency, oscillation amplitude and Reynolds number. It can be found from this figure and table that the pitch-to-diameter ratio greatly influences the time delay. With the increase of pitch-to-diameter ratio, the time delay is getting larger, which can be explained as follows: as the pitch-to-diameter ratio increases, the outer layer velocity increases as shown in the Figure 14, the boundary layer development will take less time than lower velocities.

If we compare figure 7(a-c) and figure 17(a-c), it can be found that in the region from the point near stagnation point to $\overline{x} = 1.44$, the time constant for a cylinder array is larger than that for a single cylinder, but after this region the time constant for a single cylinder is larger than that of a cylinder array. The increase rate of time constant for a single cylinder is greater that of a cylinder array, which is caused by the increase of outer velocity in this region.

5.4 The Comparison with the Time Delay in Weaver's Model

In Weaver's time delay model, the effect of pitch-to-diameter ratio is not considered. As our time delay model and Weaver's model are based on different mechanisms, it is impossible to compare them directly, but there is one common factor that the predictions from these two models are all independent of flow Reynolds number.

CHAPTER VI

EXPERIMENTAL RESULTS

So far the preliminary theoretical study of time delays for both a single cylinder and a cylinder in a cylinder array have been done, the last part of this dissertation is the experimental study of time delay.

6.1 Experimental System and Instrumentation

All the experiments were performed on a free surface water table in the School of Mechanical and Aerospace Engineering at Oklahoma State University, with a working section 25 in. wide, 45 in. long and 3 in. deep, at Reynolds number 1350 based on the diameter of one smooth brass circular cylinder. The diameter of the cylinder is 25.4 mm. The cylinder was mounted vertically, with its bottom end free and its top end clamped to the driving mechanism which moved the cylinder in forced oscillations normal to the mean free stream flow. The mechanism was driven by an electric motor with an infinitely-variable-speed transmission connected to an adjustable eccentric circular disk. In this way, both the exciting amplitude and exciting frequency could be changed precisely. The cylinder and the driving mechanism were rigid enough to avoid deflection during oscillation.

The line diagram of the apparatus is shown in Figure 20. The measurements of time delay between cylinder oscillation and flow perturbation were made by detecting flow fluctuation around the cylinder and cylinder oscillation velocity. The flow fluctuation was measured with a DISA type 55M01 Constant Temperature Anemometer and DANTEC 55R11 cylindrical probe. The hot film probe was placed 1.2A away from the equilibrium

cylinder, here A is the oscillation amplitude of cylinder. The anemometer output signals went through a band-pass filter to eliminate the high frequency noise, and then went to a spectrum analyzer, which provided both instantaneous and averaged spectra of the signal. The oscillation velocity of the cylinder was detected by Poly-tech OFV-2600/OFV-350 vibrometer systems. The output signals from the vibrometer went to the spectrum analyzer, which provided the cross correlation of flow perturbation and cylinder oscillation velocity after which the time delay between flow perturbation and cylinder oscillation can be determined. For spectral analysis of the signal, 10 or 20 ensemble averages were used to reduce the random errors.

Before data could be received with any degree of confidence, it was necessary to determine the set-up's characteristics, through the measurement of the stationary vortex-shedding frequency at a known flow velocity. That frequency was compared with the calculated vortex shedding frequency based on the Strouhal number S=0.2. The flow velocity was measured through counting the time for a particle to travel a certain distance. The free stream velocity in this measurement is 2.1 in/sec.

Before measuring the time delay, it is necessary to estimate the boundary thickness of the cylinder under the experimental conditions. From Schlichting (Fig. 10.8), the boundary layer thickness at $\theta = 90^{\circ}$ is:

$$\delta = \frac{2.0R}{\sqrt{\frac{U_{\infty}R}{\nu}}} \tag{64}$$

where: ν is kinematic viscosity of the fluid, for water at room temperature $\nu = 10^{-6}\ m^2 / s$; R is radius of oscillation cylinder, mm; U_{∞} is free steam velocity, m/sec. If a cylinder with diameter D=25.4 mm was used, for the maximum water table velocity U_{∞}=0.053m/sec. Substitution of the above parameters into Eq. 64 the boundary layer thickness at $\theta = 90^{\circ}$ is:

$$\delta = \frac{2.0R}{\sqrt{\frac{U_\infty R}{\nu}}} = \frac{0.0254}{\sqrt{\frac{0.053 * 0.0127}{10^{-6}}}} \approx 0.001m = 1.0mm$$

So the boundary layer thickness is very small compared to the diameter of the oscillation cylinder. The measurement point of the hot film was outside the steady boundary layer.

6.2 The Experimental Results

Using the above experimental setup and instrumentation, the measurement of time delay was carried out. The Figure 21(a) shows the cross correlation between the flow velocity and cylinder oscillation velocity at 0 degree from stagnation point, where the free stream flow velocity is 53.34 mm/sec, the oscillation amplitude of the cylinder is 2.5 mm, the oscillation frequency is 1.31 Hz. From this figure, it is found that the flow velocity and cylinder oscillation correlate closely, which means that there is no time delay detected in this location. Similarly, the Figures 22(a) and 23(a) show the cross correlation at 30 and 60 degrees from the stagnation point respectively, but the cylinder oscillation frequency is 2.62 Hz, again there is no time delay detected in these locations. It is found that there is no time delay detected from 0 to 84 degrees. Figure 24(a) shows the cross correlation near 85 degree from the stagnation point. From this figure it is found that there is a distinguishable peak at τ=0.4 sec, which means that there is a 0.4 second time delay between the cylinder oscillation and flow perturbation. From fundamental experimental fluid mechanics (Schlliting, 1979), it is known that the flow separation of a single cylinder with cross flow occurs at 86 degrees, so it can be concluded that the time delay happens around the separation point. After the separation point, there is still a time delay detected but the value of the time delay varies with locations and time, which means that time delay in the wake cannot be described in a simple way. Figures 21(b) to 24(b) show the histogram of the hot wire signal under the same experimental conditions.

Figure 25(a) shows the cross correlation at 85 degrees from the stagnation point. when the hot film moves with the cylinder but outside the boundary layer. It can be found

that there is no time delay detected in this case which is different from that when the hot film does not move with the cylinder. Small high-order perturbations were observed overlaid on the fundamental fluctuations in our experiments.

CHAPTER VII

CONCLUSIONS AND DISCUSSIONS

7.1 Conclusions

A theoretical model of time delay for a single cylinder and a cylinder array with small amplitude oscillation has been developed. The model is based on the time delay in the transient boundary layer development. The cylinder oscillation will change the boundary layer and therefore the point of separation, but there is a phase lag between the cylinder oscillation and the change in the flow separation. The time delay can be predicted by solving the momentum-integral form of the unsteady boundary layer numerically. The system parameters which affect time delay have been identified and evaluated numerically. A preliminary experimental study has been carried out to verify the existence of the time delay between the cylinder oscillation and flow perturbation.

7.1.1 The theoretical conclusions

For a single cylinder with transverse oscillation, the results show that the time delay is independent of oscillation frequency and amplitude, so that the cylinder oscillation velocity does not influence the time delay. This is in agreement with the time delay model used by Weavers et al (1986) or Price et al.(1992). It is found that the time delay changes with location; when $0.09 \leq \bar{x} \leq 1.06$ the time delay increases linearly as the observer's location moves downstream, but in the region $1.06 \leq \bar{x} \leq 1.80$ the time delay increases exponentially as the observer's position moves downstream.

For a single cylinder with streamwise oscillation, the behavior of time delay is similar to that with transverse oscillation, but the magnitude of the time delay for streamwise oscillation is smaller than that of transverse oscillation.

The results show that the fluctuation of momentum thickness changes with the location. The fluctuation decays in the range from $\bar{x} = 0.09$ to $\bar{x} = 1.26$, but it increases when $\bar{x} > 1.26$, which is different from the decay function used in Weaver's model (1992).

For a cylinder array with transverse oscillation, it is found that the effect of oscillation frequency, oscillation amplitude, and Reynolds number on time delay is very small. As the time delay does not depend on the Reynolds number, it seems that incoming-flow turbulence levels should also be unimportant. The time delay for a cylinder array changes with the observer's location, but the behavior is different from that of a single cylinder. In the region from the point near stagnation point to $\bar{x} = 1.44$, the time delay for a cylinder array is larger than that of a single cylinder, but after this region, the time delay for a single cylinder is larger than that of a cylinder array. The results show that the pitch-to-diameter ratio greatly affects the time delay; with increase of pitch-to-diameter ratio, the time delay gets smaller. In Weaver's or Price's model, the effect of pitch-to-diameter ratio on time delay is not considered. As this current model and Weaver's model are based on a different mechanism, it is impossible to compare them directly, but the prediction from these two models are all independent of the flow Reynolds number. The present study gives a physical insight into the time delay, which is important for understanding the physical mechanism of the time delay.

7.1.2 The experimental conclusions

From the experimental results, the following conclusions can be drawn:

(1). The time delay is caused by the development of the boundary layer, which is in good agreement with what was expected theoretically and demonstrated numerically.

(2). Before the separation point, it was found from measurement that the flow perturbation and cylinder oscillation correlate closely, without time delay or phase lag;

(3). Near the separation point (about 85 degree), time delay is detected between the cylinder oscillation and flow perturbation;

(4). After the separation point, time delay still exists, but the value of time delay is different from moment to moment and from location to location, so that the time delay in the wake can not be described in a simple way.

(5). If the hot film probe moves with the cylinder but outside the boundary layer, there is no time delay found between the cylinder oscillation and the mean flow. Small high-order perturbations were observed overlaid on the fundamental fluctuations in our experiments.

7.2 The Discussion

We have presented a new mechanism of time delay based on fundamental fluid dynamics, developed a theoretical model of time delay and carried out a theoretical analysis of the time delay for both a single cylinder and a cylinder array. In addition to the theoretical study, a experimental study has been carried out. Both are very helpful in understanding the physical mechanism of time delay and giving physical insight to time delay.

This study presents the theoretical method to determine the time delay, numerical results, and the experimental observations. Those results have not been reported or investigated in the past. Due to experimental set-up's limitations, the experimental conditions are not in exact agreement with the conditions of the theoretical model. As discussed in the theoretical development the theoretical model is only valid for small flow perturbations $\varepsilon = \overline{A}\,\overline{\omega} = \frac{2\pi fA}{U_\infty} \le 0.05$ or $\frac{fA}{U_\infty} \le 0.008$. Since the maximum flow velocity U_∞ of the open water table is only about 2.5 in/sec, we should have $fA \le 0.02$ in / sec.

For the available oscillation measurement transducers, the oscillation frequency should be greater than 1.0 Hz for a good frequency response, so the oscillation amplitude of cylinder has to be $A \leq 0.02$ in, which is a very small oscillation amplitude and cannot be met by the present experimental setup. As the experimental amplitudes exceed the limits of the theoretical model, the comparation between the theoretical results and the experimental results can not be made at present. In order to verify the results at small amplitudes, we propose that, in the future, these measurements should be carried out in the new wind tunnel. This will confirm that the phenomenon demonstrated theoretically is indeed the same at the small amplitudes of vibration onset.

The other half of the problem, the generation of transverse forces due to shifts in the location of flow separation, deserves an investigation in the future.

REFERENCES

Abd-Rabbo, A. and Weaver, D. S., 1986, "A Flow Visualization Study of Flow Development in Staggered Tube Arrays," Journal of Sound and Vibration, Vol. 106, pp. 241-256.

Bearman, P. W, and Zdravkovich, M. M., 1978, "Flow around a Circular Cylinder near a Plane Boundary," Journal of Fluid Mechanics, 89, pp. 33-47.

Bearman, P. W. 1984, "Vortex Shedding From Oscillating Bluff Bodies," Ann. Rev. Fluid Mech., pp. 195-222 .

Bishop , R. E. D. , and Hassan , A. Y. 1964, "The Lift and Drag Forces on a Circular Cylinder Oscillating in a Flowing Fluid," Proc. of the Royal Soc. of London , Series A , Vol. 277, pp. 51-75.

Blevins, R. D., 1974, "Fluid Elastic Whirling of a Tube Row," Journal of Pressure Vessel Technology, Transaction of the ASME, 98, pp. 263-267.

Blevins, R. D., Gibert, R. J. and Villard, B., 1981, "Experiment on Vibration of Heat Exchanger Tube Arrays in Cross Flow," Trans. 6th International Conference on Structural Mechanics in Reactor Technology, Paris.

Blevins, R. D., 1990, "Flow-induced Vibration," Van Nostrand Reinhold, New York.

Bublitz, P., 1972, "Unsteady Pressure and Forces Acting on an Oscillating Circular Cylinder in Transverse Flow," IUTAML-IAHR Symposium Karlsruhe, Flow-induced Structural Vibrations, pp. 443-453.

Chen, S. S., 1978, "Cross Flow Induced Vibrations of Heat Exchangers Tube Banks," Nuclear Engineering Design, 47, pp. 147-158.

Chen, S. S. and Jendrzejczyk, J. A., 1981, "Experiments on Fluid Elastic Instability in Tube Banks Subjected to Liquid Cross Flow," Journal of Sound and Vibration, 78(3), pp. 130-135.

Chen, S. S. and Jendrzejczyk, J. A., 1981, "Flow Velocity Dependence of Damping in Tube Arrays Subjected to Liquid Cross Flow," ASME Journal of Pressure Vessel Technology 103, pp. 130-135.

Chen, S. S. and Jendrzejczyk, J. A., 1982, "Experiment and Analysis of Instability of Tube Rows Subjected to Liquid Cross Flow," Journal of Applied Mechanics 48, pp. 704-709.

Chen, S. S., 1983, "Instability Mechanisms and Stability Criteria of a Group of Circular Cylinders Subjected to Cross Flow. Part 1: Theory," Journal of Vibration, Acoustics, Stress, and Reliability in Design, 105, pp. 51-58.

Chen, S. S., 1984, "Guidelines for the Instability Flow Velocity of Tube arrays in Cross Flow," Journal of Sound and Vibration 76, pp. 439-455.

Chen, S. S. and Jendrzejczyk, J. A., 1987, "Fluid Excitation Forces Acting on a Square Tube Array," Journal of Fluid Engineering, 109, pp. 415-423.

Chen, S. S., and Jendrzejczyk, J. A., 1987, "Characteristics of Fluid-elastic Instability of Tube Rows in Cross-flow," Proceedings of the International Conference of Flow Induced Vibrations, Bowness-on-Widermere, England, Paper No. A1, May 12-14.

Chen, S. S., 1991, "Flow Induced Vibration of an Array of Cylinders," Part 1, Shock and Vibration Digest, 23(12), pp. 3-9.

Cheng, M. and Moretti, P. M., 1988, "Experimental Study of the Flow Field Downstream of a Single Tube Row," Experimental Thermal and Fluid Science, 1(1).

Cheng, M. and Moretti, P. M., 1989, "Flow Instability in Tube Bundles," ASME Symposium Flow Induced Vibrations, PVP, 154, Honolulu.

Cheng, M. and Moretti, P. M., 1991, "Lock-in Phenomena on a Single Cylinder with Forced Transverse Vibration," ASME Symposium on Flow-Induced Vibration and Wear, PVP Volume, San Diego, June 23-27, 1991, pp. 129-133.

Cheng, M. and Moretti, P. M., 1992, "Lock-in of Vortex Shedding from a Normal Pair of Cylinders with Forced Transverse Vibration," International Symposium on Flow-induced Vibration and Noise, Vol. 6, pp. 25-27.

Chilukuri, R., 1987, Journal of Fluid Engineering, Transactions of the ASME, Vol. 1909, pp. 166-171.

Connors, J. H., 1970, "Fluid-elastic Vibration of Tube Arrays Excited by Cross Flow," Flow-Induced Vibration in Heat Exchangers, Ed., d. D. Reiff, ASME, New York, pp. 42-56.

Connors, J. H., 1978, "Fluid-elastic Vibration of Heat Exchanger Tube Arrays," ASME Journal of Mechanical Design, 100, pp. 347-353.

Griffin, O. M. and Ramberg, S. E., 1974, Journal Fluid Mechanics, Vol. 66, pp. 553-576.

Fei, X. L., 1989, "Advanced Fluid Dynamics," Xi-an Jiao Tong University Press, Xi-an, China.

Glauert, M. B., 1956, "The Laminar Boundary Layer on Oscillating Plates and Cylinders," Journal of Fluid Dynamics, Vol. 1, part 1, p.97-110.

Griffin, O. M. 1991, and Hall ,M. S., "Review-vortex Shedding Lock-on and Flow Control in Bluff Body Wakes," Journal of Fluids Engineering, Vol. 113, pp. 526-537.

Grover, L. K. and Weaver, D. S., 1978, "Cross Flow Induced Vibrations in a Tube Bank-Vortex Shedding," Journal of Sound and Vibration 59, pp. 263-276.

Hara, F, 1989, "Unsteady Fluid Dynamics Forces Acting on a Single Row of Cylinders Vibrating in a Cross Flow," Journal of Fluids & Structures, 3, pp. 97-113.

Heineken, E. P. and Mohr, K. H., 1982, "Investigations on Fluid Borne Forces in Heat Exchangers with Tubes in Cross Flow," Third Vibration in Nuclear Plant Conference, Keswich.

Kabayashi, T., 1976, "Study on the Fluid Force Acting on Narrow Circular Cylinder Array and Square-Cylinder array," Journal of JSME 42, pp. 1452-1461.

Lever, J. H. and Weaver, D. S., 1982, "A Theoretical Model for the Fluid-elastic Instability in Heat Exchanger Tube Bundles," Journal of Pressure Vessel Technology 103(4), pp. 147-158.

Lever, J. H., and Weaver, D. S., 1986, "On the Stability of Heat Exchanger Tube Bundles. Part 1: Modified Theoretical Model," Journal of Sound and Vibration, 107, pp. 375-392.

Lever, J. H., and Weaver, D. S., 1986, "On the Stability of Heat Exchanger Tube Bundles. Part 2: Numerical Results and Comparison with Experiments," Journal of Sound and Vibration, 107, pp. 393-410.

Lighthill, M. J., 1954, "The Response of Laminar Skin Friction and Heat Transfer to Fluctuations in the Stream Velocity," Proceedings Royal Society London, A224, pp. 1-23.

Ljungkrona, L., and Sunden, B., 1992, "Surface Pressure Distributions on Two In-Line Tube Bundles in Cross Flow," Journal of Fluids and Structure.

Marn, J. and Catton, I., 1992, "On Stability Analysis of a Flexible Cylinder in an Array of Rigid Cylinders," Journal of Fluids Engineering, 114, pp. 12-19.

Moretti, P. M., 1986, "Caught in a Cross Flow," Mechanical Engineering, 1089(12), pp. 56-61.

Moretti, P. M., 1993, "Flow-Induced Vibrations in Arrays of Cylinders," Annual Review of Fluid Mechanics, Vol. 25, pp. 99-114.

Muraoka, K., and Tashiro, S., 1984, "The Effect of the Wake from Circular Cylinder on Boundary Layer Transition,' Journal of JSME 50, pp. 3152-3158.

Nakamura, T., and Fujita, K., 1993, " A Study on an Approximate Theory of Fluid-elastic Instability Vibration of Tube Array: Part I-Basic Concept of Fluid-elastic Force and

Instability of Tube Rows,' 1992 International Symposium on Flow-induced Vibration and Noise, PVP-VOl. 242, pp. 1-16.

Nishikawa, E., and Isgigai, S., 1977, "Structure and Pressure Drop of the Flow around a Tube in Array in Cross-flow," Journal of JSME 43, pp. 3310-3319.

Oengoeren, A., and Ziada, S., 1992, "Unsteady Fluid Forces Acting on a Square Tube Bundle in Air Cross-Flow," International Symposium on Flow-Induced Vibration and Noise, Vol. 1, pp. 55-74.

Okamoto, T., and Takeuchi, Y., 1975, "Effect of the Side Wall on a Flow Around and behind two-dimensional Circular Cylinder," Journal of JSME 41, pp. 181-188.

Paidoussis, M. P., 1979, "Flow-Induced Vibrations in Nuclear Reactor and Heat Exchangers," Proceedings of the IUTAM-IAHR Symposium on Practical Experiences with Flow-Induced Vibrations, Karlsruhe, Germany.

Paidoussis, M. P., 1981, "Fluid-elastic Vibration of Cylinder Array in Axial and Cross Flow," Journal of Sound and Vibration 76, pp. 329-359.

Paidoussis, M. P., 1987, "Flow -Induced Instabilities of Cylindrical Structures," Applied Mechanics Review, 40, pp. 163-175.

Patankar, S. V., 1980, "Numerical Heat Transfer and Fluid Flow," Hemisphere Publishing Corporation, London.

Pettigrew, M. J., Sylvestre, Y. and Campagna, A. O., 1978, "Vibration Analysis of Heat Exchanger and Steam Generator Designs," Nuclear Engineering Design, 48, pp. 97-115.

Pettigrew, M. J. and Taylor, C. E., 1991, "Fluid Elastic Instability of Heat Exchanger Tube Bundles: Review and Design Recommendations," Proceedings of Institute of Mechanical Engineers, Flow-Induced Vibration, Bedford Hotel, Brighton, pp. 349-368.

Price, S. J., Paidoussis, M. P., and Cheng, B., 1992, "A Constrained-Mode Analysis with a One-Cylinder Kernel for a Fully Flexible in-line Array in Cross-Flow," International Symposium on Flow-Induced Vibration and Noise, Vol. 2, pp. 17-30.

Price, S. J., and Paidoussis, M. P., 1984, "An Improved Mathematical Model for the Stability of Cylinder Rows Subject to Cross-Flow," Journal of Sound and Vibration, Vol. 97, pp. 615-640.

Price, S. J., and Paidoussis, M. P., 1986a, "A Constrained-Mode Analysis of the Fluid-elastic Instability of a Double Row of Circular Cylinders Subject to Cross-Flow: A Theoretical Investigation of System Parameters," Journal of Sound and Vibration, Vol. 105, pp. 121-142.

Price, S. J. and Paidoussis, M. P., 1986b, "An Improved Mathematical Model for the Stability of Cylinder Rows Subjected to Cross-Flow," Journal of Fluids Engineering, Vol. 108, pp. 121-142.

Price, S. J., Paidoussis, M. P., and Giannias, N., 1990, "A Generalized Constrained-Mode Analysis for Cylinder Arrays in Cross-Flow," Journal of Fluids and Structures, Vol. 4, pp. 171-202.

Price, S. J., Paidoussis, M. P., and Cheng, B., 1992, "A Constrained-Mode Analysis with a One-Cylinder Kernel for a Fully Flexible in-line Array in Cross-Flow," International Symposium on Flow-Induced Vibration and Noise, Vol. 2, pp. 17-30.

Rzentkowski, G., and Lever, J. H., 1992, "Modeling the Non-linear Fluid-elastic Behavior of Tube Bundle," International Symposium on Flow-Induced Vibration and Noise, Vol. 2, pp. 89-105.

Roberts, B. W., 1966, "Low Frequency, Aeroelastic Vibrations in a Cascade of Circular Cylinders," Mechanical Engineering Science Monograph, No. 4.

Schlichting, H., 1979, "Boundary Layer Theory," McGraw-Hill, New York.

Simposon, A., and Flower, J. W., 1977, "An Improved Mathematical Model for the Aerodynamic Forces on Tandem Cylinders with Aeroelastic Applications," Journal of Sound and Vibration, Vol. 51, pp. 183-217.

Southworth, P. J. and Zdravkovich, M. M., 1975, "Cross Flow Induced Vibrations of Finite Tube Banks in In-Line Arrangement, " Journal of Mechanical Engineering Science 17, pp. 190-198.

Soper, M. M., 1980, "The Effect of Tube Layout on the Fluid-elastic Instability of Tube Bundles in Cross Flow, " Flow-Induced Heat Exchanger Tube Vibration, HTD-Vol. 9, ASME, New York.

Soper, M. M., 1983, "The Effect of Tube Layout on the Fluid-elastic Instability of Tube Bundles in Cross Flow, " ASME Journal of Heat Transfer, 105, pp. 744-750.

Stansby, P. K., 1976, "Base Pressure of Oscillating Cylinders," Journal of Engineering Mechanics, 104, pp. 649-661.

Tanaka, H. and Takahara, S., 1980, "Unsteady Fluid Dynamic Force on Tube Bundle and Its Dynamic Effect on Vibration," Flow Induced Vibration in Heat Exchangers, Ed. D. d. Reiff, ASME, New York.

Tanaka, H. and Takahara, S., 1981, "Fluid Elastic Vibration of Tube Arrays in Cross Flow," Journal of Sound and Vibration, 77, pp. 19-37.

Tanaka, h. and Ohta, K., 1982, "Flow-Induced Vibration of Tube Arrays with Various Pitch-to-Diameter Ratios," Journal of Pressure Vessel Technology, 104, pp. 168-174.

Tanida, Y., Okajima, A. and Watanabe, P., 1973, "Stability of Circular Cylinder Oscillating in Uniform Flow or in a Wake," Journal of Fluid Mechanics, 61, pp. 769-784.

Thwaites, B, Aeronaut. Q., 1, pp. 245-280.

Weaver, D. S. and Grover, L. K., 1978, "Cross-Flow Induced Vibrations in a Tube Bank-Turbulent Buffeting and Fluid Elastic Instability," Journal of Sound and Vibration, 59, pp. 277-294.

Weaver, D. S. and Korogannakis, d., 1981, "The Cross Flow Response of a Tube Array in Water -- A Comparison with the Same Array in Air," Flow-Induced Vibration Design Guidelines. PVP-Vol. 52, ASME, New York.

Weaver, D. S., and Abd-Rabbo, A., 1985, "A Flow Visualization Study of a Square Array of Tubes in Water Cross-Flow," ASME Journal of Fluids Engineering, Vol. 107, pp. 354-363.

Weaver, D. S. and Fitzpatric, J. A., 1987, "A Review of Flow Induced Vibrations in Heat Exchangers," Proceedings of the International Conference of Flow Induced Vibrations, Bowness-on-winwemere, England, Paper No. A1, pp. 1-17.

Yetisir, M., and Weaver, D. S., 1992, "A Theoretical Study of Fluid-elastic Instability in a Flexible Array of Tubes," International Symposium on Flow-Induced Vibration and Noise, Vol. 2, pp. 69-87.

Zdravkovich, M. M. and Namork, J. E., 1978, "Flow Structure Within Both Stationary and Vibrating Tube Banks and Triangular Pitch," Proceedings BNES International Conference of Vibration in Nuclear Plant, Keswick, U. K..

Zdravkovich, M. M. and Namork, J. E., 1980, "Structure of Interstitial Flow Between Closely Spaced Tubes in Staggered Array," Flow Induced Vibrations, ASME Publication, pp. 41-46.

Zdravkovich, M. M. and Stonebanks, 1990, "Intrinsically Non-uniform and Metastable Flow in and Behind Tube Arrays," Journal of Fluids and Structure, 4, pp. 305-309.

Zdravkovich, M. M., 1991, "On Suppressing Metastable Interstitial Flow behind a Tube Array," Proceedings of the Institute of Mechanical Engineers, Flow-Induced Vibration, pp. 185-191, Bedford Hotel, Brighton.

Table 1 The Time Constants, Time Delay and Phase Lag
at Different Locations with Different Freqencies
for Single Cylinder with Transverse Oscillation (ε=0.05)

1. The Time Constant Changes with Locations at Different Frequencies						
X	ω=0.10π	ω=0.20π	ω=0.30π	ω=0.40π	ω=0.50π	
0.09	0.150	0.150	0.150	0.150	0.150	
0.18	0.400	0.410	0.420	0.440	0.480	
0.36	0.500	0.510	0.520	0.540	0.570	
0.54	0.550	0.550	0.560	0.580	0.600	
0.72	0.600	0.610	0.610	0.620	0.640	
0.90	0.670	0.680	0.680	0.680	0.690	
1.08	0.770	0.770	0.770	0.770	0.770	
1.26	0.900	0.890	0.880	0.870	0.860	
1.44	1.070	1.060	1.040	1.020	1.000	
1.62	1.310	1.270	1.240	1.200	1.170	
1.80	1.640	1.580	1.510	1.460	1.420	
2. The Time Delay Changes with Locations at Different Frequencies						
X	ω=0.10π	ω=0.20π	ω=0.30π	ω=0.40π	ω=0.50π	
0.09	0.000	0.000	0.000	0.000	0.000	
0.18	0.250	0.260	0.270	0.290	0.330	
0.36	0.350	0.360	0.370	0.390	0.420	
0.54	0.400	0.400	0.410	0.430	0.450	
0.72	0.450	0.460	0.460	0.470	0.490	
0.90	0.520	0.530	0.530	0.530	0.540	
1.08	0.620	0.620	0.620	0.620	0.620	
1.26	0.750	0.740	0.730	0.720	0.710	
1.44	0.920	0.910	0.890	0.870	0.850	
1.62	1.160	1.120	1.090	1.050	1.020	
1.80	1.490	1.430	1.360	1.310	1.270	
3. The Phase Lag Changes with Locations at Different Frequencies						
X	ω=0.10π	ω=0.20π	ω=0.30π	ω=0.40π	ω=0.50π	
0.09	0.000	0.000	0.000	0.000	0.000	
0.18	4.500	9.360	14.580	20.880	29.700	
0.36	6.300	12.960	19.980	28.080	37.800	
0.54	7.200	14.400	22.140	30.960	40.500	
0.72	8.100	16.560	24.840	33.840	44.100	
0.90	9.360	19.080	28.620	38.160	48.600	
1.08	11.160	22.320	33.480	44.640	55.800	
1.26	13.500	26.640	39.420	51.840	63.900	
1.44	16.560	32.760	48.060	62.640	76.500	
1.62	20.880	40.320	58.860	75.600	91.800	
1.80	26.820	51.480	73.440	94.320	114.300	

Table 2 Time Constants, Time Delay and Phase Lag
at Different Locations with Different Amplitudes
for Single Cylinder with Transverse Oscillation ($\omega=0.20\pi$)

1. The Time Constant Changes with Locations at Different Amplitudes						
X	A=0.01	A=0.02	A=0.03	A=0.04	A=0.05	
0.090	0.230	0.210	0.200	0.190	0.180	
0.180	0.490	0.480	0.470	0.460	0.440	
0.360	0.540	0.540	0.530	0.530	0.520	
0.540	0.570	0.570	0.570	0.560	0.560	
0.720	0.620	0.610	0.610	0.610	0.610	
0.900	0.680	0.680	0.680	0.680	0.680	
1.080	0.760	0.760	0.760	0.760	0.760	
1.260	0.880	0.880	0.880	0.880	0.890	
1.440	1.040	1.050	1.050	1.050	1.050	
1.620	1.270	1.270	1.270	1.270	1.270	
1.800	1.600	1.590	1.590	1.590	1.590	
2. The Time Delay Changes with Locations at Different Amplitudes						
X	A=0.01	A=0.02	A=0.03	A=0.04	A=0.05	
0.099	0.000	0.000	0.000	0.000	0.000	
0.252	0.260	0.270	0.270	0.270	0.260	
0.423	0.310	0.330	0.330	0.340	0.340	
0.594	0.340	0.360	0.370	0.370	0.380	
0.765	0.390	0.400	0.410	0.420	0.430	
0.936	0.450	0.470	0.480	0.490	0.500	
1.107	0.530	0.550	0.560	0.570	0.580	
1.278	0.650	0.670	0.680	0.690	0.710	
1.449	0.810	0.840	0.850	0.860	0.870	
1.620	1.040	1.060	1.070	1.080	1.090	
1.800	1.370	1.380	1.390	1.400	1.410	
3. The Phase Lag Changes with Locations at Different Amplitudes						
X	A=0.01	A=0.02	A=0.03	A=0.04	A=0.05	
0.099	0.000	0.000	0.000	0.000	0.000	
0.252	9.360	9.720	9.720	9.720	9.360	
0.423	11.160	11.880	11.880	12.240	12.240	
0.594	12.240	12.960	13.320	13.320	13.680	
0.765	14.040	14.400	14.760	15.120	15.480	
0.936	16.200	16.920	17.280	17.640	18.000	
1.107	19.080	19.800	20.160	20.520	20.880	
1.278	23.400	24.120	24.480	24.840	25.560	
1.449	29.160	30.240	30.600	30.960	31.320	
1.620	37.440	38.160	38.520	38.880	39.240	
1.800	49.320	49.680	50.040	50.400	50.760	

Table 3 Time Constants, Time Delay and Phase Lag
at Different Locations with Different Freuqencies
for Single Cylinder with Streamwise Oscillation (ε=0.05)

1. The Time Constant Changes with Locations at Different Frequencies						
X	ω=0.10π	ω=0.20π	ω=0.30π	ω=0.40π	ω=0.50π	
0.09	0.230	0.230	0.230	0.230	0.240	
0.18	0.490	0.490	0.490	0.490	0.500	
0.36	0.530	0.530	0.530	0.540	0.540	
0.54	0.560	0.560	0.560	0.570	0.570	
0.72	0.600	0.600	0.600	0.610	0.610	
0.90	0.650	0.660	0.660	0.670	0.680	
1.08	0.730	0.740	0.740	0.750	0.760	
1.26	0.850	0.850	0.860	0.870	0.890	
1.44	1.000	1.010	1.030	1.040	1.060	
1.62	1.220	1.230	1.250	1.280	1.290	
1.80	1.540	1.560	1.590	1.620	1.630	
2. The Time Delay Changes with Locations at Different Frequencies						
X	ω=0.10π	ω=0.20π	ω=0.30π	ω=0.40π	ω=0.50π	
0.09	0.000	0.000	0.000	0.000	0.000	
0.18	0.260	0.260	0.260	0.260	0.260	
0.36	0.300	0.300	0.300	0.310	0.300	
0.54	0.330	0.330	0.330	0.340	0.330	
0.72	0.370	0.370	0.370	0.380	0.370	
0.90	0.420	0.430	0.430	0.440	0.440	
1.08	0.500	0.510	0.510	0.520	0.520	
1.26	0.620	0.620	0.630	0.640	0.650	
1.44	0.770	0.780	0.800	0.810	0.820	
1.62	0.990	1.000	1.020	1.050	1.050	
1.80	1.310	1.330	1.360	1.390	1.390	
3. The Phase Lag Changes with Locations at Different Frequencies						
X	ω=0.10π	ω=0.20π	ω=0.30π	ω=0.40π	ω=0.50π	
0.09	0.000	0.000	0.000	0.000	0.000	
0.18	4.680	9.360	14.040	18.720	23.400	
0.36	5.400	10.800	16.200	22.320	27.000	
0.54	5.940	11.880	17.820	24.480	29.700	
0.72	6.660	13.320	19.980	27.360	33.300	
0.90	7.560	15.480	23.220	31.680	39.600	
1.08	9.000	18.360	27.540	37.440	46.800	
1.26	11.160	22.320	34.020	46.080	58.500	
1.44	13.860	28.080	43.200	58.320	73.800	
1.62	17.820	36.000	55.080	75.600	94.500	
1.80	23.580	47.880	73.440	100.080	125.100	

Table 4 Time Constants,Time Delay and Phase Lag
at Different Locations with Different Amplitudes for Single Cylinder
with Streamwise Oscillation ($\omega=0.20\pi$)

1. The Time Constant Changes with Locations at Different Amplitudes						
X	A=0.01	A=0.02	A=0.03	A=0.04	A=0.05	
0.090	0.240	0.240	0.240	0.240	0.240	
0.180	0.500	0.500	0.500	0.500	0.500	
0.360	0.550	0.540	0.540	0.540	0.540	
0.540	0.570	0.570	0.570	0.570	0.560	
0.720	0.610	0.610	0.610	0.610	0.600	
0.900	0.670	0.670	0.670	0.670	0.660	
1.080	0.760	0.750	0.750	0.750	0.750	
1.260	0.870	0.870	0.870	0.860	0.860	
1.440	1.040	1.030	1.030	1.030	1.020	
1.620	1.260	1.260	1.250	1.250	1.250	
1.800	1.590	1.590	1.580	1.580	1.580	
2. The Time Delay Changes with Locations at Different Amplitudes						
X	A=0.01	A=0.02	A=0.03	A=0.04	A=0.05	
0.099	0.000	0.000	0.000	0.000	0.000	
0.252	0.260	0.260	0.260	0.260	0.260	
0.423	0.310	0.300	0.300	0.300	0.300	
0.594	0.330	0.330	0.330	0.330	0.320	
0.765	0.370	0.370	0.370	0.370	0.360	
0.936	0.430	0.430	0.430	0.430	0.420	
1.107	0.520	0.510	0.510	0.510	0.510	
1.278	0.630	0.630	0.630	0.620	0.620	
1.449	0.800	0.790	0.790	0.790	0.780	
1.620	1.020	1.020	1.010	1.010	1.010	
1.800	1.350	1.350	1.340	1.340	1.340	
3. The Phase Lag Changes with Locations at Different Amplitudes						
X	A=0.01	A=0.02	A=0.03	A=0.04	A=0.05	
0.099	0.000	0.000	0.000	0.000	0.000	
0.252	9.360	9.360	9.360	9.360	9.360	
0.423	11.160	10.800	10.800	10.800	10.800	
0.594	11.880	11.880	11.880	11.880	11.520	
0.765	13.320	13.320	13.320	13.320	12.960	
0.936	15.480	15.480	15.480	15.480	15.120	
1.107	18.720	18.360	18.360	18.360	18.360	
1.278	22.680	22.680	22.680	22.320	22.320	
1.449	28.800	28.440	28.440	28.440	28.080	
1.620	36.720	36.720	36.360	36.360	36.360	
1.800	48.600	48.600	48.240	48.240	48.240	

Table 5. The Effect of Location of First Node on Time Constant

							($\varepsilon = 0.01$, $\omega = 0.2\pi$)					
N	x(rad)	x(deg)	t	t	t	t	t	t	t	t	t	t
2	0.018	1.031	0.310									
3	0.036	2.063	0.400	0.290								
4	0.054	3.094	0.450	0.390	0.270							
5	0.072	4.125	0.470	0.450	0.370	0.240						
6	0.090	5.157	0.490	0.470	0.430	0.340	0.220					
7	0.108	6.188	0.500	0.490	0.460	0.410	0.320	0.200				
8	0.126	7.219	0.500	0.500	0.490	0.450	0.390	0.300	0.180			
9	0.144	8.251	0.510	0.510	0.500	0.480	0.430	0.370	0.280	0.170		
10	0.162	9.282	0.510	0.510	0.510	0.490	0.460	0.410	0.350	0.260	0.160	
11	0.180	10.313	0.510	0.510	0.510	0.510	0.490	0.450	0.400	0.330	0.250	0.150
21	0.360	20.626	0.540	0.540	0.540	0.540	0.540	0.540	0.540	0.540	0.530	0.520
31	0.540	30.940	0.570	0.570	0.570	0.570	0.570	0.570	0.570	0.570	0.570	0.570
41	0.720	41.253	0.620	0.620	0.620	0.620	0.620	0.620	0.620	0.620	0.620	0.620
51	0.900	51.566	0.680	0.680	0.680	0.680	0.680	0.680	0.680	0.680	0.680	0.680
61	1.080	61.879	0.760	0.760	0.760	0.760	0.760	0.760	0.760	0.760	0.760	0.760
71	1.260	72.193	0.880	0.880	0.880	0.880	0.880	0.880	0.880	0.880	0.880	0.880
81	1.440	82.506	1.040	1.040	1.040	1.040	1.040	1.040	1.040	1.040	1.040	1.040
91	1.620	92.819	1.270	1.270	1.270	1.270	1.270	1.270	1.270	1.270	1.270	1.270
101	1.800	103.132	1.590	1.590	1.590	1.590	1.590	1.590	1.590	1.590	1.590	1.590

Table 6 Time Constants, Time Delay and Phase Lag
at Different Locations with Different Freuqencies (Cylinder Arrays)

	Re=2000, T/D=1.44 , A=0.01, Tmax=3.0					
1. The Time Constant Changes with Locations at Different Frequencies						
X	ω=0.10π	ω=0.20π	ω=0.30π	ω=0.40π	ω=0.50π	
0.099	0.289	0.287	0.289	0.302	0.310	
0.252	0.871	0.868	0.891	0.924	0.941	
0.423	0.977	0.977	1.009	1.053	1.075	
0.594	1.003	1.005	1.041	1.091	1.116	
0.765	1.015	1.018	1.056	1.109	1.135	
0.936	1.028	1.031	1.071	1.126	1.152	
1.107	1.046	1.050	1.090	1.145	1.173	
1.278	1.071	1.075	1.115	1.171	1.198	
1.449	1.103	1.108	1.147	1.202	1.230	
1.620	1.142	1.147	1.186	1.241	1.268	
1.800	1.187	1.192	1.231	1.285	1.311	
2. The Time Delay Changes with Locations at Different Frequencies						
X	ω=0.10π	ω=0.20π	ω=0.30π	ω=0.40π	ω=0.50π	
0.099	0.000	0.000	0.000	0.000	0.000	
0.252	0.582	0.581	0.602	0.622	0.631	
0.423	0.688	0.690	0.720	0.751	0.765	
0.594	0.714	0.718	0.752	0.789	0.806	
0.765	0.726	0.731	0.767	0.807	0.825	
0.936	0.739	0.744	0.782	0.824	0.842	
1.107	0.757	0.763	0.801	0.843	0.863	
1.278	0.782	0.788	0.826	0.869	0.888	
1.449	0.814	0.821	0.858	0.900	0.920	
1.620	0.853	0.860	0.897	0.939	0.958	
1.800	0.898	0.905	0.942	0.983	1.001	
3. The Phase Lag Changes with Locations at Different Frequencies						
X	ω=0.10π	ω=0.20π	ω=0.30π	ω=0.40π	ω=0.50π	
0.099	0.000	0.000	0.000	0.000	0.000	
0.252	10.476	20.916	32.508	44.784	56.790	
0.423	12.384	24.840	38.880	54.072	68.850	
0.594	12.852	25.848	40.608	56.808	72.540	
0.765	13.068	26.316	41.418	58.104	74.250	
0.936	13.302	26.784	42.228	59.328	75.780	
1.107	13.626	27.468	43.254	60.696	77.670	
1.278	14.076	28.368	44.604	62.568	79.920	
1.449	14.652	29.556	46.332	64.800	82.800	
1.620	15.354	30.960	48.438	67.608	86.220	
1.800	16.164	32.580	50.868	70.776	90.090	

Table 7 Time Constants, Time Delay and Phase Lag at Different Locations with Different Amplitudes (Cylinder Arrays)

Re=2000, T/D=1.44, Tmax=3.0						
	(ω=0.20π)					
1. The Time Constant Changes with Locations at Different Amplitudes						
X	A=0.01	A=0.02	A=0.03	A=0.04	A=0.05	
0.099	0.287	0.284	0.281	0.278	0.275	
0.252	0.868	0.856	0.845	0.836	0.826	
0.423	0.977	0.963	0.949	0.935	0.921	
0.594	1.005	0.990	0.974	0.959	0.944	
0.765	1.018	1.002	0.986	0.971	0.955	
0.936	1.031	1.015	0.999	0.984	0.968	
1.107	1.05	1.034	1.018	1.003	0.987	
1.278	1.075	1.060	1.044	1.028	1.013	
1.449	1.108	1.092	1.077	1.061	1.046	
1.620	1.147	1.132	1.117	1.101	1.087	
1.800	1.192	1.177	1.162	1.147	1.133	
2. The Time Delay Changes with Locations at Different Amplitudes						
X	A=0.01	A=0.02	A=0.03	A=0.04	A=0.05	
0.099	0.000	0.000	0.000	0.000	0.000	
0.252	0.581	0.572	0.564	0.558	0.551	
0.423	0.690	0.679	0.668	0.657	0.646	
0.594	0.718	0.706	0.693	0.681	0.669	
0.765	0.731	0.718	0.705	0.693	0.680	
0.936	0.744	0.731	0.718	0.706	0.693	
1.107	0.763	0.750	0.737	0.725	0.712	
1.278	0.788	0.776	0.763	0.750	0.738	
1.449	0.821	0.808	0.796	0.783	0.771	
1.620	0.860	0.848	0.836	0.823	0.812	
1.800	0.905	0.893	0.881	0.869	0.858	
3. The Phase Lag Changes with Locations at Different Amplitudes						
X	A=0.01	A=0.02	A=0.03	A=0.04	A=0.05	
0.099	0.000	0.000	0.000	0.000	0.000	
0.252	20.916	20.592	20.304	20.088	19.836	
0.423	24.840	24.444	24.048	23.652	23.256	
0.594	25.848	25.416	24.948	24.516	24.084	
0.765	26.316	25.848	25.380	24.948	24.480	
0.936	26.784	26.316	25.848	25.416	24.948	
1.107	27.468	27.000	26.532	26.100	25.632	
1.278	28.368	27.936	27.468	27.000	26.568	
1.449	29.556	29.088	28.656	28.188	27.756	
1.620	30.960	30.528	30.096	29.628	29.232	
1.800	32.580	32.148	31.716	31.284	30.888	

Table 8 Time Constants, Time Delay and Phase Lag
at Different Locations With Different Pitch Ratios

Re=2000, A=0.01, Tmax=3.0						
	(ω=0.20π)					
1. The Time Constant Changes with Locations at Different Pitch Ratios						
X	T/D=1.10	T/D=1.20	T/D=1.30	T/D=1.40	T/D=1.50	T/D=1.60
0.099	0.129	0.168	0.210	0.260	0.312	0.351
0.252	0.485	0.593	0.706	0.821	0.937	1.043
0.423	0.551	0.671	0.797	0.926	1.050	1.160
0.594	0.574	0.696	0.825	0.955	1.076	1.179
0.765	0.587	0.710	0.840	0.969	1.086	1.183
0.936	0.599	0.723	0.854	0.983	1.099	1.192
1.107	0.612	0.739	0.872	1.002	1.118	1.210
1.278	0.627	0.757	0.893	1.026	1.144	1.238
1.449	0.645	0.779	0.920	1.056	1.179	1.276
1.620	0.666	0.806	0.951	1.094	1.221	1.323
1.800	0.690	0.835	0.987	1.136	1.270	1.379
2. The Time Delay Changes with Locations at Different Pitch Ratios						
X	T/D=1.10	T/D=1.20	T/D=1.30	T/D=1.40	T/D=1.50	T/D=1.60
0.099	0.000	0.000	0.000	0.000	0.000	0.000
0.252	0.356	0.425	0.496	0.561	0.625	0.692
0.423	0.422	0.503	0.587	0.666	0.738	0.809
0.594	0.445	0.528	0.615	0.695	0.764	0.828
0.765	0.458	0.542	0.630	0.709	0.774	0.832
0.936	0.470	0.555	0.644	0.723	0.787	0.841
1.107	0.483	0.571	0.662	0.742	0.806	0.859
1.278	0.498	0.589	0.683	0.766	0.832	0.887
1.449	0.516	0.611	0.710	0.796	0.867	0.925
1.620	0.537	0.638	0.741	0.834	0.909	0.972
1.800	0.561	0.667	0.777	0.876	0.958	1.028
3. The Phase Lag Changes with Locations at Different Pitch Ratios						
X	T/D=1.10	T/D=1.20	T/D=1.30	T/D=1.40	T/D=1.50	T/D=1.60
0.099	0.000	0.000	0.000	0.000	0.000	0.000
0.252	12.816	15.300	17.856	20.196	22.500	24.912
0.423	15.192	18.108	21.132	23.976	26.568	29.124
0.594	16.020	19.008	22.140	25.020	27.504	29.808
0.765	16.488	19.512	22.680	25.524	27.864	29.952
0.936	16.920	19.980	23.184	26.028	28.332	30.276
1.107	17.388	20.556	23.832	26.712	29.016	30.924
1.278	17.928	21.204	24.588	27.576	29.952	31.932
1.449	18.576	21.996	25.560	28.656	31.212	33.300
1.620	19.332	22.968	26.676	30.024	32.724	34.992
1.800	20.196	24.012	27.972	31.536	34.488	37.008

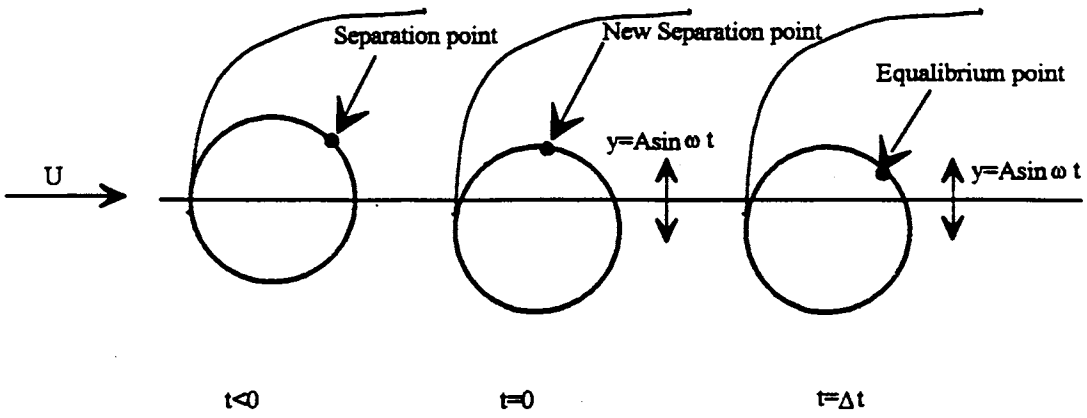

Fig. 1 The Movement of Separation Point

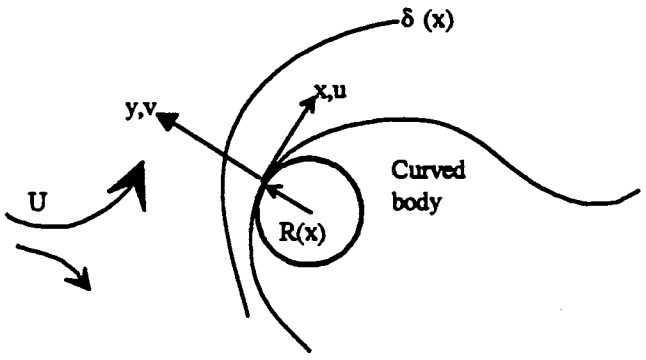

Fig.2 Boundary-layer flow over a curved body shape

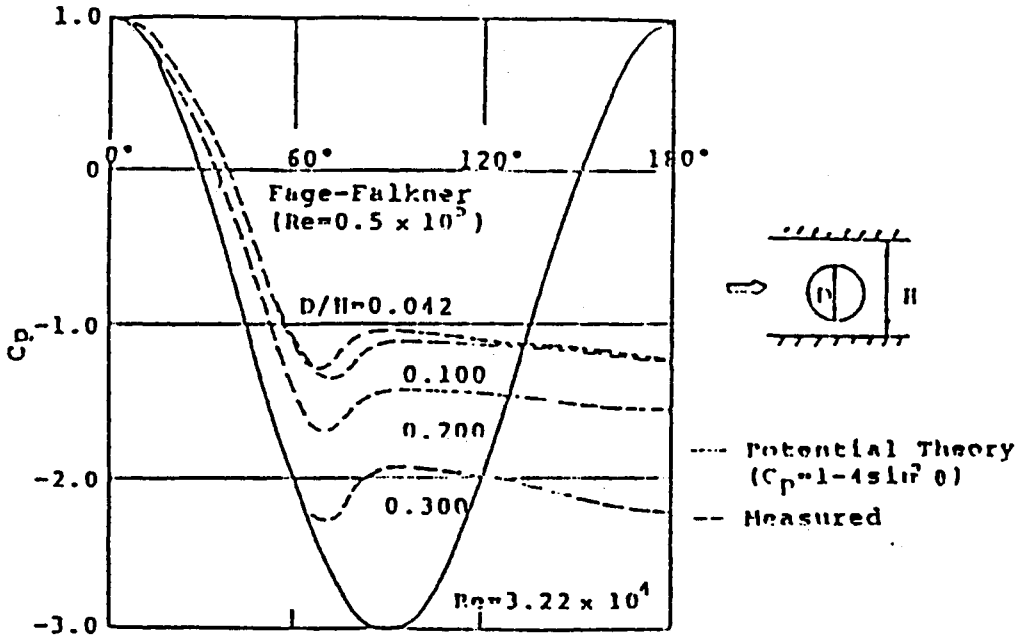

Fig. 3 Nondimensional Pressure Distribution [Nakamura et al., 1992]

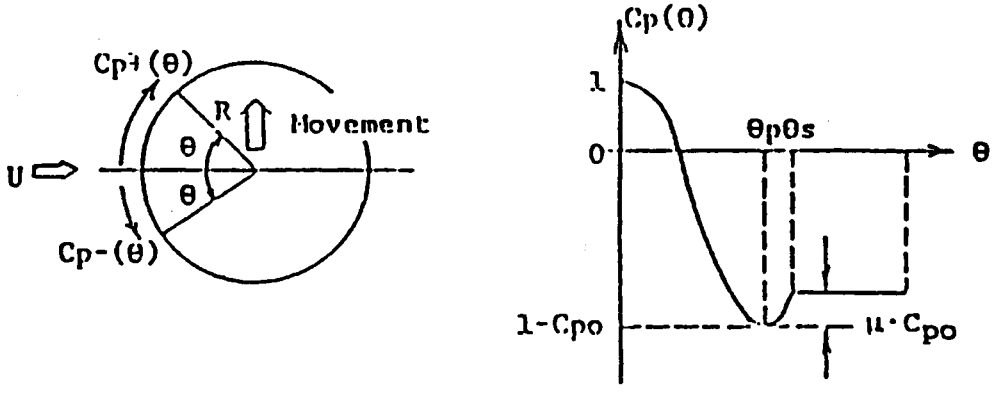

Fig. 4 Approximation of Pressure Distribution [Nakamura et al., 1992]

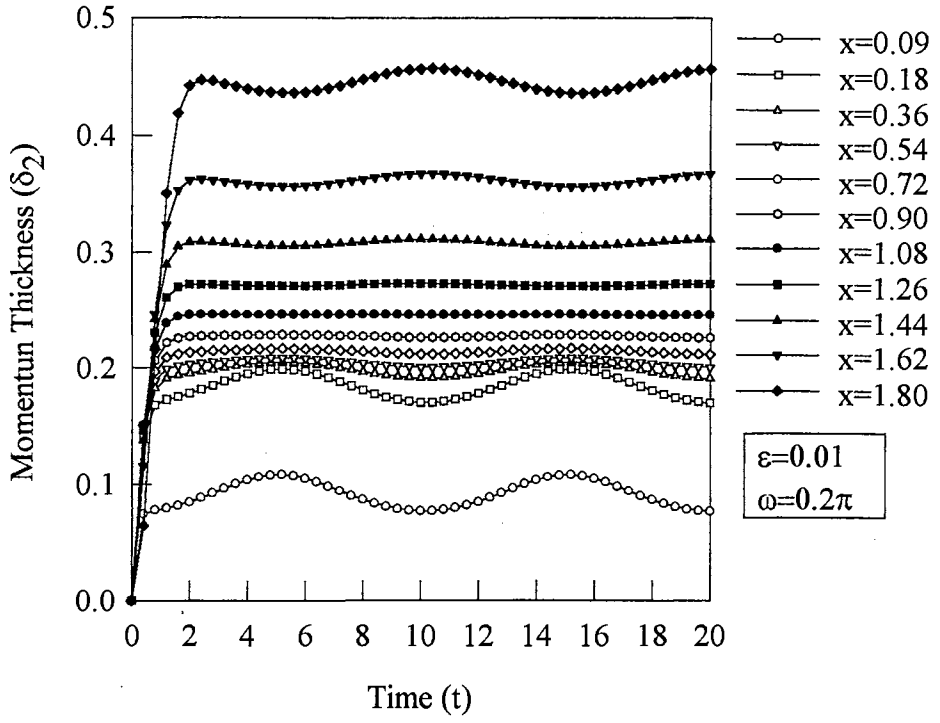

Fig. 5 The Development of Momentum Thickness at Different Locations

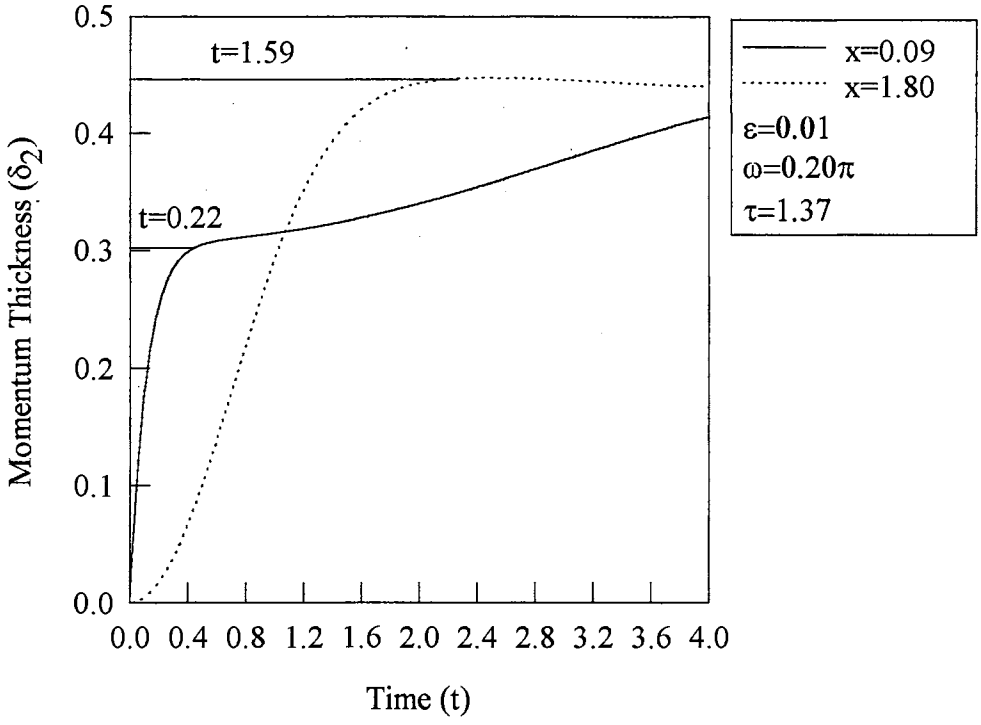

Fig. 6 The Time Constant Difference Between x=0.09 and x=1.80

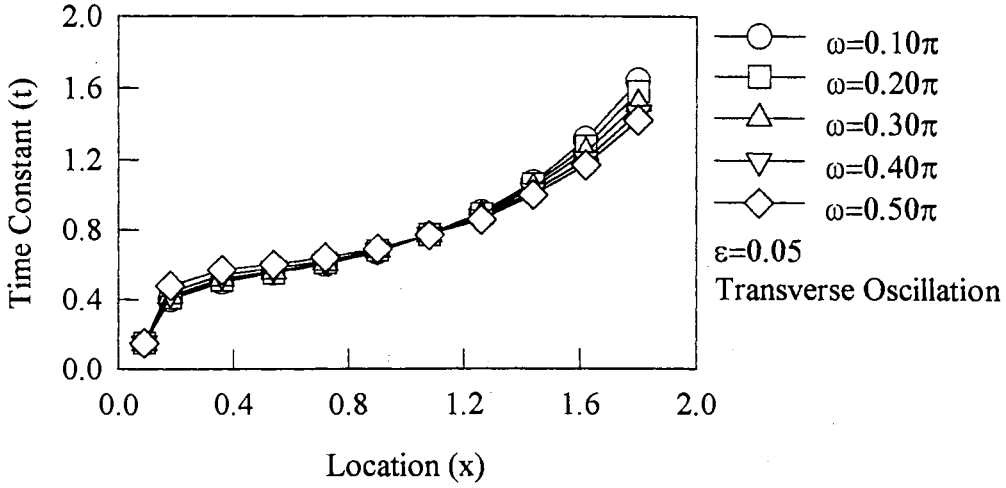

Fig. 7(a) The Time Constants vs. Location at Different Frequencies

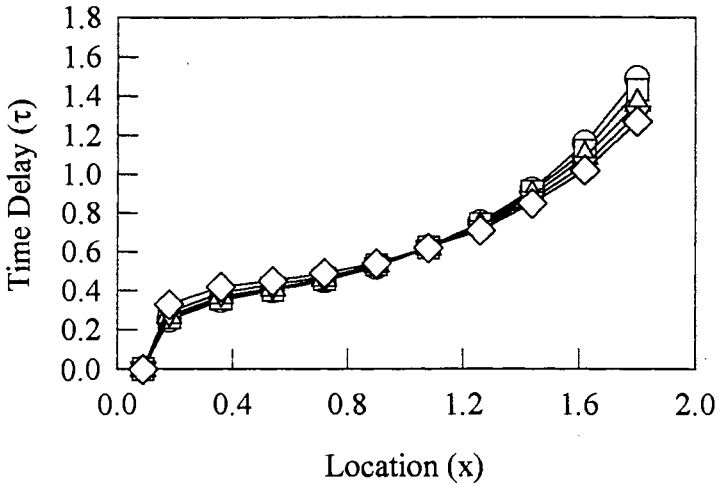

Fig. 7(b) The Time Delay vs. Location at Different Frequencies

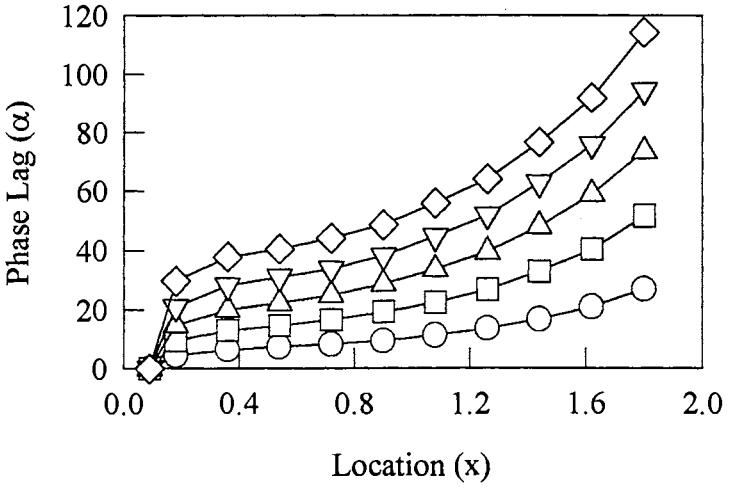

Fig. 7(c) The Phase Lag vs. Location at Different Frequencies

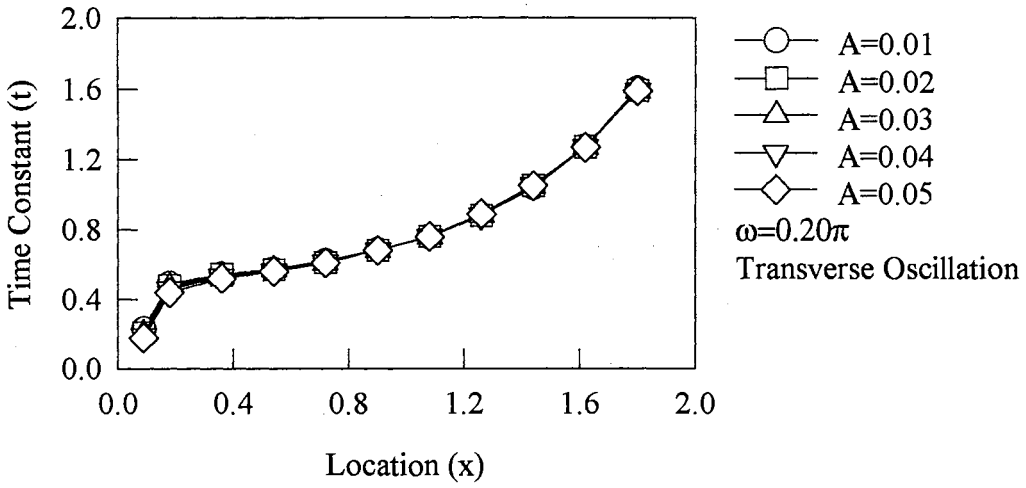

Fig. 8(a) The Time Constants vs. Location at Different Oscillation Amplitudes

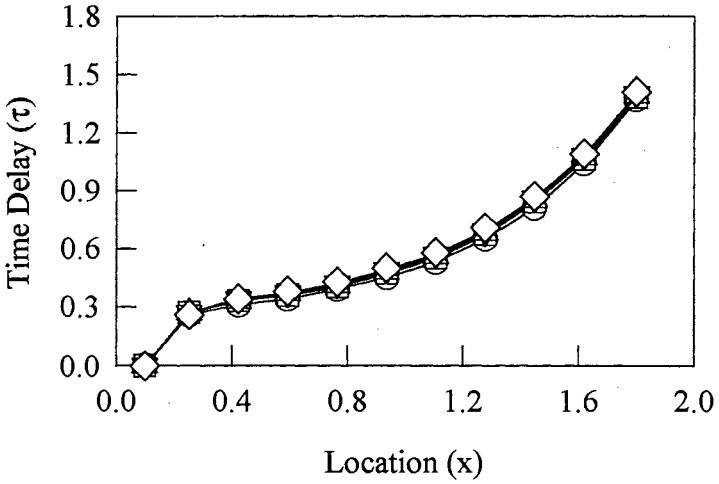

Fig. 8(b) The Time Delay vs. Location at Different Oscillation Amplitudes

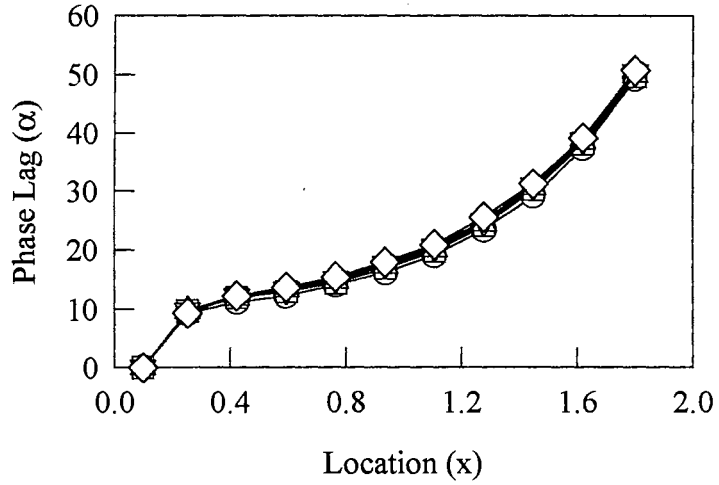

Fig. 8(c) The Phase Lag vs. Location at Different Oscillation Amplitudes

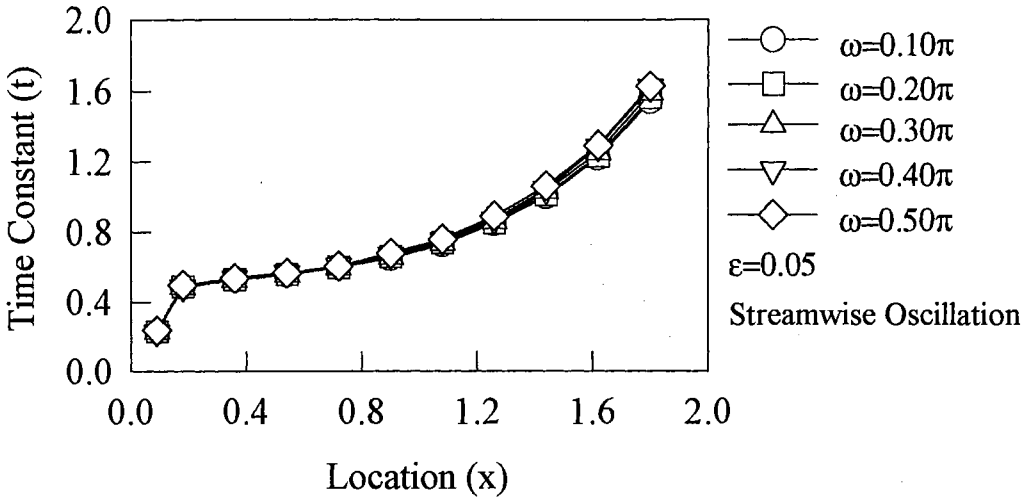

Fig. 9(a) The Time Constant vs. Location at Different Frequencies

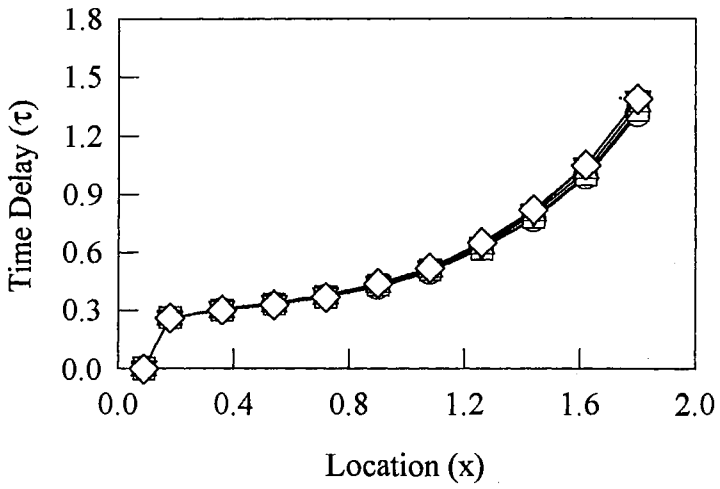

Fig. 9(b) The Time Delay vs. Location at Different Frequencies

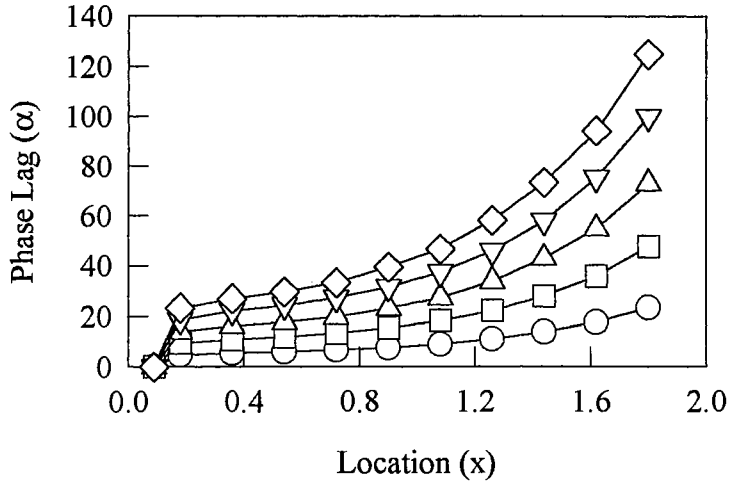

Fig. 9(c) The Phase Lag vs. Location at Different Frequencies

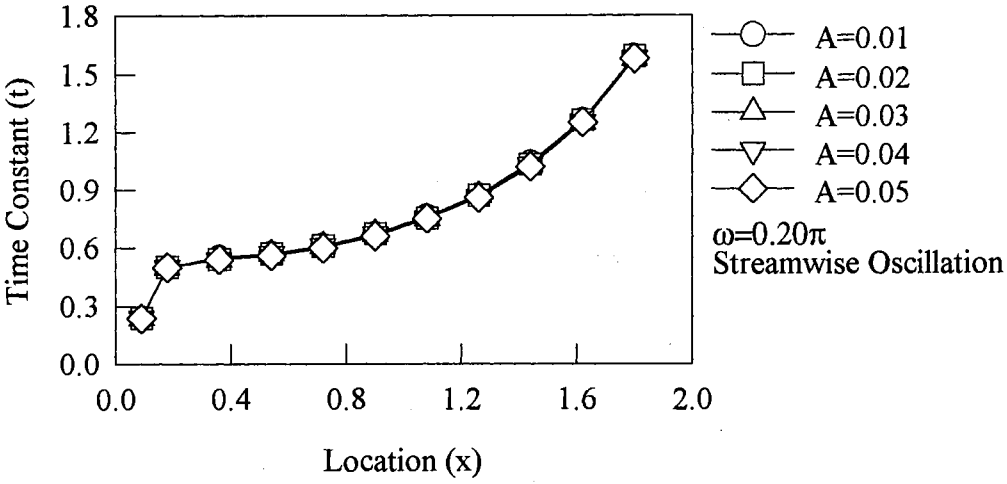

Fig. 10(a) The Time Constant vs. Location at Different Amplitudes

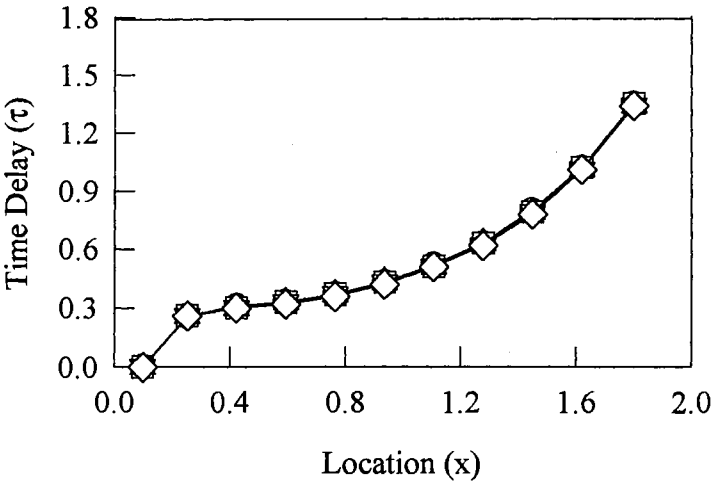

Fig. 10(b) The Time Delay vs. Location at Different Amplitudes

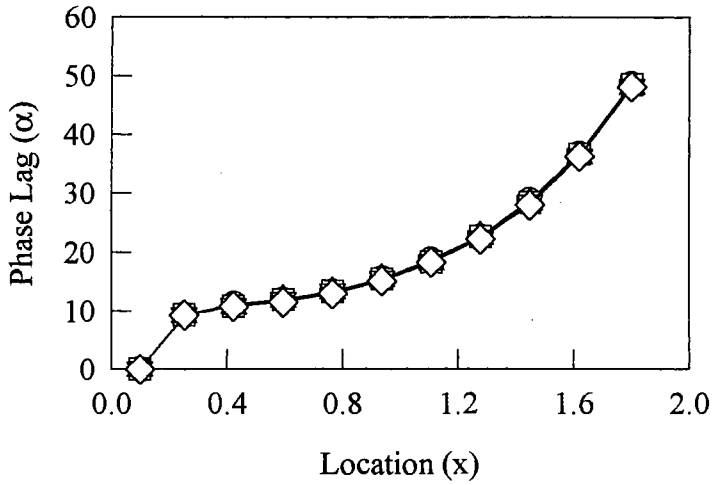

Fig. 10(c) The Phase Lag vs. Location at Different Amplitudes

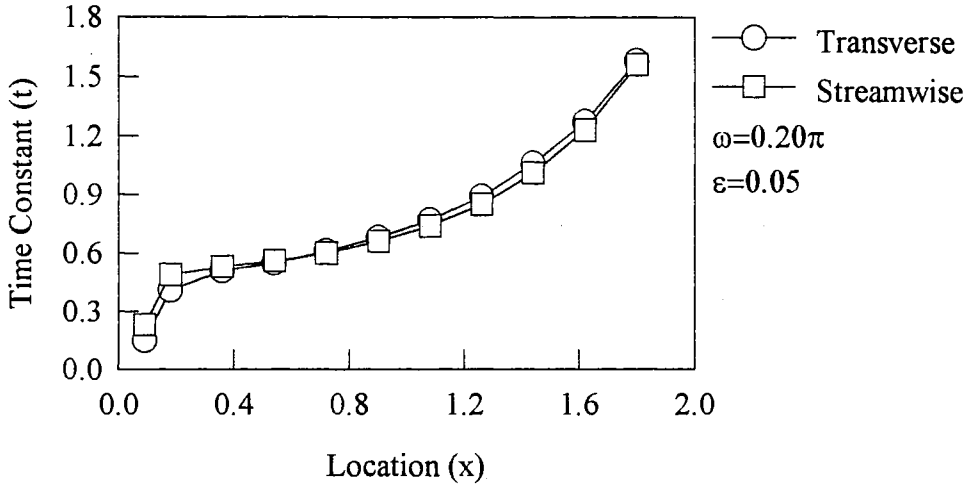

Fig. 11(a) The Time Constant vs. Location

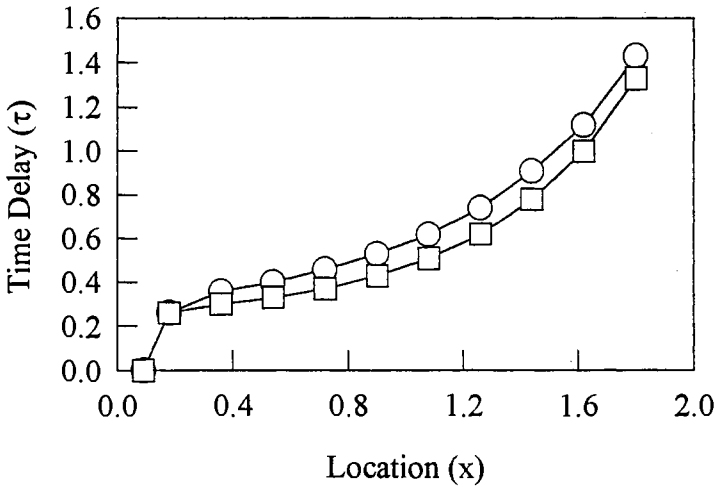

Fig. 11(b) The Time Delay vs. Location

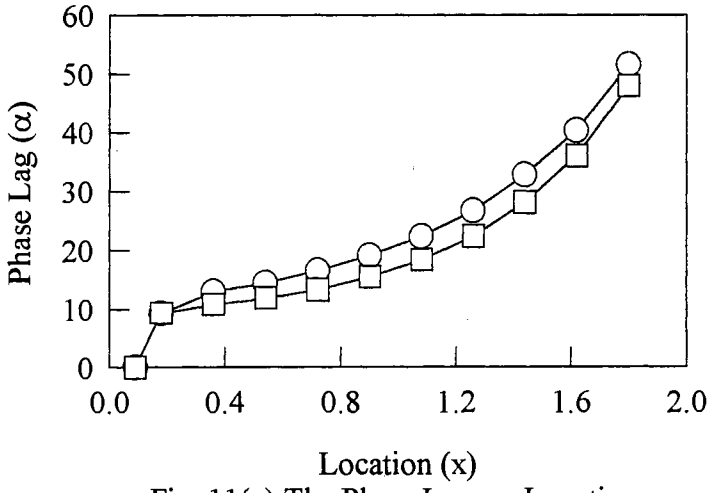

Fig. 11(c) The Phase Lag vs. Location

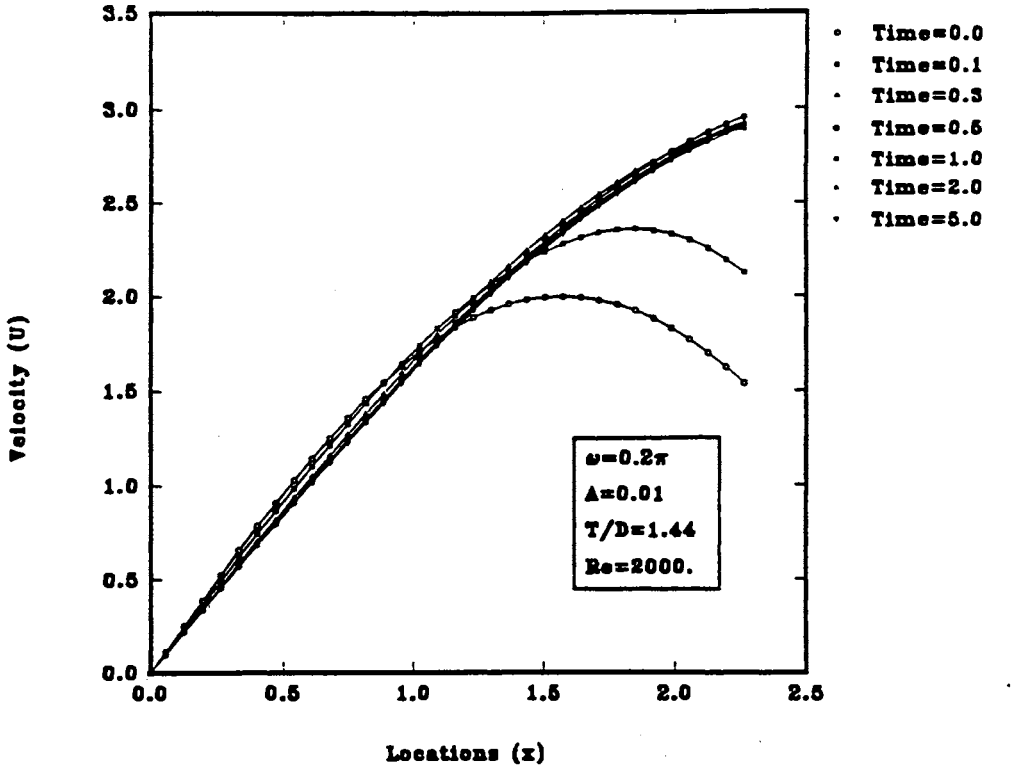

Fig. 12 The Velocity Distribution at Different Time

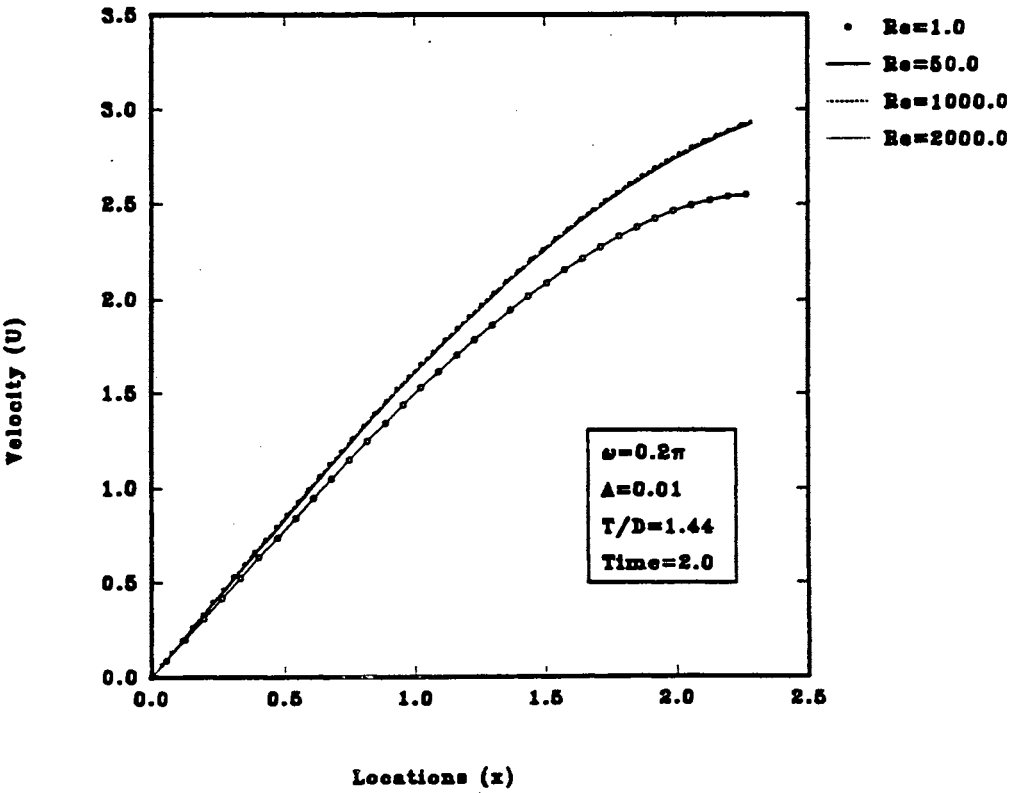

Fig. 13 The Velocity distribution at Different Reynolds Number

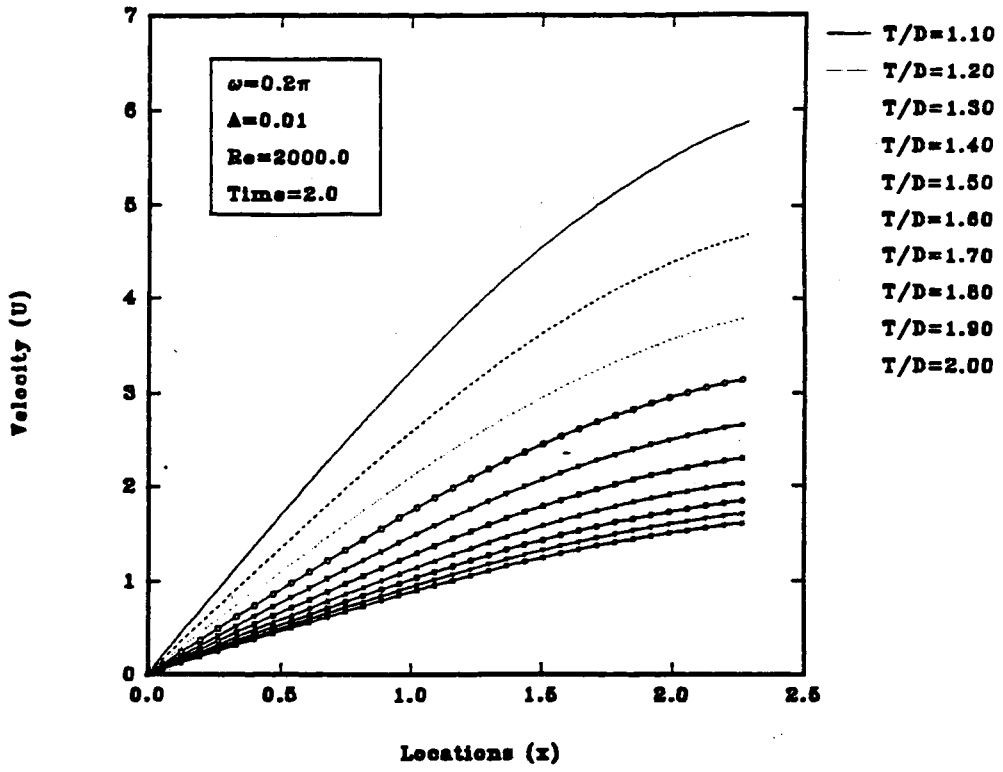

Fig. 14 The Velocity Distribution at Different Pitch Ratios

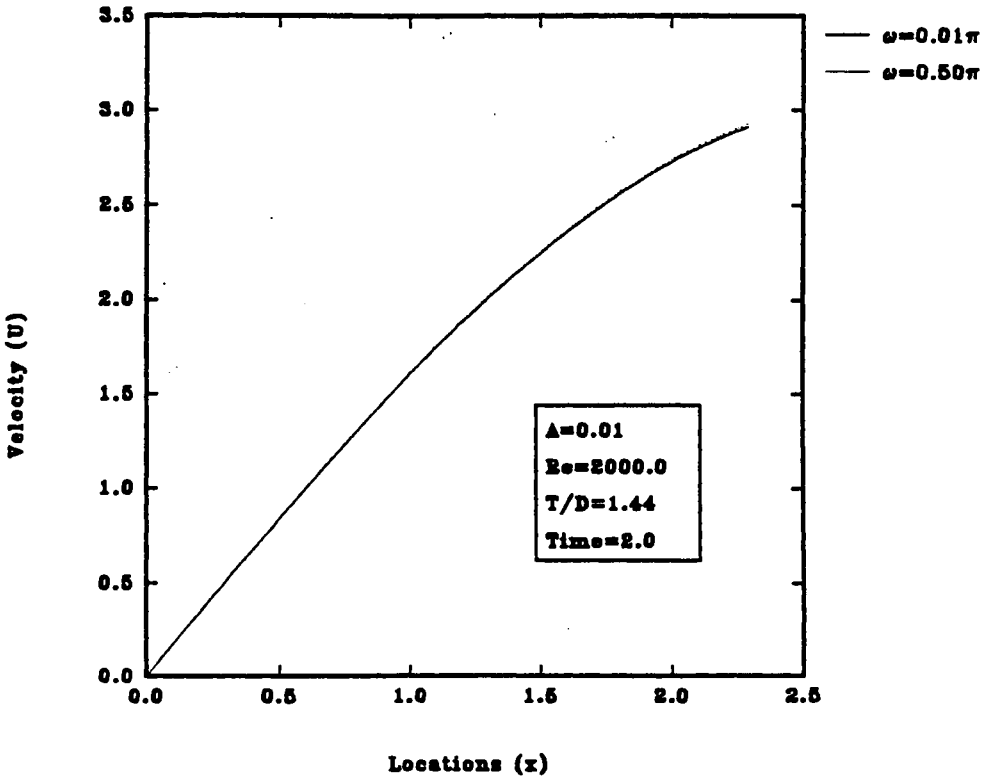

Fig. 15 The Velocity Distribution at Different Oscillation Frequencies

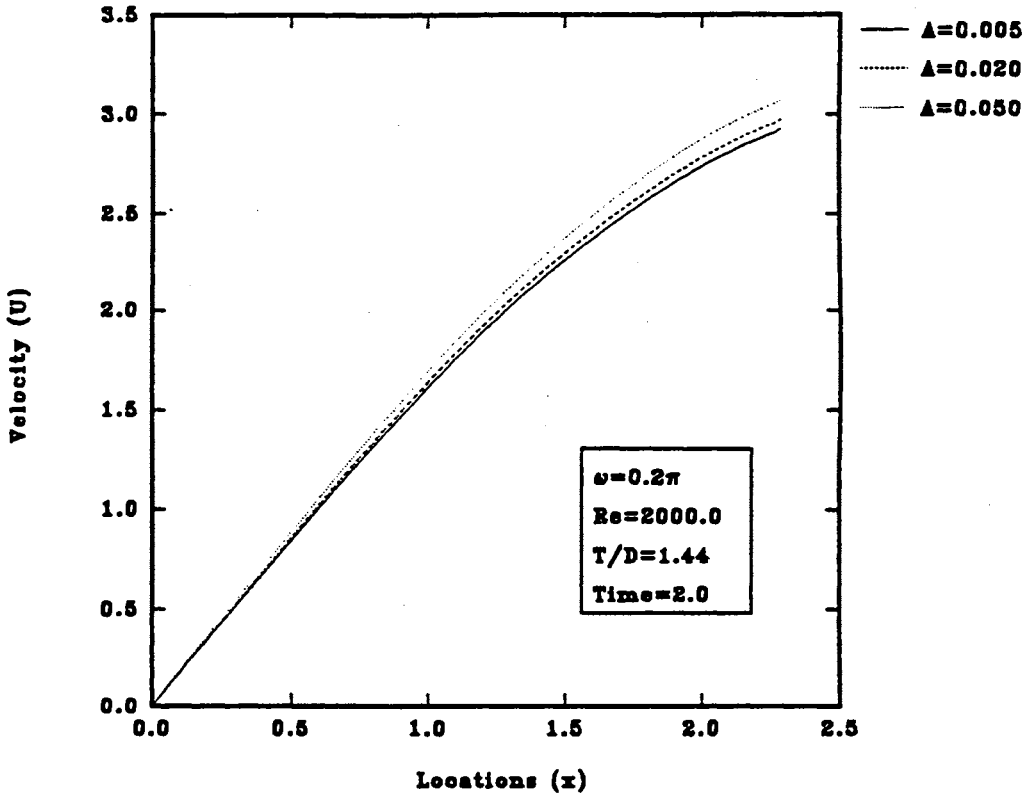

Fig. 16 The Velocity Distribution at different Amplitudes

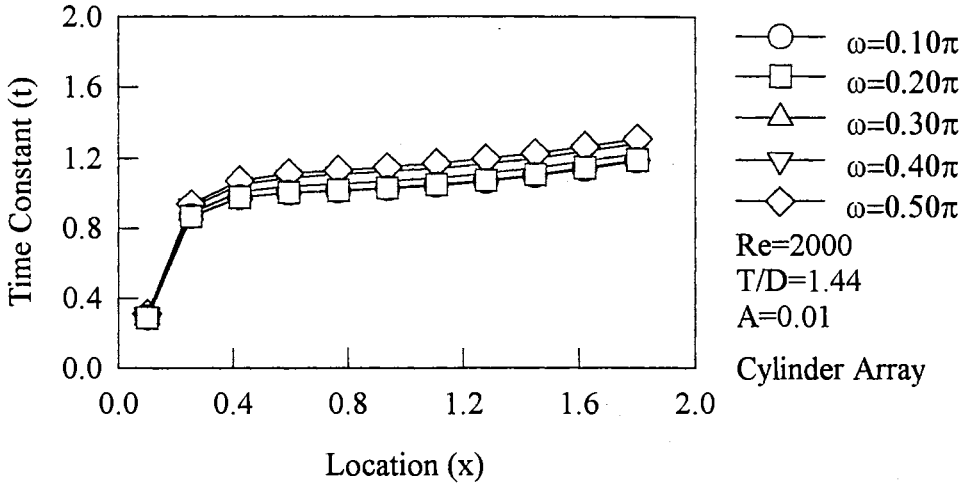

Fig. 17(a) The Time Constant vs. Location at Different Frequencies

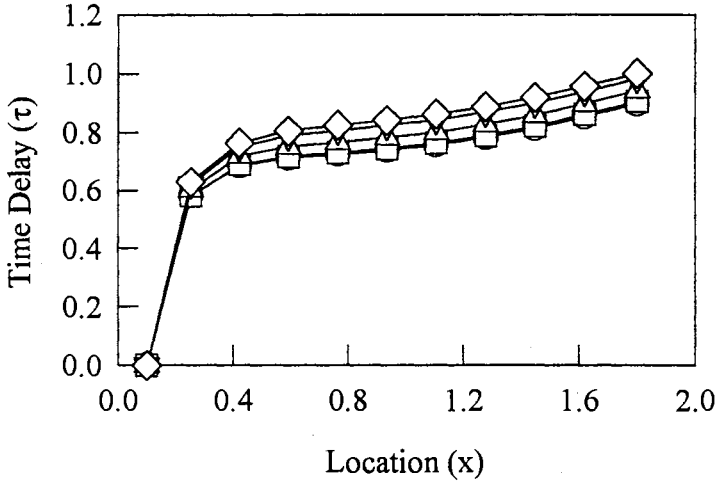

Fig. 17(b) The Time Delay vs. Location at Different Frequencies

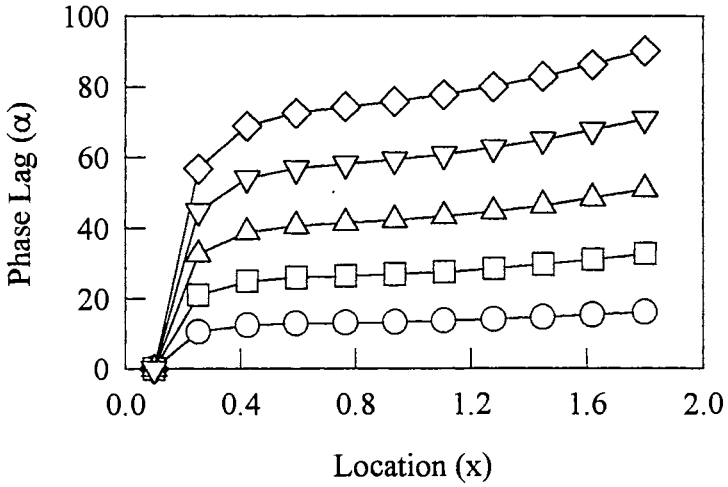

Fig. 17(c) The Phase Lag vs. Location at Different Frequencies

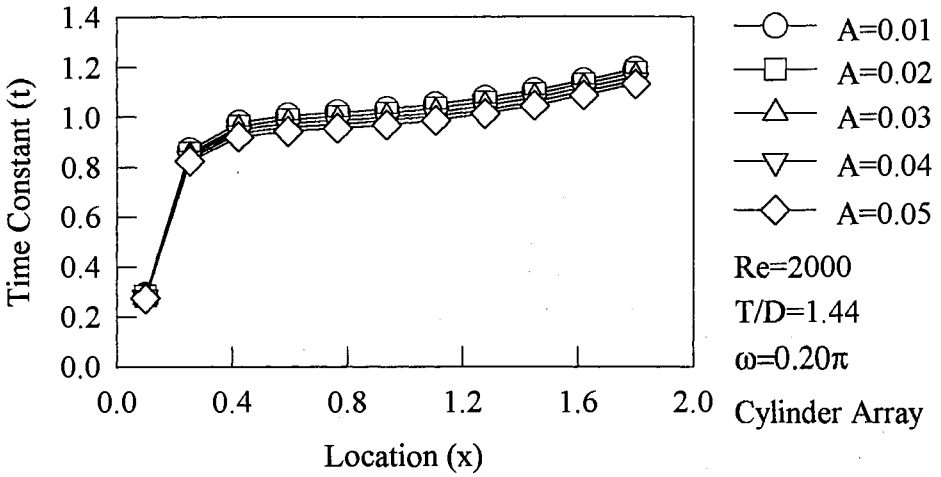

Fig. 18(a) The Time Constant vs. Location at Different Amplitudes

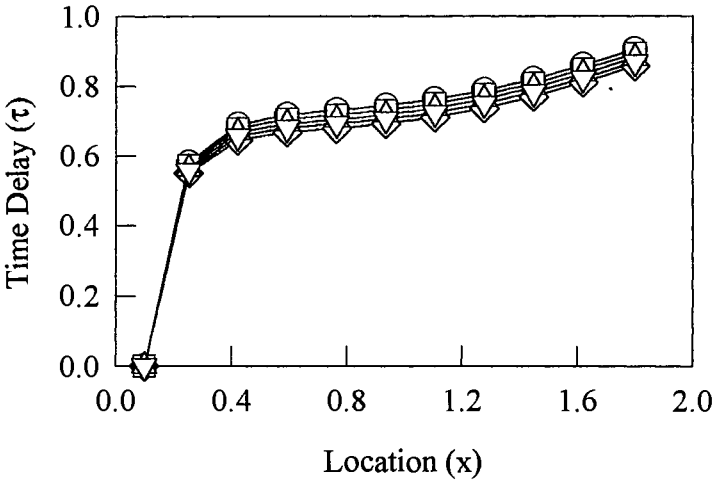

Fig. 18(b) The Time Delay vs. Location at Different Amplitudes

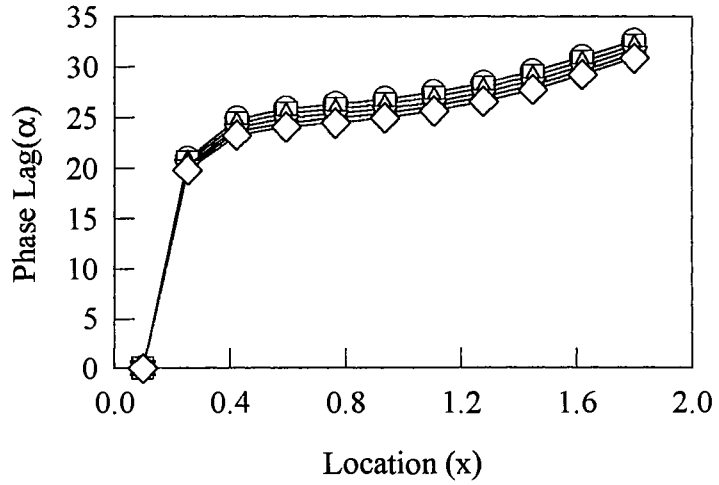

Fig. 18(c) The Phase Lag vs. Location at Different Amplitudes

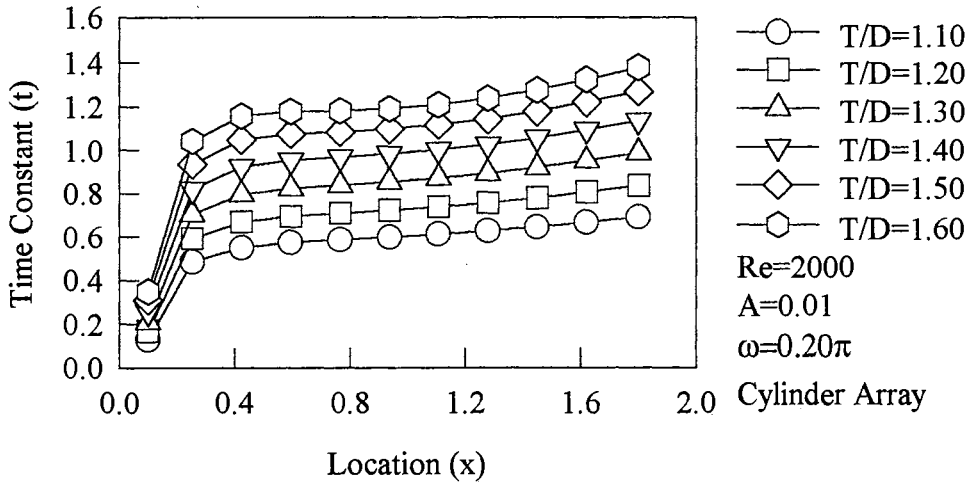

Fig. 19(a) The Time Constant vs. Location at Different Pitch Ratios

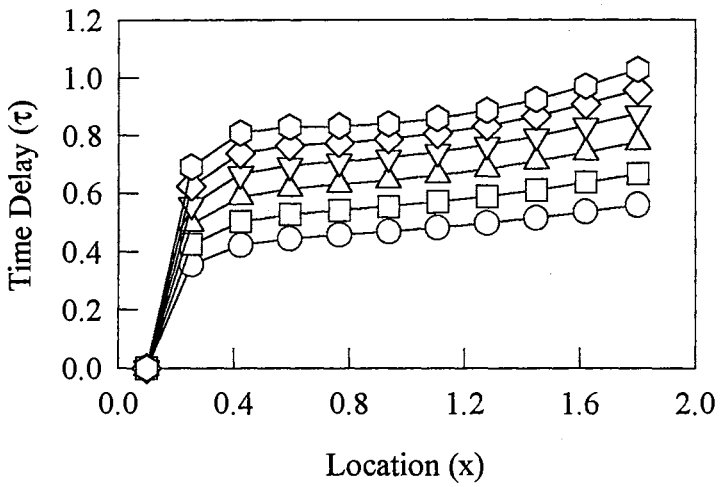

Fig. 19(b) The Time Delay vs. Location at Different pitch Ratios

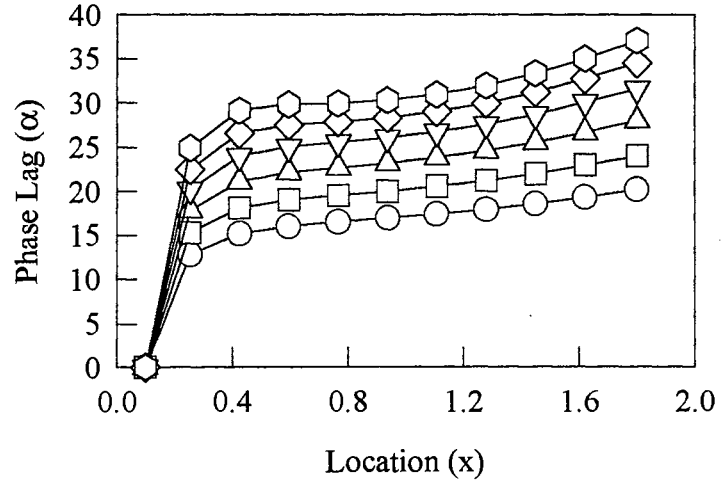

Fig. 19(c) The Phase Lag vs. Location at Different Pitch Ratios

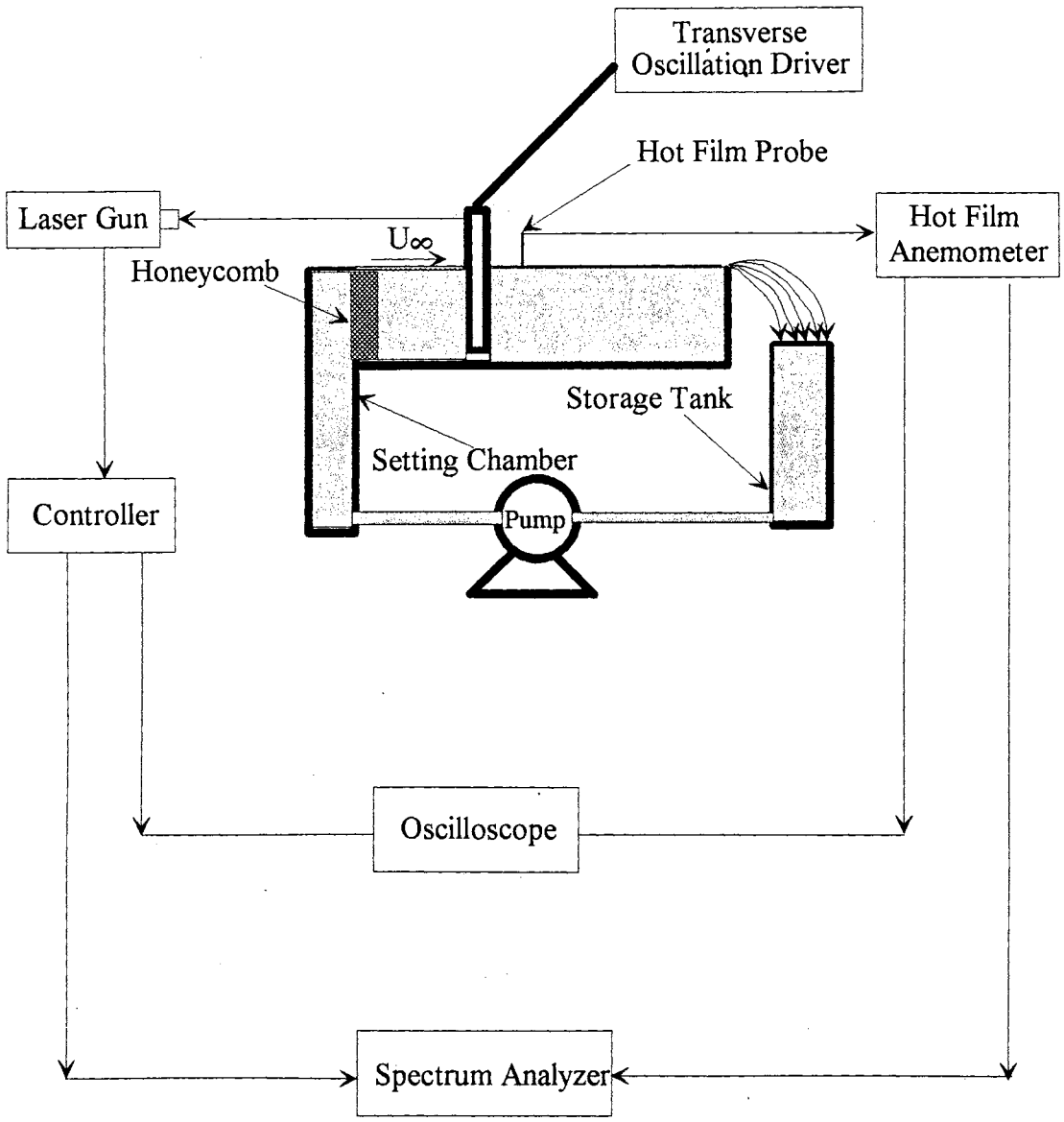

Figure 20 The line diagram of experimental system and instrumentation

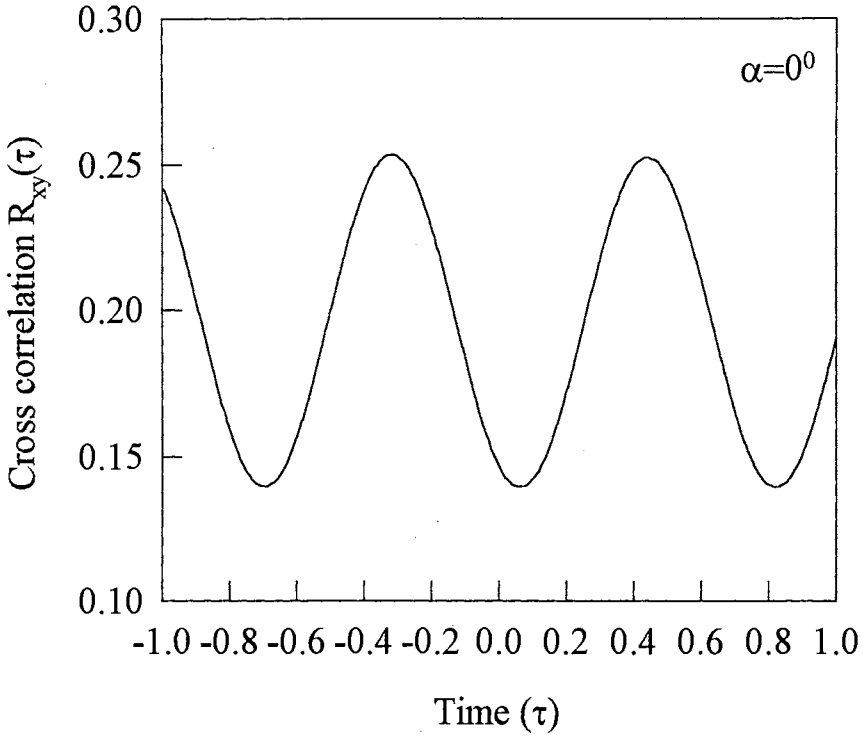

Figure 21(a) The cross correlation of perturbation and oscillation

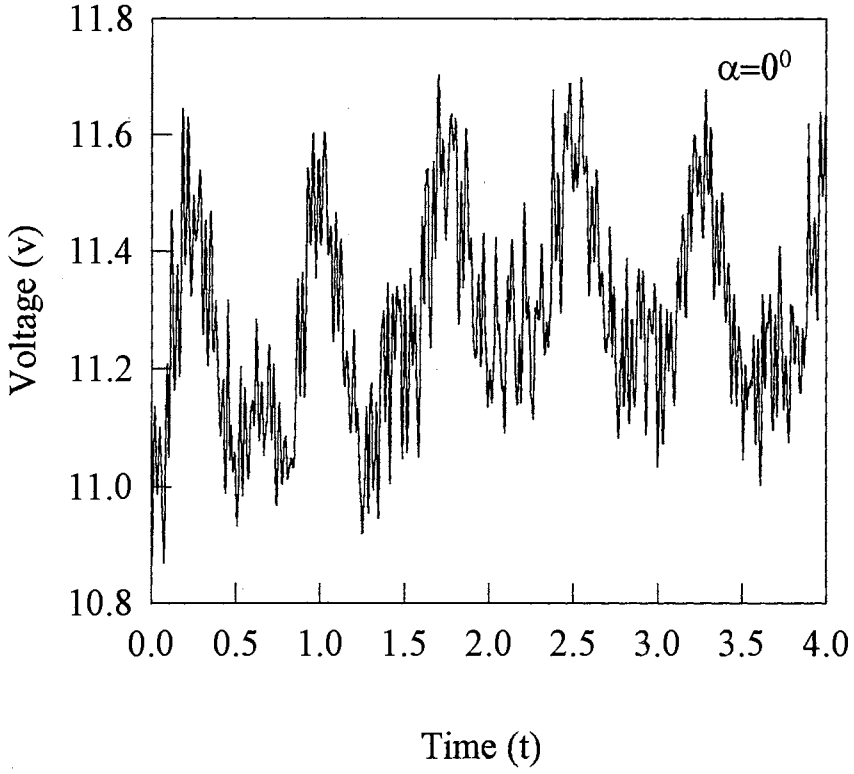

Figure 21(b) The flow perturbation vs time

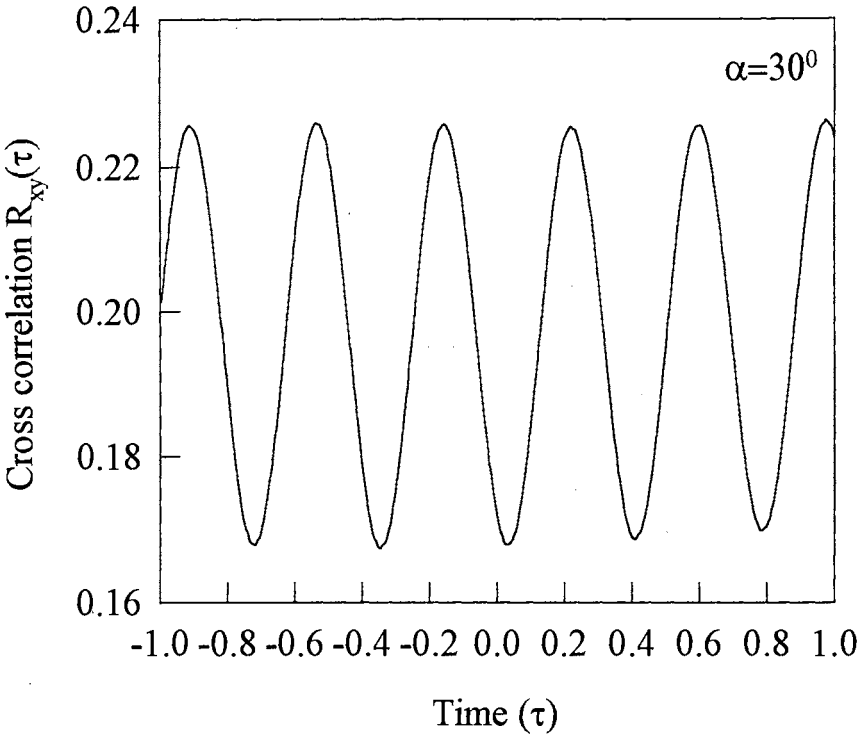

Figure 22(a) The cross correlation of perturbation and oscilation

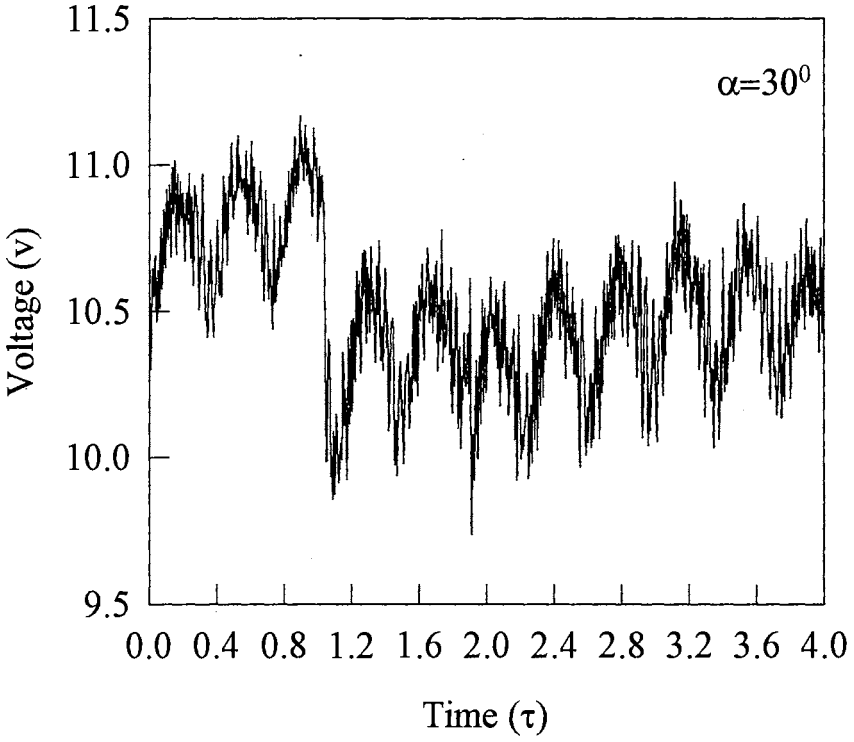

Figure 22(b) The flow perturbation vs time

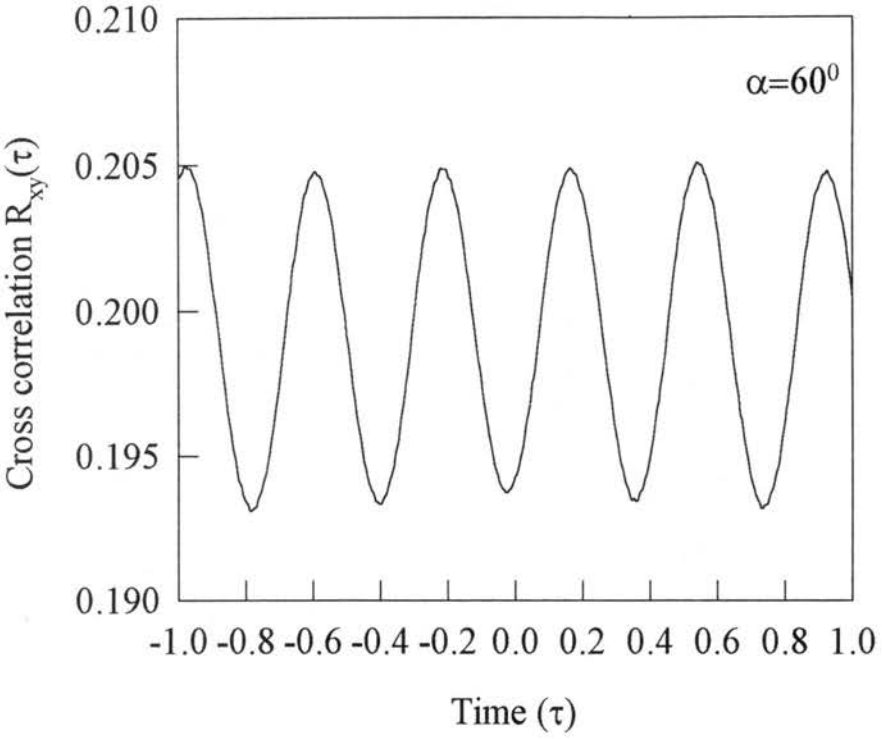

Figure 23(a) The cross correlation of perturation and oscillation

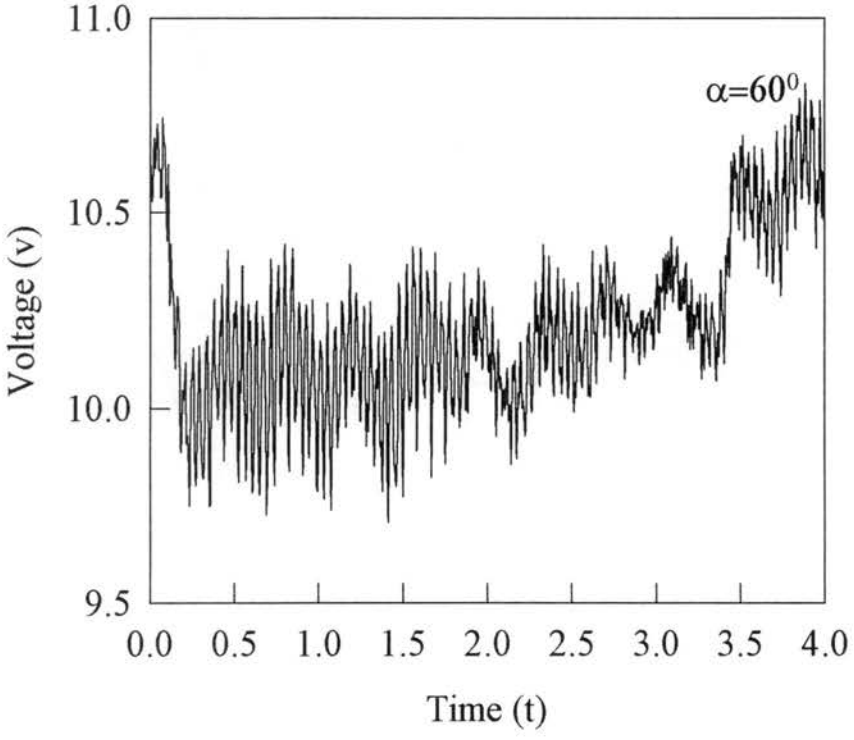

Figure 23(b) The flow perturbation vs time

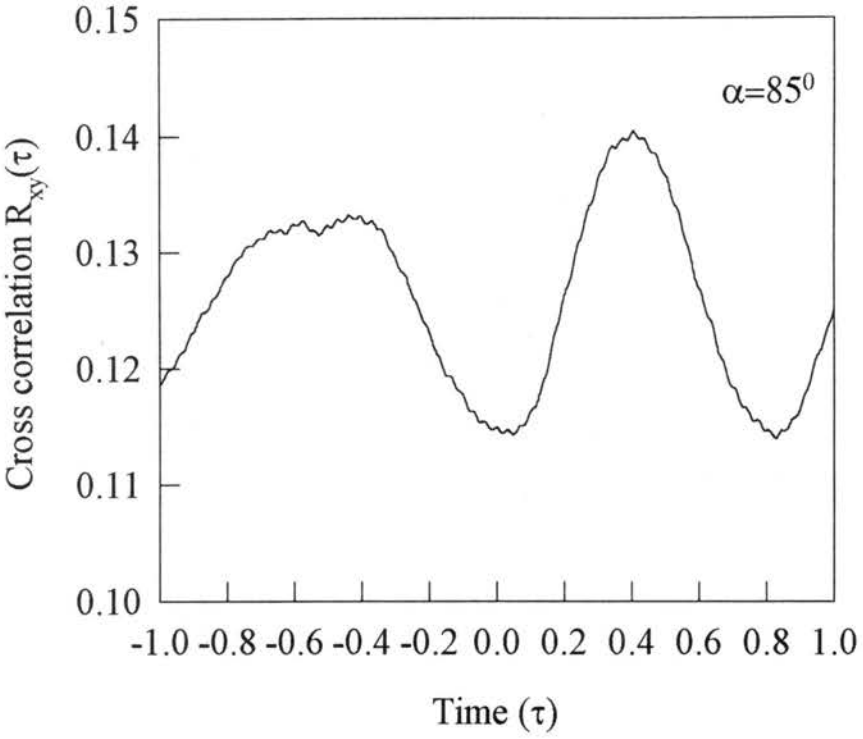

Figure 24(a) The cross correlation of perturbation and oscillation

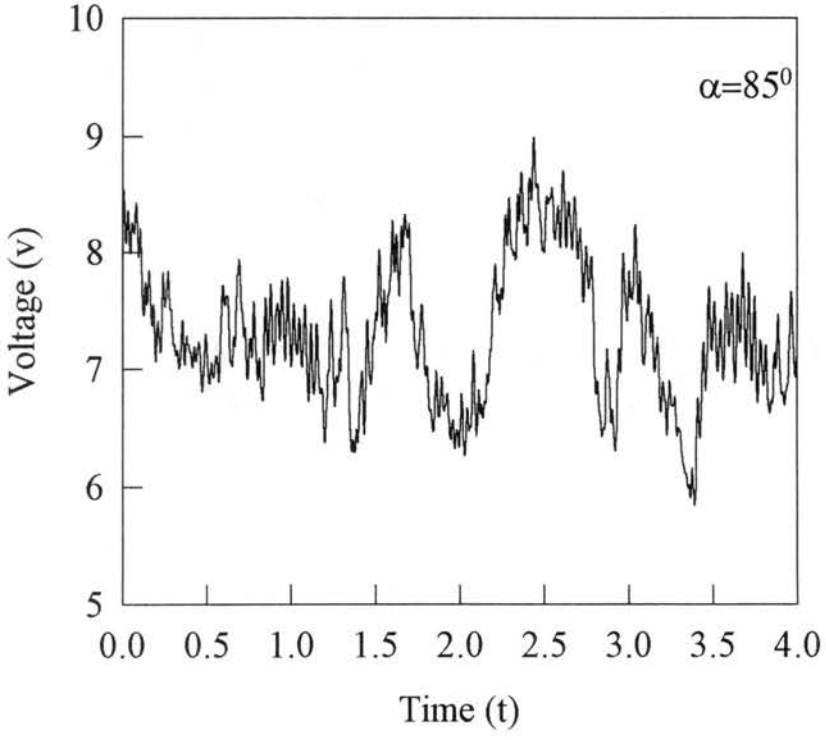

Figure 24(b) The flow perturbation vs time

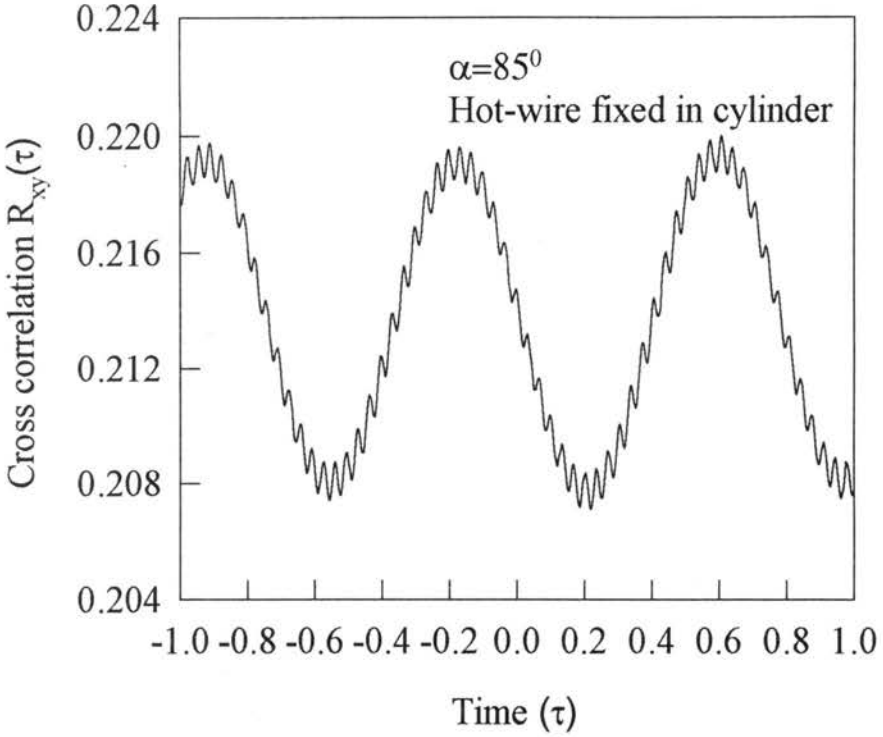

Figure 25(a) The cross correlation of perturbation and oscillation

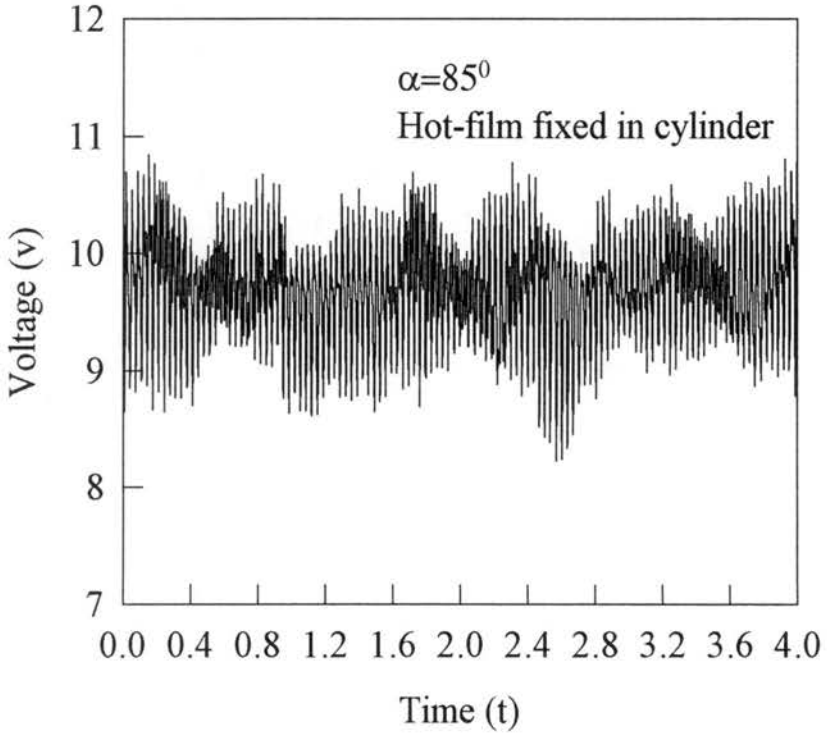

Figure 25(b) The flow perturbation vs time

VITA

Jiaqi Cai

Candidate for the Degree of

Doctor of Philosophy

Thesis: A STUDY OF TIME DELAYS ON A SINGLE CYLINDER AND A CYLINDER IN AN ARRAY OSCILLATING IN UNIFORM FLOW

Major Field: Mechanical Engineering

Biographical:

Personal Data: Born in Tianjin, China, on September 19, 1964,, the son of Shouwen Cai and Sujin Chen; Citizenship: China.

Education: Graduated from Tianjin Railway 3rd High school, Tianjin, China in July 1979; received Bachelor of Science Degree in Chemical Engineering from Tianjin University, Tianjin, China in July 1983; received Master of Science Degree in Chemical Engineering from Tianjin University, Tianjin, China in June 1986; completed requirements for Doctor of Philosophy degree at Oklahoma State University in May 1995.

Experience: Assistant Professor in Zhejiang University of Technology from June 1986 to August 1990; Teaching Assistant in Mechanical and Aerospace Engineering Department of Oklahoma State University from August 1990 to May 1995.

Professional Membership: Member of Chinese Society of Mechanical Engineers; Member of American Society of Mechanical Engineers.